4

Black Hole Binaries

Jeffrey E. McClintock
Harvard–Smithsonian Center for Astrophysics, 60 Garden St., Cambridge, MA 02138, USA

Ronald A. Remillard
Center for Space Research, MIT, Cambridge, MA 02139, USA

4.1 Introduction

4.1.1 Scope of this review

We focus on 18 black holes with measured masses that are located in X–ray binary systems. These black holes are the most visible representatives of an estimated ∼300 million stellar–mass black holes that are believed to exist in the Galaxy (van den Heuvel 1992; Brown & Bethe 1994; Timmes et al. 1996; Agol et al. 2002). Thus the mass of this particular form of dark matter, assuming $\sim 10 M_\odot$ per black hole, is ∼4% of the total baryonic mass (i.e., stars plus gas) of the Galaxy (Bahcall 1986; Bronfman et al. 1988). Collectively this vast population of black holes outweighs the Galactic–center black hole, SgrA*, by a factor of ∼1000. These stellar–mass black holes are important to astronomy in numerous ways. For example, they are one endpoint of stellar evolution for massive stars, and the collapse of their progenitor stars enriches the universe with heavy elements (Woosley et al. 2002). Also, the measured mass distribution for even the small sample of 18 black holes featured here are used to constrain models of black hole formation and binary evolution (Brown et al. 2000a; Nelemans & van den Heuvel 2001; Fryer & Kalogera 2001). Lastly, some black hole binaries appear to be linked to the hypernovae believed to power gamma–ray bursts (Israelian et al. 1999; Brown et al. 2000b; Orosz et al. 2001).

This review is focused on the X–ray timing and spectral properties of these 18 black holes, plus a number of black hole candidates, with an eye to their importance to physics as potential sites for tests of general relativity (GR) in the strongest possible gravitational fields. There are now several current areas of research that probe phenomena in these systems that are believed to occur very near the event horizon. These X–ray phenomena include quasi–periodic oscillations (QPOs) at high frequency (40–450 Hz) observed from seven systems, relativistically broadened iron lines from the inner accretion disk, and thermal disk emission from near the innermost stable circular orbit allowed by GR. We also comment on evidence for the existence of the event horizon, which is based on a comparison of black–hole and neutron–star binaries and on models for advective accretion flows.

The black hole binaries featured here are mass–exchange binaries that contain an accreting black hole primary and a nondegenerate secondary star. They comprise about 10% of all bright X–ray binaries. For background on X–ray binaries, see Chapter 1, and references therein. For comprehensive reviews on black hole binaries, see

Tanaka & Lewin (1995; hereafter TL95) and Tanaka and Shibazaki (1996; hereafter TS96). In this review, we emphasize the results of the past decade. Throughout we make extensive use of the extraordinary data base amassed since January 1996 by NASA's *Rossi X–ray Timing Explorer* (Swank 1998). Because of our page limit, several important topics are omitted such as X–ray reflection studies (Done & Nayakshin 2001), the estimated number of black–hole X–ray novae in the Galaxy (which is ~1000; van den Heuvel 1992; TS96; Romani 1998), and the present and projected rates of discovery of black hole binaries.

The main elements of the review are organized as follows. In the remainder of this section we catalog a total of 40 black–hole binaries and candidate black–hole binaries and discuss several introductory subjects, notably the physics of accretion onto black holes. In §4.2 we present seven–year X-ray light curves for 20 systems. In §4.3 we provide modified definitions of the canonical states of black hole binaries. Both low– and high–frequency quasi–periodic oscillations are discussed in §4.4. A recurring theme of the review is the importance of these black holes as potential sites for tests of general relativity.

4.1.2 The 18 black hole binaries

The first black hole binary (BHB), Cygnus X–1, was established by Webster and Murdin (1972) and Bolton (1972); the second, LMC X–3, was identified by Cowley et al. (1983). Both of these systems are persistently bright in X–rays; furthermore, they are classified as high–mass X–ray binaries (HMXBs) because their secondaries are massive O/B stars (White et al. 1995). The third BHB to be established, A0620–00, is markedly different (McClintock & Remillard 1986). A0620–00 was discovered as an X–ray nova in 1975 when it suddenly brightened to an intensity of 50 Crab* to become the brightest nonsolar X–ray source ever observed (Elvis et al. 1975). Then, over the course of a year, the source decayed back into quiescence to become a feeble (1 μCrab) source (McClintock et al. 1995). Similarly, the optical counterpart faded from outburst maximum by $\Delta V \approx 7.1$ mags to $V \approx 18.3$ in quiescence, thereby revealing the optical spectrum of a K–dwarf secondary.

During the past 20 years, black holes (BHs) have been established in 15 additional X–ray binaries. Remarkably, nearly all these systems are X–ray novae like A0620–00. Thus, in all there are now 18 confirmed BHBs. They are listed in Table 4.1 in order of right ascension. The coordinate name of each source is followed in the second column by its variable star name (or other name, such as Cyg X–1), which is useful for web–based literature searches. For X–ray novae, the third column gives the year of discovery and the number of outbursts that have been observed. As indicated in the table, among the confirmed BHBs, there are six recurrent X–ray novae and three persistent sources, Cyg X–1, LMC X–3 and LMC X–1. As indicated in the fourth column, these latter three sources are high–mass X–ray binaries and are the only truly persistent sources among the BHBs.

Two of the X–ray novae are peculiar: GRS 1915+105 has remained bright for more than a decade since its eruption in August 1992; GX339–4 (1659–487), which was

* 1 Crab = 2.6×10^{-9} erg cm^{-2} s^{-1} keV^{-1} (averaged over 2-11 keV) = 1.06 mJy @ 5.2 keV for a Crab–like spectrum with photon index $\Gamma = 2.1$.

Table 4.1. *Confirmed black hole binaries: primary properties*

Source	Alternative name[a]	Year[b]	Type[c]	$F_{x,max}$ (μJy[d])	D (kpc)	P_{orb} (hr)	Spec.	References
0422+32	V518 Per	1992/1	L,T	3000	2.6 ± 0.7	5.1	M2V	1,2
0538–641	LMC X–3	–	H,P	60	50 ± 2.3	40.9	B3V	3,4
0540–697	LMC X–1	–	H,P	30	50 ± 2.3	101.5	O7III	3,5,6
0620–003	V616 Mon	1975/2	L,T	50000	1.2 ± 0.1	7.8	K4V	7,8,9,10
1009–45	MM Vel	1993/1	L,T	800	5.0 ± 1.3	6.8	K7/M0V	11,12
1118+480	KV UMa	2000/1	L,T	40	1.8 ± 0.5	4.1	K5/M0V	13,14
1124–684[e]	GU Mus	1991/1	L,T	3000	5 ± 1.3	10.4	K3/K5V	15,15a,16
1543–475	IL Lupi	1971/4	L,T	15000	7.5 ± 0.5	26.8	A2V	17,18
1550–564	V381 Nor	1998/5	L,T	7000	5.3 ± 2.3	37.0	G8/K8IV	19
1655–40	V1033 Sco	1994/2	L,T	3900	3.2 ± 0.2	62.9	F3/F5IV	20,21,22
1659–487[f]	V821 Ara	1972/[f]	L,T	1100	4	42.1:	–	23,24
1705–250	V2107 Oph	1977/1	L,T	3600	8 ± 2	12.5	K3/7V	7,25,26
1819.3–2525	V4641 Sgr	1999/1	L,T	13000	7.4–12.3	67.6	B9III	27
1859+226	V406 Vul	1999/1	L,T	1500	11	9.2:	–	28,29
1915+105	V1487 Aql	1992/1	L,T	3700	11–12	804.0	K/MIII	30,31,32,33
1956+350	Cyg X–1	–	H,P	2300	2.0 ± 0.1	134.4	O9.7Iab	34,35
2000+251	QZ Vul	1988/1	L,T	11000	2.7 ± 0.7	8.3	K3/K7V	35a,7,36,37
2023+338	V404 Cyg	1989/3	L,T	20000	2.2–3.7	155.3	K0III	38,39,40

[a] Name recognized by the SIMBAD Database and the Astrophysics Data System (ADS).
[b] Year of discovery/number of outbursts observed (Chen et al. 1997; this work).
[c] 'H' – HMXB, 'L' – LMXB, 'T' – transient, 'P' – persistent; Liu et al. 2000, 2001; this work.
[d] $1\ \mu\text{Jy} = 10^{-29}$ ergs cm^{-2} s^{-1}Hz^{-1} = 2.42×10^{-12}ergs cm^{-2} s^{-1}keV^{-1}.
[e] Commonly known as Nova Muscae 1991.
[f] Commonly known as GX339–4; number of outbursts ~ 10 (Kong et al. 2002).

REFERENCES: [1]Esin et al. 1997; [2]Filippenko et al. 1995a; [3]Freedman et al. 2001; [4]Cowley et al. 1983; [5]Hutchings et al. 1987; [6]Cowley et al. 1995; [7]Barret et al. 1996b; [8]Gelino et al. 2001b; [9]Marsh et al. 1994; [10]McClintock & Remillard 2000; [11]Barret et al. 2000; [12]Filippenko et al. 1999; [13]McClintock et al. 2001a; [14]Wagner et al. 2001; [15]Orosz et al. 1996; [15a]Gelino et al. 2001a; [16]Shahbaz et al. 1997; [17]Orosz et al. 2002b; [18]Orosz et al. 1998; [19]Orosz et al. 2002a; [20]Hjellming & Rupen 1995; [21]Orosz & Bailyn 1997; [22]Shahbaz et al. 1999; [23]Cowley et al. 1987; [24]Hynes et al. 2003; [25]Remillard et al. 1996; [26]Filippenko et al. 1997; [27]Orosz et al. 2001; [28]Zurita et al. 2002; [29]Filippenko & Chornock 2001; [30]Mirabel & Rodriguez 1994; [31]Fender et al. 1999b; [32]Greiner et al. 2001a; [33]Greiner et al. 2001b; [34]Mirabel & Rodrigues 2003; [35]Gies & Bolton 1982; [35a]Harlaftis et al. 1996; [36]Filippenko et al. 1995b; [37]Casares et al. 1995; [38]Shahbaz et al. 1994; [39]Casares & Charles 1994; [40]Casares et al. 1993.

discovered by Markert et al. in 1973, undergoes frequent outbursts followed by very faint states, but it has never been observed to reach the *quiescent* state (Hynes et al. 2003). Columns 5 and 6 give the peak X–ray flux and a distance estimate for each source. The orbital period is given in the seventh column (a colon denotes an uncertain value) and the spectral type in the eighth. The first one or two references listed for each binary contain information on the orbital period and the spectral type. The remaining references support the distance estimates.

The data in Table 4.1 reveal considerable diversity among the BHBs. For example, these 18 binaries range in size from tiny XTE J1118+480 with $P_{\rm orb} = 0.17$ days and a separation between the BH and its companion of $a \approx 2.8\ R_\odot$ to GRS 1915+105 with $P_{\rm orb} = 33.5$ days and $a \approx 95 R_\odot$. Only six of these 18 systems were established as BHBs a decade ago (van Paradijs & McClintock 1995). As indicated in Table 4.1, all of the 15 X–ray novae are low–mass X–ray binaries (LMXBs), which typically contain a secondary with a mass of roughly 1 $M_\odot$ or less (White et al. 1995). The BHBs 4U1543–47 and SAX J1819.3–2525 have relatively massive secondaries: 2.7 ± 1.0 $M_\odot$ and 2.9 ± 0.2 $M_\odot$, respectively (Orosz et al. 2002b). We classify them as LMXBs because their secondary masses are comparable to the mass of the secondary of Her X–1 (2.3 ± 0.3 $M_\odot$; Reynolds et al. 1997), which is a well–known LMXB (Liu et al. 2001). Furthermore, a 2–3 $M_\odot$ secondary is much less massive than the O/B secondaries ($\gtrsim$10 $M_\odot$) found in HMXB systems.

BHBs manifest themselves in five rather distinct spectral/temporal states defined in the 1–10 keV band (e.g., van der Klis 1994; TL95; TS96). The three most familiar are (1) the *high/soft* (HS) state, a high–intensity state dominated by thermal emission from an accretion disk; (2) the *low/hard* (LH) state, a low–intensity state dominated by power–law emission and rapid variability; and (3) the *quiescent* state an extraordinarily faint state also dominated by power–law emission. The remaining two states, (4) the *very high* (VH) state and (5) the *intermediate* state, are more complex; recently they have come to the fore, as they have now been observed in an appreciable number of sources. These five BH states and the transitions between them are the focus of §4.3, where they are redefined and illustrated in detail.

Additional data specific to the BH primaries are contained in Table 4.2. Of special importance is the mass function, $f(M) \equiv P_{\rm orb}K_2^3/2\pi G = M_1 \sin^3 i/(1+q)^2$. The observables on the left side of the equation are the orbital period, $P_{\rm orb}$, and the half–amplitude of the velocity curve of the secondary, K_2. On the right, the quantity of most interest is the BH mass, M_1; the other parameters are the orbital inclination angle, i, and the mass ratio, $q \equiv M_2/M_1$, where M_2 is the mass of the secondary. Thus a secure value of the mass function can be determined for a quiescent X–ray nova or an HMXB by simply measuring the radial velocity curve of the secondary star. The mass function values are given in the second column of Table 4.2. An inspection of the equation for $f(M)$ shows that the value of the mass function is the absolute minimum mass of the compact primary. Thus, for 12 of the 18 BHBs, the very secure value of f(M) alone is sufficient to show that the mass of the compact X–ray source is at least 3 $M_\odot$ (Table 4.2), which is widely agreed to exceed the maximum stable mass of a neutron star (NS) in GR (Rhoades & Ruffini 1974; Kalogera & Baym 1996). For the remaining half–dozen systems, some additional data are required to make the case for a BH. The evidence for BHs in these 18 systems is generally very strong (see Ch. 5). Thus, assuming that GR is valid in the strong–field limit, we choose to refer to these compact primaries as BHs, rather than as BH candidates. We note, however, our reservations about three of the systems listed in Table 4.2: (1) The mass function of LMC X–1 (0540-697) is quite uncertain; (2) the orbital period of XTE J1859+226 is not firmly established (Filippenko & Chornock 2001; Zurita et al. 2002); and (3) the dynamical data for GX 339–4 (1659-487) were determined in outburst by a novel technique, and neither the orbital period nor the velocity amplitude are securely determined (Hynes et al. 2003).

The mass of a BH can be derived from the measurement of its mass function in combination with estimates for M_2 and sin i. The ratio of the mass of the BH to the mass of the secondary star is usually deduced by measuring the rotational velocity

Table 4.2. *Confirmed black hole binaries: X–ray and optical data*

Source	f(M)[a] ($M_\odot$)	M_1^a ($M_\odot$)	f(HFQPO) (Hz)	f(LFQPO) (Hz)	Radio[b]	E^c_{max} (MeV)	References
0422+32	1.19±0.02	3.2–13.2	–	0.035–32	P	0.8,1–2:	1,2,3,4,5
0538–641	2.3±0.3	5.9–9.2	–	0.46	–	0.05	6,7
0540–697	0.14±0.05	4.0–10.0:	–	0.075	–	0.02	8,7
0620–003	2.72±0.06	3.3–12.9	–	–	P,J?	0.03:	9,10,11,11a
1009–45	3.17±0.12	6.3–8.0	–	0.04–0.3	–[d]	0.40, 1:	12,4,13
1118+480	6.1±0.3	6.5–7.2	–	0.07–0.15	P	0.15	14,15,16,17
1124–684	3.01±0.15	6.5–8.2	–	3.0-8.4	P	0.50	18,19,20,21
1543–475	0.25±0.01	7.4–11.4[e]	–	7	–[f]	0.20	22,4
1550–564	6.86±0.71	8.4–10.8	92,184,276	0.1-10	P,J	0.20	23,24,25,26,27
1655–40	2.73±0.09	6.0–6.6	300,450	0.1–28	P,J	0.80	28,29,30,31,54
1659–487	$> 2.0^g$	–	–	0.09–7.4	P	0.45, 1:	32,33,4,13
1705–250	4.86±0.13	5.6–8.3	–	–	–[d]	0.1	34,35
1819.3–2525	3.13±0.13	6.8–7.4	–	–	P,J	0.02	36,37
1859+226	7.4±1.1	7.6–12:	190	0.5–10	P,J?	0.2	38,39,40,41
1915+105	9.5±3.0	10.0–18.0:	41,67,113,168	0.001-10	P,J	0.5, 1:	42,43,44,4,13
1956+350	0.244±0.005	6.9–13.2	–	0.035–12	P,J	2–5	45,46,47,48,49
2000+251	5.01±0.12	7.1–7.8	–	2.4–2.6	P	0.3	18,50,51
2023+338	6.08±0.06	10.1–13.4	–	–	P	0.4	52,53

[a] Orosz et al. 2002b, except for 1659–487; colon denotes uncertain value.
[b] Radio properties: 'P' - persistent over 10 or more days and/or inverted spectrum; 'J' - relativistic jet detected.
[c] Maximum energy reported; colon denotes uncertain value.
[d] No observations made.
[e] Orosz, private communication.
[f] Very faint (e.g., see IAUC 7925).
[g] For preferred period, $P = 1.76$ days, $f(M) = 5.8 \pm 0.5\ M_\odot$; Hynes et al. 2003.

REFERENCES: [1]van der Hooft et al. 1999; [2]Vikhlinin et al. 1992; [3]Shrader et al. 1994; [4]Grove et al. 1998; [5]van Dijk et al. 1995; [6]Boyd et al. 2000; [7]Nowak et al. 2001; [8]Ebisawa et al. 1989; [9]Owen et al. 1976; [10]Kuulkers et al. 1999; [11]Coe et al. 1976; [11a] Marsh et al. 1994; [12]van der Hooft et al. 1996; [13]Ling et al. 2000; [14]Wood et al. 2000; [15]Revnivtsev et al. 2000b; [16]Fender et al. 2001; [17]McClintock et al. 2001a; [18]Rutledge et al. 1999; [19]Belloni et al. 1997; [20]Ball et al. 1995; [21]Sunyaev et al. 1992; [22]This work; [23]Remillard et al. 2002b; [24]Corbel et al. 2001; [25]Wu et al. 2002; [26]Corbel et al. 2003; [27]Sobczak et al. 2000b; [28]Remillard et al. 1999; [29]Strohmayer 2001a; [30]Hjellming & Rupen 1995; [31]Hannikainen et al. 2000; [32]Revnivtsev et al. 2001; [33]Corbel et al. 2000; [34]Wilson & Rothschild 1983; [35]Cooke et al. 1984; [36]Hjellming et al. 2000; [37]Wijnands & van der Klis 2000; [38]Cui et al. 2000a; [39]Markwardt 2001; [40]Brocksopp et al. 2002; [41]Dal Fiume et al. 1999; [42]Morgan et al. 1997; [43]Strohmayer 2001b; [44]Mirabel & Rodriguez 1994; [45]Vikhlinin et al. 1994; [46]Cui et al. 1997b; [47]Stirling et al. 2001; [48]Ling et al. 1987; [49]McConnell et al. 2002; [50]Hjellming et al. 1988; [51]Sunyaev et al. 1988; [52]Han & Hjellming 1992; [53]Sunyaev et al. 1991b; [54]Tomsick et al. 1999.

of the latter. The binary inclination angle can be constrained in several ways; commonly, one models the photometric variations associated with the gravitationally-distorted secondary star that is seen to rotate once per binary orbit in the plane of the sky (e.g., Greene, Bailyn, & Orosz 2001). Mass estimates for the known BHBs are given in the third column of Table 4.2. In an astrophysical environment, a BH is completely specified in general relativity by two numbers, its mass and its specific angular momentum or spin, $a = J/cM_1$, where J is the BH angular momentum and c

is the speed of light (e.g., Kato et al. 1998). The spin value is conveniently expressed in terms of a dimensionless spin parameter, $a_* = a/r_g$, where the gravitational radius is $r_g \equiv GM/c^2$. The value of a_* lies between 0 for a Schwarzschild hole and 1 for a maximally–rotating Kerr hole. The radius of the BH event horizon depends on both M_1 and a_*; this topic is discussed further in §4.1.5.

High frequency QPOs (HFQPOs) in the range 40–450 Hz are observed for the four systems with data given in the fourth column. Low–frequency QPOs (LFQPOs) are also observed from these systems and ten others, as indicated in column 5. Most of the systems were at one time or another detected as radio sources and at least five have exhibited resolved radio jets (column 6; see Mirabel & Rodriguez 1999). An X–ray jet (two–sided) has been observed from XTE J1550–564 (Corbel et al. 2002). As shown in column 7, power–law emission extending to ∼1 MeV has been observed for six sources. The references listed in the last column support the X–ray QPO, radio, and E_{max} data given in columns 4–7.

The dynamical evidence for massive ($M > 3\ M_\odot$) collapsed stellar remnants is indisputable. However, this evidence alone can never establish the existence of BHs. At present, the argument for BHs depends on the assumption that GR is the correct theory of strong gravity. To make an airtight case that a compact object is a BH with an event horizon, we must make clean quantitative measurements of relativistic effects that occur near the collapsed object. That is, we must measure phenomena that are predicted by GR to be unique to BHs. A possible route to this summit is to measure and interpret the effects of strong–field gravity that are believed to be imprinted on both HFQPOs (§4.4.3) and X–ray emission lines (§4.2.3). Another approach, which is discussed in §4.3.4, is based on sensing the qualitative differences between an event horizon and the material surface of a NS.

4.1.3 Black hole candidates

Certain characteristic X–ray properties of the 18 established BHs are often used to identify a candidate BH when the radial velocities of the secondary cannot be measured (e.g., because the secondary is too faint). These frequently observed characteristics of the established BHBs, which are discussed in detail by TL95, include an ultrasoft X–ray spectrum (1–10 keV), a power–law spectral tail that extends beyond 20 keV, characteristic state transitions (§4.1.2; §4.3), and rapid temporal variability. However, none of these putative BH signatures has proved to be entirely reliable; each of them has been forged by one or more systems known to contain a NS primary (TL95). This is not surprising since the X–ray spectral/temporal properties originate in an accretion flow that is expected to be fairly similar whether the primary is a BH or a weakly magnetized NS. Another characteristic of all BHBs is a complete absence of either periodic pulsations or type I X–ray bursts, which are the very common signatures of NS systems.

Nevertheless, despite the limitations of these spectral/temporal identifiers, they have served as useful guides and have allowed the identification of a number of probable BH primaries, which we refer to as BH candidates or BHCs. In order to economize on acronyms, we also use BHC to refer to the binary system that hosts the BH candidate. A list of 22 BHCs is given in Table 4.3. These systems are less well–known than the BHBs listed in Table 4.1. Therefore, to aid in their identification we

Table 4.3. *Candidate black hole binaries*[a]

Source	RA(2000)	DEC(2000)	r_x[b]	BH trait[c]	Grade[d]	References
1354–645 (BW Cir)	13 58 09.74	-64 44 05.2		LH,HS	A	1,2,3,4
1524–617 (KY TrA)	15 28 16.7	-61 52 58		LH,HS	A	5,6,7
4U 1630–47	16 34 01.61	-47 23 34.8		LH,HS	A	8,9,10,11,83
XTE J1650–500	16 50 01.0	-49 57 45		LH,HS,VH	A	12,13,14,15,16
SAX J1711.6–3808	17 11 37.1	-38 07 06		LH,HS	B	17,18
GRS 1716–249[e]	17 19 36.93	-25 01 03.4		LH	B	19,20,21
XTE J1720–318	17 19 59.06	-31 44 59.7		LH:,HS	C	22,23,24
KS 1730–312	17 33 37.6	-31 13 12	30″	LH,HS	C	25,26
GRS 1737–31	17 40 09	-31 02.4	30″	LH	B	27,28,29
GRS 1739–278	17 42 40.03	-27 44 52.7		LH,HS,VH	A	30,31,32,33,34
1E 1740.7–2942	17 43 54.88	-29 44 42.5		LH,HS,J	A	35,36,37,38,39
H 1743–322	17 46 15.61	-32 14 00.6		HS,VH	A	40,41,42,80,81,82
A 1742–289	17 45 37.3	-29 01 05		HS:	C	43,44,45,46
SLX 1746–331	17 49 50.6	-33 11 55	35″	HS:	C	47,48,49
XTE J1748–288	17 48 05.06	-28 28 25.8		LH,HS,VH,J	A	50,51,52,53,54
XTE J1755–324	17 55 28.6	-32 28 39	1′	LH,HS	B	55,56,57,58
1755–338 (V4134 Sgr)	17 58 40.0	-33 48 27		HS	B	59,42,60,61,62
GRS 1758–258	18 01 12.67	-25 44 26.7		LH,HS,J	A	63,38,64,65,66
EXO 1846–031	18 49 16.9	-03 03 53	11″[f]	HS	C	67
XTE J1908+094	19 08 53.08	+09 23 04.9		LH,HS	B	68,69,70,71
1957+115 (V1408 Aql)	19 59 24.0	+11 42 30		HS	C	72,42,73,74,75
XTE J2012+381	20 12 37.70	+38 11 01.2		LH,HS	B	76,77,78,79

[a] For additional references and information, see TL95 and Liu et al. 2001.
[b] Positional uncertainty given if $r_x > 10''$.
[c] 'LH' – *low/hard* state, 'HS' – *high/soft* state, 'VH' – *very high* state, 'J' – radio jet.
[d] Qualitative grade indicating the likelihood that the candidate is in fact a BH.
[e] GRS 1716–249 = GRO J1719–24 = X–ray Nova Oph 1993.
[f] Alternative position also possible; see Parmar et al. 1993.

REFERENCES: [1]Kitamoto et al. 1990; [2]Brocksopp et al. 2001; [3]Revnivtsev et al. 2000a; [4]McClintock et al. 2003b; [5]Murdin et al. 1977; [6]Kaluzienski et al. 1975; [7]Barret et al. 1992; [8]Hjellming et al. 1999; [9]Tomsick & Kaaret 2000; [10]Dieters et al. 2000; [11]Augusteijn et al. 2001; [12]Groot et al. 2001; [13]Kalemci et al. 2002; [14]Homan et al. 2003a; [15]Miller et al. 2002b; [16]Sanchez–Fernandez et al. 2002; [17]in 't Zand et al. 2002a; [18]Wijnands & Miller 2002; [19]Mirabel et al. 1993; [20]van der Hooft et al. 1996; [21]Revnivtsev et al. 1998b; [22]Rupen et al. 2003; [23]Remillard et al. 2003a; [24]Markwardt & Swank 2003; [25]Borozdin et al. 1995; [26]Vargas et al. 1996; [27]Ueda et al. 1997; [28]Cui et al. 1997a; [29]Trudolyubov et al. 1999; [30]Marti et al. 1997; [31]Vargas et al. 1997; [32]Borozdin et al. 1998; [33]Wijnands et al. 2001; [34]Greiner et al. 1996; [35]Cui et al. 2001; [36]Churazov et al. 1993; [37]Smith et al. 1997; [38]Smith et al. 2002; [39]Marti et al. 2000; [40]Gursky et al. 1978; [41]Cooke et al. 1984; [42]White & Marshall 1984; [43]Davies et al. 1976; [44]Wilson et al. 1977; [45]Branduardi et al. 1976; [46]Kennea & Skinner 1996; [47]Skinner et al. 1990; [48]White & van Paradijs 1996; [49]Motch et al. 1998; [50]Hjellming et al. 1998b; [51]Revnivtsev et al. 2000c; [52]Kotani et al. 2000; [53]Miller et al. 2001; [54]Rupen et al.1998;; [55]Remillard et al. 1997; [56]Ogley et al. 1997; [57]Revnivtsev et al. 1998a; [58]Goldoni et al. 1999; [59]Bradt & McClintock 1983; [60]White et al. 1988; [61]Pan et al. 1995; [62]Seon et al. 1995; [63]Rodriguez et al. 1992; [64]Sunyaev et al. 1991a; [65]Smith et al. 2001; [66]Rothstein et al. 2002; [67]Parmar et al. 1993; [68]Rupen et al. 2002; [69]in't Zand et al. 2002b; [70]Woods et al. 2002; [71]Chaty et al. 2002; [72]Margon et al. 1978; [73]Wijnands et al. 2002; [74]Yaqoob et al. 1993; [75]Nowak & Wilms 1999; [76]Hjellimg et al. 1998a; [77]Campana et al. 2002; [78]Vasiliev et al. 2000; [79]Hynes et al. 1999; [80]Revnivtsev et al. 2003; [81]Steeghs et al. 2003; [82]Homan et al. 2003b; [83]Remillard & McClintock 1999.

have included in most cases the prefix to the coordinate source name that identifies the discovery mission (e.g., EXO = *EXOSAT*). For the four sources with variable star names, the prefix is omitted. In columns 2–4, we give the best available coordinates and their uncertainties (if they exceed $10''$). These coordinates are also an excellent resource for interrogating ADS and SIMBAD.

In column 5 we list the characteristics that indicate the BHC classification, e.g., an observation of one or more of the canonical states of a BHB. A source classified as "ultrasoft" in the older literature (e.g., White & Marshall 1984) is assumed here to have been observed in the HS state. Three BHCs with resolved radio jets are also noted in column 5. Variability characteristics (§4.4) and broad Fe Kα emission lines (§4.2.3) can also be important BH indicators, but these are not explicitly noted in Table 4.3. Selected references are cited in the last column. The coordinate data can be found in the first reference. The following few references support the BH characteristics given in column 5. For several sources, a few additional references provide limited information on optical/IR/radio counterparts, etc.

We have assigned a grade to each BHC that is based both on how thoroughly the candidate has been observed and on the characteristics it displayed. In fact, this grade is qualitative and subjective and meant only as a guide. Our sense of the grade is as follows: We would be surprised if even one of the nine A–grade BHCs contains a NS, but not surprised if one of the six C–grade BHCs contains a NS. In compiling Table 4.3, we have been selective. For example, we did not include SAX J1805.5–2031 (Lowes et al. 2002) and XTE J1856+053 (Barret et al. 1996a) primarily because we judged that the available information was too scanty. Thus the total number of BH or BHC cases considered here is 40. For narrative discussions about many of the systems in Tables 4.1 and 4.3, see TL95. For additional data and as a supplement to the list of references given in Table 4.3, see Liu et al. (2001).

4.1.4 X–ray novae

If we include the X–ray novae observed during the past decade, then about 300 bright binary X–ray sources are known (van Paradijs 1995; Liu et al. 2000; Liu et al. 2001). More than half of them are LMXBs, and roughly half of each type (i.e., LMXB and HMXB) are classified as transient sources. The HMXB transients are neutron–star/Be–star binaries, which are not relevant to this review. The well–studied LMXB transients, on the other hand, include all of the X–ray novae that are listed in Tables 4.1–4.3. The principal hallmarks of an X–ray nova include both the discovery of the source during a violent outburst and a very large ratio of maximum to minimum X–ray intensity. The behavior of A0620–00, described in §4.1.2 provides a classic example of an X–ray nova. Indeed, it is the extreme faintness of the quiescent accretion disk in these systems that allows one to view the companion star, leading to secure dynamical measurements of the BH mass (§4.1.2, §4.3.4; Ch. 5).

Recurrent eruptions have been observed for several of the X–ray novae listed in Table 4.1: e.g., A0620–00 in 1917 and 1975; H1743–322 in 1977 and 2003; GS 2023+338 in 1938, 1956 and 1987; 4U 1543–47 in 1971, 1983, 1992 and 2002; and 4U 1630–472 and GX 339–4 at $\sim 1-2$ year intervals. (Outbursts prior to 1970 are inferred from studies of optical plates ex post facto.) Most X–ray novae, however, have been observed to erupt only once. Nevertheless, all X–ray novae are thought to be recurrent, with cycle times for some possibly as long as several centuries or more. TS96 suggest an average cycle time of 10–50 years. The infrequent outbursts are due to a sudden surge in the mass accretion rate onto the BH. The generally accepted mechanism driving the outburst cycle is that described by the disk instability model, which was developed initially for dwarf novae (Smak 1971; Osaki 1974; Cannizzo 1993; Lasota et al. 2001) and extended to X–ray novae (e.g., Dubus et al. 2001).

4.1.5 Accretion onto black holes

The desire to understand observations of BHBs compels us to model the hydrodynamics and radiation processes of gas orbiting in the gravitational potential of a compact object (see Ch. 13 for a detailed review). The best–known such model is the thin accretion disk (Pringle & Rees 1972; Shakura & Sunyaev 1973; Novikov & Thorne 1973; Lynden–Bell & Pringle 1974). For nearly all of the systems included in Tables 4.1–4.3, the companion star fills its Roche equipotential lobe and a narrow stream of gas escapes the star through the inner Lagrangian (L_1) point. This gas has high specific angular momentum and cannot accrete directly onto the BH. It feeds into a thin disk of matter around the BH known as an accretion disk. Once entrained in the disk, the gas moves in Keplerian orbits with angular velocity $(GM/R^3)^{1/2}$. However, viscous dissipation slowly taps energy from the bulk orbital motion, and viscosity transports angular momentum outward. As a result, the gas gets hotter as it sinks deeper into the gravitational potential well of the BH. Near the BH the disk terminates because there are no stable particle orbits possible in the extreme gravitational field. The existence of an innermost stable circular orbit (ISCO) and other properties of BHs are discussed in many texts (e.g. Shapiro & Teukolsky 1983; Kato et al. 1998). A defining property of a BH is its event horizon, the immaterial surface that bounds the interior region of spacetime that cannot communicate with the external universe. The radius of the event horizon of a Schwarzschild BH ($a_* = 0$) is $R_{\rm S} \equiv 2R_{\rm g} \equiv 2(GM/c^2) = 30$ km$(M/10M_\odot)$, the ISCO lies at $R_{\rm ISCO} = 6R_{\rm g}$, and the corresponding maximum orbital frequency is $\nu_{\rm ISCO} = 220$ Hz$(M/10M_\odot)^{-1}$ (see §4.1.2 for the definition of a_*). For an extreme Kerr BH ($a_* = 1$), the radii of both the event horizon and the minimum stable (prograde) orbit are identical, $R_{\rm K} = R_{\rm ISCO} = R_{\rm g}$, and the maximum orbital frequency is $\nu_{\rm ISCO} = 1615$ Hz$(M/10M_\odot)^{-1}$. For the Kerr BH, it is well known that the rotational energy can be tapped electromagnetically (Blandford & Znajek 1977). The gas flows driven by this process are both anisotropic and self–collimating (Blandford 2002, and references therein), and they may be the source of the relativistic jets seen from several BHBs and BHCs (Tables 4.2–4.3).

Even for XTE J1118+480, the smallest system in Table 4.1, the outer radius of the accretion disk is expected to be roughly one solar radius, $\sim 10^5 R_{\rm g}$, vastly larger than the BH event horizon. Thus a gas element of mass m that is destined to enter the BH starts far out with negligible binding energy. However, when it reaches the ISCO it will have radiated $0.057mc^2$ for a Schwarzschild BH or $0.42mc^2$ for an extreme Kerr BH. Moreover, 90% of this colossal binding energy is radiated within about $20R_{\rm g}$ of the center. At all disk radii, the binding energy liberated by viscous dissipation is radiated locally and promptly and results in a gas temperature that increases radially inward reaching a maximum of $T \sim 10^7$ K near the BH. This picture is the basis of the standard thin accretion disk model (Shakura & Sunyaev 1973). A nonrelativistic approximation to this thin disk spectrum has been formulated conveniently as a multi–temperature blackbody (Mitsuda et al. 1984; Makishima et al. 1986). The total disk luminosity in a steady state is $L_{\rm disk} = GM\dot{M}/2R_{\rm in}$, where $\dot{M}$ is the mass accretion rate and $R_{\rm in}$ is the radius of the inner edge of the disk. This model, often referred to as the Multicolor Disk (MCD) model, is used to describe the thermal component that is dominant in the HS state and is also present in the VH state (§4.2.2; §4.3.5; §4.3.7). The MCD model has been available within XSPEC ("diskbb"; Arnaud & Dorman 2002) for many years and has been widely used. Despite the successes of the MCD model, it is important to note a significant limitation, namely, the neglect of a torque–free boundary condition at the ISCO (Gierlinski et al. 1999). In the MCD model, the temperature profile is simply $T(R) \propto R^{-3/4}$, which rises to a maximum at the ISCO, whereas a proper inner boundary condition produces null dissipation at the ISCO with the temperature peaking at $R > R_{\rm ISCO}$ (Pringle 1981; Gierlinski et al. 1999). The current MCD model requires attention and improvement.

Efforts have also been made to include relativistic corrections to the MCD model (e.g., Ebisawa et al. 1991; Zhang et al. 1997a; Gierlinski et al. 2001). However, quantitative analyses (e.g., a spectroscopic measurement of the inner disk radius when the source distance and inclination angle is known) will require more sophisticated models. Accretion disk models are being developed to incorporate MHD effects in the context of GR (e.g., McKinney & Gammie 2002), with additional considerations for radiation pressure and radiative transfer (Turner et al. 2002; Shimura & Takahara 1995). Early results show that magnetic fields may couple matter in the "plunging region" to matter at radii greater than the ISCO, and thereby extract energy from very near the horizon (Agol & Krolik 2000). In the case of a rapidly–rotating Kerr hole, the spin/electromagnetic effects mentioned above may not only drive relativistic jets, but also may modify grossly the spectrum of the inner accretion disk (Wilms et al. 2001b; Miller et al. 2002b).

At lower mass accretion rates corresponding to several percent of the Eddington luminosity, a BHB usually enters the LH (i.e., *low/hard*) state and at very low accretion rates it reaches the *quiescent* state, which may be just an extreme example of the LH state. In both of these states, the spectrum of a BHB is dominated by a hard, nonthermal power–law component (photon index ∼1.7; §4.3.4 & §4.3.6), which cannot be accounted for by a thermal accretion disk model; it is most plausibly explained as due to Comptonization of soft photons by a hot optically–thin plasma. Early models for the spectrum of the *quiescent* state postulated that the disk does not extend all the way down to the ISCO (Narayan 1996; Narayan et al. 1996). The disk is truncated at some larger radius and the interior volume is filled with a hot ($T_e \sim 100$ keV) advection–dominated accretion flow or ADAF (Narayan & Yi 1994, 1995; Narayan et al. 1996; Quataert & Narayan 1999). In an ADAF, most of the energy released via viscous dissipation remains in the accreting gas rather than being radiated away (as in a thin disk). The bulk of the energy is advected with the flow. Only a small fraction of the energy is radiated by the optically thin gas before the gas reaches the center. Consequently, the radiative efficiency of an ADAF (which depends on the uncertain fraction of the viscous energy that is channeled to the electrons) is expected to be only ∼0.1–1%, whereas the radiative efficiency discussed

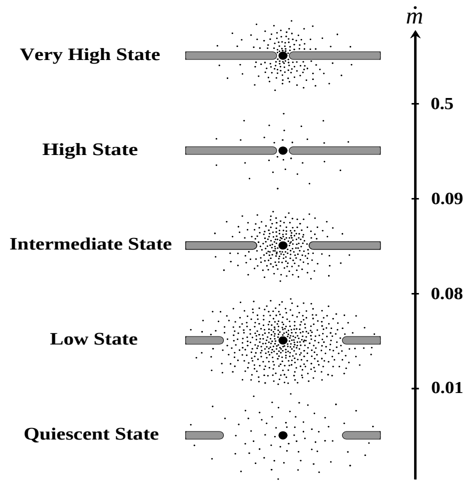

Fig. 4.1. Schematic sketch of the accretion flow in different spectral states as a function of the total Eddington–scaled mass accretion rate $\dot{m}$. The ADAF is represented by dots and the thin disk by the horizontal bars. The *very high* state is illustrated, but it is not included in the unification scheme (Esin et al. 1997).

above for disk accretion is definitely $\geq$ 5.7%. There is wide agreement that these radiatively inefficient flows have been observed in quiescent BHBs (§4.3.4) and from galactic nuclei (Baganoff et al. 2001; Loewenstein et al. 2001). However, the theoretical picture has become complex with variant models involving winds (ADIOS; Blandford & Begelman 1999) and convection (CDAFs; Igumenshchev & Abramowicz 1999; Stone et al. 1999; Narayan et al. 2000; Quataert & Gruzinov 2000)

One attempt has been made to unify four of the five states of a BHB using both the MCD and ADAF models (Esin et al. 1997). This approach is illustrated in Figure 4.1, which shows how the geometry of the accretion flow changes as the mass accretion rate $\dot{m}$ varies ($\dot{m}$ is the mass accretion rate expressed in Eddington units). The scenario indicates how a BH system progresses through five distinct states of increasing $\dot{m}$ from the *quiescent* state to the VH state. In the three states at lower $\dot{m}$, the flow consists of two zones (disk and ADAF), as described above. For the two states of highest $\dot{m}$, the disk extends down to the ISCO. In all five states, the disk is bathed in a corona that is a seamless continuation of the ADAF. Apart from the VH state, the model treats consistently the dynamics of the accreting gas, the thermal balance of the ions and electrons in the ADAF and corona, and the radiation processes. The model has had significant successes in describing the spectral evolution of several BHBs (Esin et al. 1997; Esin et al. 1998; for further discussion of the ADAF model, see §4.3.4.)

However, the multistate model of Esin et al. (1997) has important limitations. For example, it does not unify the most luminous state, the *very high* state, which is characterized by an unbroken power–law spectrum extending out to a few hundred keV or more (§4.3.7). Also, this simple ordering of the states by $\dot{m}$ or luminosity is naive (§4.3). Moreover, the model does not account for the dynamic behavior of the corona, including strong flares and powerful low–frequency quasi–periodic oscillations (§4.4), nor does it account for the radio emission observed from most BHBs (Table 4.2). Finally, the "evaporation" process by which the cold gas in a thin disk feeds into a hot ADAF is at best qualitatively understood, and there is no quantitative model relating the disk truncation radius to the accretion rate $\dot{m}$ (Narayan 2002, and references therein).

There are alternative models of the X–ray states, and many of them invoke a dynamic accretion disk corona that is fed by MHD instabilities in the disk. For example, in the model of Merloni & Fabian (2001a, 2001b) the hot corona that generates the power–law component is intimately connected with the thin accretion disk. Magnetic energy generated (presumably) by the sheared Keplerian disk creates magnetic flares that rise out of the disk because of the Parker instability. Within the framework of this model, Di Matteo et al. (1999) present a magnetic flare model for the two common states of GX339–4. In the HS state, the flares occur near the disk and heat it. The disk reradiates the observed soft thermal component, whereas the faint hard component is produced by Comptonization of the soft flux. In the LH state, the flares occur far above the disk and the density of soft seed photons is greatly reduced. Thus, the system is photon–starved, and the resultant Comptonized spectrum is hard. Merloni and Fabian (2002) also consider coronae as sources of powerful jets/outflows. They find that such outflows can render a source radiatively inefficient even if advection of energy into the BH is unimportant.

It is generally agreed that the temperatures in the corona are in the range 100–300 keV, with optical depths of 0.1–1 (e.g., Merloni & Fabian 2001b). There is little agreement, however, on the geometry and physical properties of the corona. Thus, a wide range of coronal models have been proposed (e.g., Haardt & Maraschi 1991; Dove et al. 1997a, 1997b; Meyer et al. 2000; Rozanska & Czerny 2000; Kawaguchi et al. 2000; Nowak et al. 2002; Liu et al. 2002). Liu et al. conclude that the primary difficulty in modeling the corona is the magnetic field that produces time variations and spatial inhomogeneities; in addition, one must consider complicated radiation/energy interactions between the disk and the corona. Because of the complexity of the problem, some students of the corona choose to apply their models to large quantities of X–ray (and radio) data, an approach that has proved fruitful (Zdziarski et al. 2002, 2003; Wardzinski et al. 2002).

Timing studies have been used to isolate the fast X–ray variability in BHBs as primarily emanating from the corona rather than from the accretion disk (Churazov et al. 2001). Timing studies have also created requirements to explain X–ray QPOs, such as the strong low–frequency QPOs that are prevalent in the VH state. Many coronal models do not deal with fast variability or QPOs explicitly, although there are exceptions, such as the "Accretion–Ejection Instability" model (Tagger & Pellat 1999). In this model, magnetic spiral waves heat and accelerate material at those locations where the spiral waves and the disk are in corotation. During BHB outbursts, it has become exceedingly clear that spectral and timing characteristics at both X–ray and radio frequencies may change dramatically and abruptly. Therefore, no single model can account for all of the complex behavior, and our goal in this review is to summarize what is known about each X–ray state and to then discuss physical models in the context of a given state.

In addition to the models discussed above, we mention briefly the jet model (e.g., Falcke & Biermann 1995). This model is motivated by the observations of resolved radio and X–ray jets (Tables 4.2–4.3), by observations of radio/X–ray correlations (e.g., Hannikainen et al. 2001; Corbel et al. 2000), and by successes in modeling the broadband spectra of some systems as synchrotron radiation.

4.1.6 Some consequences of an event horizon

The properties of BHs and BH accretion flows are discussed in many texts (e.g., Shapiro & Teukolsky 1983; Kato et al. 1998; Abramowicz 1998). As mentioned above, a defining feature of a BH is its event horizon. Since BHs lack a material surface, some effects observed for NSs (e.g., type I bursts) are absent for a BH. Similarly, a BH cannot sustain a magnetic field anchored within it, and hence they cannot generate periodic X–ray pulsations, which are observed for many NSs.

Both type I bursts and periodic pulsations are considered firm signatures of a NS (TL95). It is interesting to ask what fraction of cataloged, bright sources show either pulsations or type I bursts. We examined this question using the catalog of van Paradijs (1995), selecting only the brighter sources ($F_x > 30$ μJy) that have been optically identified. We excluded the confirmed and candidate BH systems listed in Tables 4.1–4.3. For the 21 HMXB systems that met our selection criteria, we found that 18 out of 21 (86%) pulse. For 21 LMXB systems, we found that 12 burst and 2 pulse (67% burst or pulse). Thus a very high fraction of these sources manifest behavior that identifies them as NSs. It is also interesting to consider which systems have failed to produce detectable bursts or pulsations because they are either an unusual NS source or they contain a BH. The three non–pulsing HMXB sources are 1700–37, 1947+30 and Cyg X–3; the six corresponding LMXB sources are LMC X–2, 1543–62, Sco X–1, GX349+2, GX9+9 and 1822–00.

4.1.7 The Rossi X–ray Timing Explorer (RXTE): 1996.0 – present

RXTE has been in continuous operation since its launch on 1995 December 30. Its prime objective is to investigate the fundamental properties of BHs, NSs and white dwarfs by making high time resolution observations of extremely hot material located near BH event horizons or stellar surfaces. It is the largest X–ray detector array ever flown, and it provides energy coverage from 2–200 keV. It features high throughput (up to ∼150,000 counts s^{-1}) and ~ 1 μs time resolution. *RXTE's* year–round, wide–sky coverage and its fast response time has made it an important vehicle for the study of transient phenomena and for the support of multiwavelength science.

The observatory is comprised of two large area instruments (PCA and HEXTE) that act in concert, viewing the sky through a common 1^o field of view. The third instrument is an All–Sky Monitor (ASM) that surveys about 80% of the sky each orbit. For descriptions of the instruments, see Levine et al. (1996), Swank (1998), Rothschild et al. (1998), and Bradt et al. (2001). The Proportional Counter Array (PCA), which has a total net area of 6250 cm^2, is the chief instrument. The PCA consists of five sealed proportional–counter detectors. It is effective over the range 2–60 keV with 18% energy resolution at 6 keV. The High Energy Timing Experiment (HEXTE) covers the energy range 20–200 keV. It is comprised of eight NaI/CsI phoswich detectors with a combined net area of 1600 cm^2. The HEXTE has provided important spectral information beyond the reach of the PCA, but the modest count rates of the HEXTE (e.g., 289 counts s^{-1} for the Crab) limit its use for timing studies. Indeed, it is the PCA (12,800 counts s^{-1} for the Crab with 5 PCUs) that has achieved groundbreaking results in high–energy astrophysics.

The ASM is comprised of three wide–field proportional counters that are mounted on a rotating boom. On a daily basis, it surveys about 90% of the sky and obtains about 5–10 observations per source. It locates bright sources to a typical accuracy of $\sim 5'$. In uncrowded regions it can monitor known sources down to about 35 mCrab ($2\ \sigma$) in one 90–s exposure or about 10 mCrab in one day. On many occasions, the ASM has proved indispensable in alerting PCA/HEXTE observers to targets of opportunity, such as the appearance of a new transient or a state–change in a cataloged source. Furthermore, the ASM public archive containing the continuous light curves of ~400 X–ray sources (both Galactic and extragalactic) has been invaluable in studying the multiyear behavior of X–ray sources and in supplementing X–ray and multiwavelength (e.g., *Chandra* and *HST*) studies of individual sources. The data are also important to observers of AGN and gamma–ray bursts.

4.2 X–ray light curves, spectra and luminosity data

4.2.1 ASM light curves of BH binaries and BH candidates

To illustrate the diversity of behavior among BHBs and BHCs, we show in Figure 4.2–4.5 the 1.5–12 keV ASM light curves and the (5–12 keV)/(3–5 keV) hardness ratio (HR2) for 20 of the systems listed in Tables 4.1–4.3 that were active during the past seven years. These light curves should be compared to the heterogeneous collection of ~20 X–ray light curves collected by Chen et al. (1997). In making such comparisons, note that we use a linear intensity scale, whereas Chen et al. and most authors use a log scale. The light curves in Figures 4.2–4.5 are ordered by RA, although we discuss them roughly in order of increasing complexity. An intensity of 1 Crab corresponds to 75.5 ASM c s^{-1}. A hardness ratio (HR2) of 0.5 (1.5) generally corresponds to the HS state (LH state). All good data are included, although the time interval for binning the counts has been tailored to the source intensity. The hardness ratio is not plotted in the absence of a detectable 5-12 keV flux. References are cited sparingly in the narrative descriptions of the light curves given below; see Tables 4.1–4.3 for further references. In the following, the term "classic" light curve refers to an outburst profile that exhibits a fast rise and an exponential decay, like those observed for several pre–*RXTE* BH X–ray novae, including A0620–00, GS/GRS 1124–68, GS 2000+25 and GRO J0422+32 (TL95; Chen et al. 1997). Such classic light curves often show a secondary maximum (roughly a doubling of intensity) that occurs during the decline phase about 40–100 days after the onset of the outburst (TL95; Chen et al. 1997).

4.2.1.1 Black hole binaries

Figure 4.2 shows the light curves of all six of the X–ray novae with short outburst cycles that were detected by the ASM (Tables 4.1–4.2). *4U 1543–47:* An exceptionally clean example of a classic light curve with an e–folding decay time of ≈ 14 days. It lacks a secondary maximum, presumably because the outburst is so brief. For details and references on three prior outbursts of this source, see Chen et

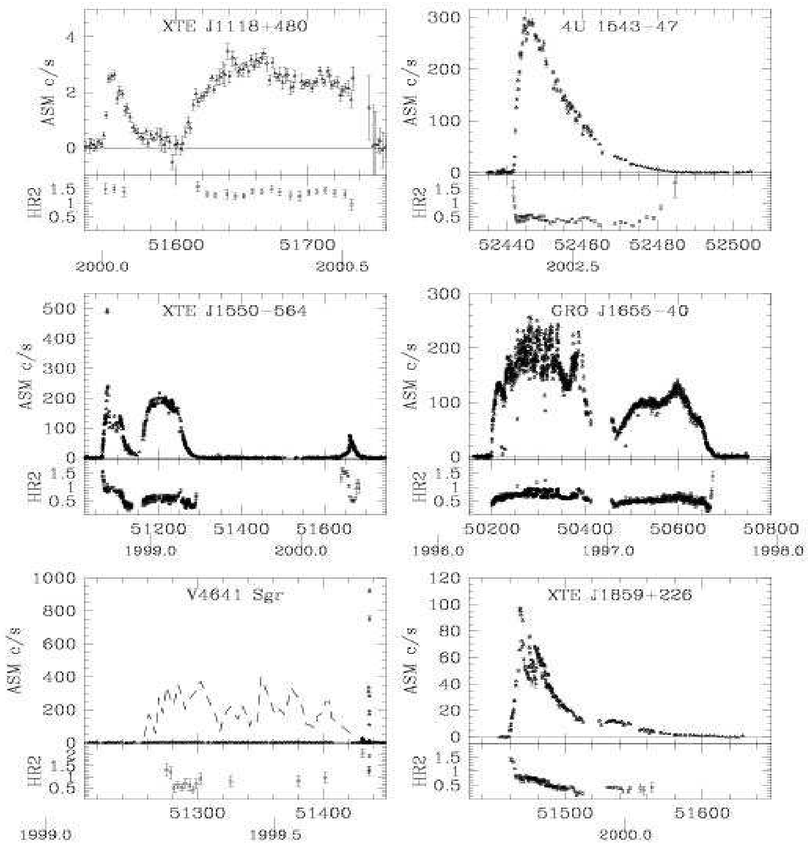

Fig. 4.2. Transient ASM light curves of six black hole binaries. For V4641 Sgr, the dashed line shows intensity x50 in order to highlight the low-level activity that preceded the violent and short–lived flare.

al. (1997). *XTE J1859+226:* A second example of a classic light curve that does show a secondary maximum (at about 75 days after discovery). Note the intense variability near the primary maximum. *XTE J1118+480:* One of five X–ray novae that remained in a hard state throughout the outburst and failed to reach the HS state. Note the prominent precursor peak.

Also shown in Figure 4.2 are the complex and similar light curves of two X–ray novae with long orbital periods, GRO J1655–40 and XTE J1550–564. *GRO J1655–40:* This source has undergone two outbursts since its discovery in 1994 July. Shown here is the full light curve of the second, 16–month outburst. The double–peaked profile is quite unlike the classic profile of 4U 1543–47. During the first maximum in 1996, the source exhibited strong flaring and intense nonthermal emission (VH state). In 1997 the source spectrum was soft and thermal except for a hard episode at the very end of the outburst (Sobczak et al. 1999). Note the several absorption dips in the light curve of this high inclination system (Kuulkers et al. 1998). *XTE J1550–564:* The complex profile includes two dominant peaks during 1998–99, followed several

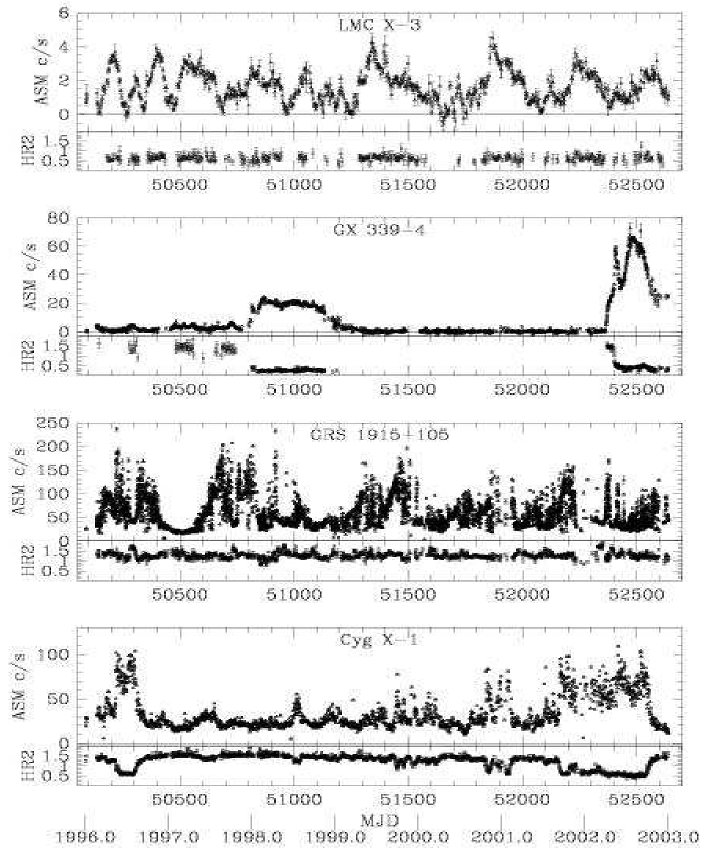

Fig. 4.3. Seven–year ASM light curves of four black hole binaries.

hundred days later by a smaller peak in 2000. Not shown here are three very small outbursts (LH states) that have occurred subsequently. Some unusual characteristics include the slow 10–day rise following the source's discovery on 1998 September 6, followed by the dominant X–ray flare (6.8 Crab; September 19-20), and the abrupt ∼10–day decay timescale following each outburst. The source was predominately in the VH or *intermediate* states during the first peak (1998), softening to the HS state during the second peak (1999). The spectral evolution through all of the X–ray states occurred much more rapidly during the small peak in 2000. *SAX J1819.3–2525 = V4641 Sgr:* As this extraordinary light curve shows, the source became active at a low level in the spring of 1999 (dashed line shows intensity x50). Five months later it underwent a brief, violent flare during which the 1.5–12 keV intensity increased very rapidly (within 7 hours) from 1.6 to 12.2 Crab. Within two hours thereafter, the intensity declined to less than 0.05 Crab (Wijnands & van der Klis 2000, and references therein).

Figure 4.3 shows the light curves of the two persistent BHBs (LMC X–3 and Cyg X–1) and two other BHBs that have been active throughout the *RXTE* era.

LMC X–3: The light curve shows the large–amplitude cyclic modulation in the flux reported by Cowley et al. (1991); however, their ∼198–day cycle time is shorter than is indicated by these data. As the hardness ratio plot shows, the source remains in the HS state most of the time. However, at the local intensity minima, where there are gaps in the HR2 plot due to statistical limitations, the PCA observations show transitions to the LH state (Wilms et al. 2001a). *GX 339–4:* As shown, the source underwent major eruptions into a soft spectral state (HR $\approx$ 0.5) in 1998 and 2002. In the time between these two outbursts, the source was very faint ($<$ 2 mCrab) compared to its customary hard–state intensity of ∼30 mCrab, which it enjoyed prior to its 1998 outburst. Remarkably, this transient BHB has never been observed in a fully *quiescent* state (Hynes et al. 2003). *GRS 1915+105:* This source exhibits extraordinary variations in both the X–ray and radio bands. Astonishing and yet repetitive patterns are sometimes seen in the X–ray light curves (Muno et al. 1999; Belloni et al. 2000; Klein–Wolt et al. 2002). For a 1992 X–ray light curve showing the birth of this source, see Chen et al. (1997). *Cyg X–1:* Transitions between the LH and HS states were first observed in this archetypal BH source (§4.3.1). However, as this record shows, there are both gradual and rapid variations in the hardness ratio that suggest both rapid state transitions and intermediate conditions between the HS and hard states (see §4.3.9).

4.2.1.2 Black hole candidates

Figure 4.4 displays the light curves of six BHCs with short outburst cycles. *XTE J748–288:* This short duration outburst that begins and ends in a hard spectral state is similar to the classic light curve of 4U 1543–47 (Fig. 4.2). The 1/e decay time is $\approx$ 16 days. This source is heavily absorbed, and the values of the hardness ratio are consequently increased. *GRS 1739–278:* A somewhat longer duration outburst with a nearly classic profile that includes a precursor peak, ∼40% variability near maximum, and undulations in intensity during the decay. Again, the outburst begins and ends with a hard spectrum. *XTE J1755–324:* This brief outburst, which follows an abrupt rise, provides yet another example of a classic light curve. This outburst is locked in the HS state. *XTE J2012+381:* This unusual light curve combines a classic rise to maximum followed directly by a precipitous drop in intensity. Also unusual are a large secondary maximum occurring just 30 days after discovery plus an additional late maximum at ∼140 days. *XTE J1650–500:* A complex light curve. At the onset of the outburst there is a very rapid rise followed by a slow rise. This unusual behavior is accompanied by a remarkable, slow (∼15–day) transition from a hard spectral state to a soft one. *4U 1354–64:* A slow rise followed by a rather rapid decline. During this outburst, the source remained in the LH state (Brocksopp et al. 2001), whereas the HS state was reached during a brighter outburst in 1987 (Kitamoto et al. 1990). This source may be identical to Cen X–2, which reached a peak intensity of 13 Crab in 1967 (Brocksopp et al. 2001).

In Figure 4.5 we show the light curves of the BHB LMC X–1 and the light curves of three BHCs. *LMC X–1:* The source is continually in a soft spectral state and maintains a relatively steady intensity. *4U 1630–47:* The ∼600–day recurrence time has been known for 25 years (Jones et al. 1976). Here we see five, nearly equally–spaced outbursts. Note the very different profiles and fluences of the outbursts. Note

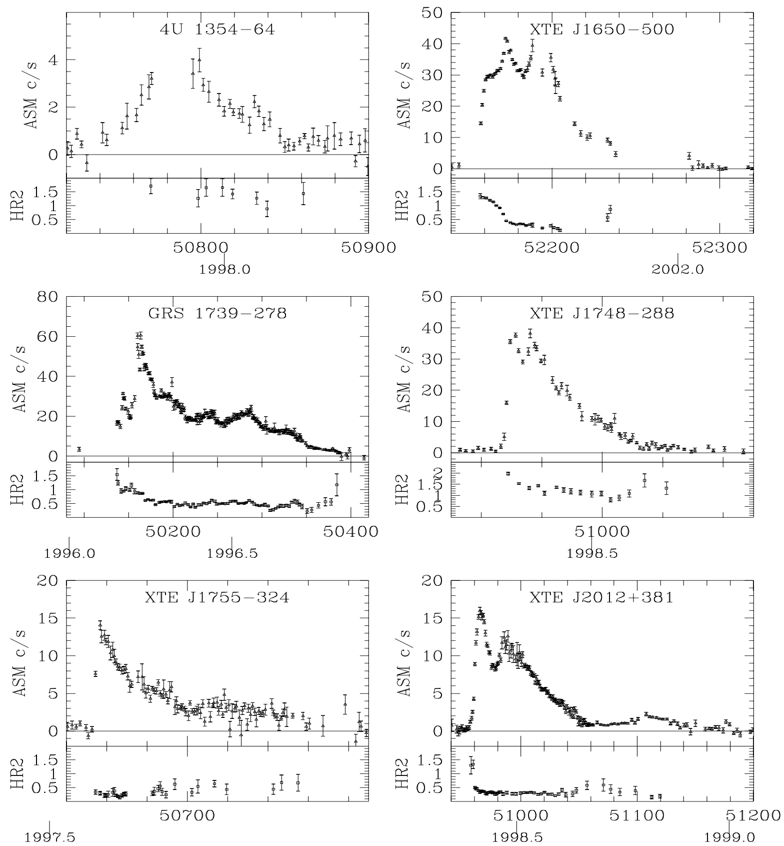

Fig. 4.4. Transient ASM light curves of six black hole candidates.

also that the 1996 outburst starts with a soft spectrum. *GRS1758–258:* This hard Galactic center source was discovered by GRANAT/SIGMA in 1991. Its spectrum extends to at least 300 keV (Sunyaev et al. 1991a). During 2001 it underwent a transition to an unusual soft state of very low intensity (Smith et al. 2001; Miller et al. 2002d); the low flux level during that event is evident in the ASM record shown here. *4U 1957+11:* The source has long been considered a BHC based on its "ultrasoft" spectrum (White & Marshall 1984), although Yaqoob et al. (1993) have argued that the primary is a NS. The source displays a consistent flaring behavior and a soft spectrum over the 7–year interval.

It is often said that during its initial rise the spectrum of a BH X–ray nova transitions from a hard spectral state to a soft one. For several sources, the data in Figures 4.2–4.5 support this view: 4U 1543–47, XTE J1550–564, XTE J1859+226, XTE J1650–500, GRS 1739–278, and XTE J2012+381. However, there are two clear counter–examples, sources whose spectra *hardened* during the initial rise: GRO J1655–40 (Fig. 4.2) and 4U 1630–47 (Fig. 4.5; first of 5 outbursts).

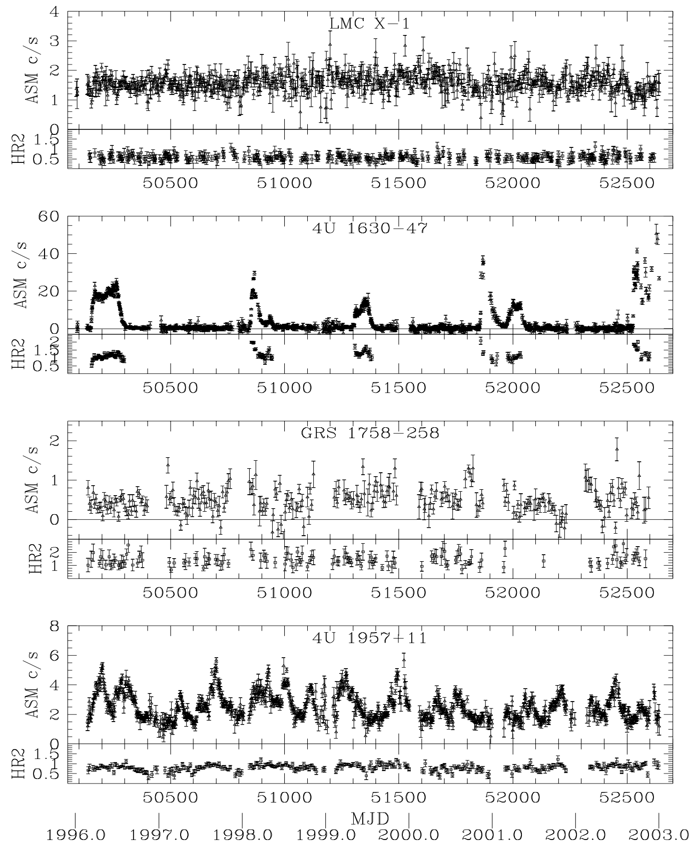

Fig. 4.5. Seven–year ASM light curves of three black hole candidates and the black hole binary LMC X–1.

4.2.2 Synoptic studies of selected black hole binaries

It is important to follow the several–month spectral evolution of individual sources and to construct unified spectral models that can be used to represent the energy spectra of all BHBs. The necessary elements of such models can be deduced from a simple appraisal of the observational data: e.g., Cyg X–1 and other BHBs in the LH state show that the model must contain a nonthermal component, which can be well represented by a power–law function (TL95). On the other hand, the soft spectra observed for most BH X–ray novae in the HS state is most widely modeled as a multi–temperature blackbody, which approximates the emission from an optically–thick (relativistic) accretion disk. Many studies of spectral evolution therefore choose a composite model comprised of disk blackbody and power–law components. Although this simple model has significant limitations, nevertheless it has proven to be widely applicable and quite effective in monitoring the spectra of BHBs, as we now discuss briefly by pointing to two examples.

Important studies of *Ginga* spectra using this model were made by Ebisawa et al.

(1991, 1993, 1994). The authors added one refinement to the model, namely, a broad absorption feature above 7 keV. This feature is associated with the reflection of X–rays by an optically thick accretion disk (Ebisawa et al. 1994). With this model a successful and quantitative comparison was made of the spectra of Cyg X–1, LMC X–3, GS 2000+25, LMC X–1, GX339–4 and GS/GRS 1124–68 (Nova Mus 1991). This latter source, which exhibited a classic light curve, was observed 51 times in 1991 over a span of 235 days using the *Ginga* Large Area Counter (LAC). We direct the reader's attention to Figure 15 in Ebisawa et al. (1994) which shows the evolution over a full outburst cycle of the spectral parameters and fluxes for GS/GRS 1124–68. In their figure, it is evident that an important transition occurs 130 days into the outburst. For example, the photon spectral index suddenly decreases from 2.2–2.6 to a value near 1.6, the hard flux increases substantially and the soft disk flux decreases. This characteristic behavior, which has been observed for a number of BH X–ray novae, marks the transition from the HS (*high/soft*) state to the LH (*low/hard*) state.

We now compare the results obtained for GS/GRS 1124–68 to the results of an analogous study of the irregular BH X–ray nova XTE J1550–564, which was observed extensively by *RXTE* during its 1997–1998 outburst (Sobczak et al. 2000b). A total of 209 pointed observations spanning the entire 255–day outburst were made using the PCA and HEXTE detectors. The 1998–1999 light curve of the source is complex and includes a slow (10 day) rise to maximum, an intense (6.8 Crab) flare that occurred early in the outburst, and a "double–peaked" profile that roughly separates the outburst into two halves of comparable intensity (Fig. 4.2). Sobczak et al. adopted very nearly the same spectral model and methodology as Ebisawa et al. (1994). We direct the reader's attention to Figure 4 and the accompanying text in Sobczak et al. (2000b), which describes a complex course of evolution relative to that of GS/GRS 1124–68. Very briefly, Sobczak et al. show that during the first half of the outburst QPOs are ubiquitous and the spectrum is dominated by the power–law component, which are conditions that mark the *very high/intermediate* state. In contrast, during the second half of the outburst QPOs are scarce and the spectrum is dominated by emission from the accretion disk, which corresponds to the *high/soft* state. During this state, the inner disk radius (§4.1.5) remained nearly constant for 4 months (Sobczak et al. 2000b). Very similar behavior has been observed for GS/GRS 1124–68 (Ebisawa et al. 1994) and for several other sources (TL95). The constancy of the disk inner radius is remarkable, given the accompanying, large variations in luminosity that are usually observed (TL95).

In overview, in both GS/GRS 1124–68 and XTE J1550–564, one sees time intervals where thermal emission from the disk dominates the spectrum, while at other times the disk spectrum is substantially modified and a *power–law component may dominate at either high or low luminosity.* In other sources, such as Cyg X–1, the nonthermal LH state may be stable for many months or years, but its soft–state spectrum does not resemble the thermal spectra seen from GS/GRS 1124–68 and XTE J1550–564. These results highlight the need to specify the physical properties of X–ray states while avoiding the confusing terminology that has developed during the past 30 years. Accordingly, in §4.3 we address this issue and seek clearer definitions of the X–ray states.

4.2.3 Relativistic iron emission lines

Strong evidence for accretion disks in active galactic nuclei has come from X–ray observations of broad iron Kα lines. In particular, in some Seyfert galaxies the very asymmetric profile of the Fe Kα line (e.g., its extended red wing) suggests strongly that the emission arises in the innermost region of a relativistic accretion disk (for reviews see Fabian et al. 2000, Reynolds & Nowak 2003). The good energy resolution of *ASCA* provided the first clear evidence for such a line profile (Tanaka et al. 1995). In some cases, the line profile indicates the presence of an accretion disk extending down to the ISCO (Weaver et al. 2001). The broad Fe Kα fluorescence line is thought to be generated through the irradiation of the cold (weakly–ionized) disk by a source of hard X–rays (likely an optically–thin, Comptonizing corona). Relativistic beaming and gravitational redshifts in the inner disk region can serve to create an asymmetric line profile.

In fact, the first broad Fe Kα line observed for either a BHB or an AGN was reported in the spectrum of Cyg X–1 based on *EXOSAT* data (Barr et al. 1985). It was this result that inspired Fabian et al. (1989) to investigate the production of such a line in the near vicinity of a Schwarzschild BH, a result that was later generalized by Laor (1991) to include the Kerr metric. Other early studies of relativistically smeared Fe Kα lines from BHBs were conducted by Done et al. (1992) and others. Their work was one part of a broader examination of the accretion geometry that is produced as hard X–rays from an overlying corona illuminate an optically–thick accretion disk. An Fe Kα line and a reflected continuum are always generated in this case (George & Fabian 1991; Matt et al. 1991). One example is a *Ginga* study of the reflected spectrum of V404 Cyg (Zycki et al. 1999a, 1999b). A limitation of this study is the use of proportional counter detectors (e.g., the *Ginga* LAC and *RXTE* PCA, which have an energy resolution of only FWHM $\approx$ 1.2 keV at Fe Kα). Such iron Kα studies suffer both because the energy resolution is marginal and because the response matrices of the detectors are uncertain at the 1–2 % level, while the Fe line profile in BHBs is typically only 1–5 % above the X–ray continuum. Consequently, the results from these instruments must be considered with caution. Some iron Kα sources that have been studied with *RXTE* include: GRO J1655–40 (Balucinska–Church & Church 2000); XTE J1748–288 (Miller et al. 2001); and GX 339–4 (Feng et al. 2001; Nowak et al. 2002).

More telling studies of the Fe Kα line have been achieved using the MECS and HP–GSPC detectors aboard *BeppoSAX*, which have a resolution of $\approx$ 0.6 keV at Fe Kα. Broad line profiles ($\sim$4–9 keV) have been observed for SAX J1711.6–3808 (in't Zand et al. 2002a) and XTE J1908+094 (in't Zand et al. 2002b); however, these profiles are rather symmetric and may be more a product of Compton scattering than relativistic broadening. *BeppoSAX* studies have also revealed other systems with broad, asymmetric Fe K profiles that resemble the predictions of relativistic smearing: GRS 1915+105 (Martocchia et al. 2002) and V4641 Sgr (Miller et al. 2002a). Interestingly, for both of these systems the inner disk radius deduced from the line profile is consistent with the radius of the ISCO for a Schwarzschild BH, suggesting that rapid spin is not required.

Spectral studies at higher resolution have been made recently with *XMM–Newton* and *Chandra*. Using the *XMM* EPIC–MOS1 detector, Miller et al. (2002b) find for

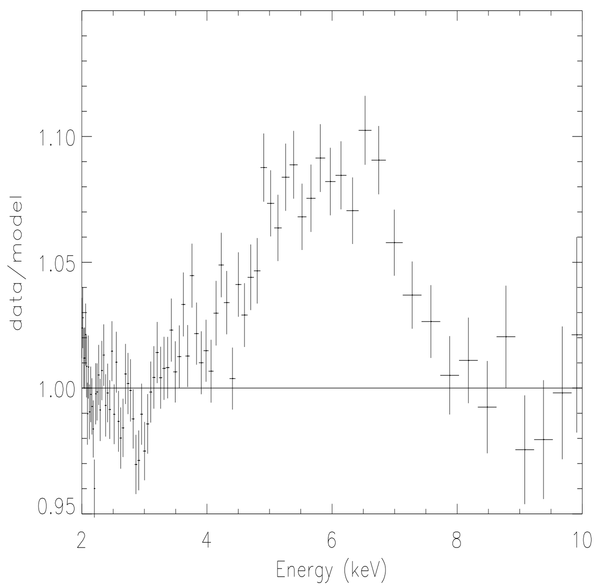

Fig. 4.6. Data/model ratio for XTE J1650–500. The model consists of multicolor disk blackbody and power–law components (Miller et al. 2002b). Note the non–Gaussian shape and low–energy extent of the line profile.

XTE J1650–500 a broad, skewed Fe Kα emission line (Fig. 4.6) which suggests the presence of an extreme Kerr BH and indicates a steep radial falloff of disk emissivity with radius. An observation of Cyg X–1 with the HETGS grating and ACIS–S detector aboard *Chandra* revealed a broad line centered at $\approx$ 5.82 keV with a FWHM of $\approx$ 1.9 keV (Miller et al. 2002c). Also present was a smeared Fe edge at $\approx$ 7.3 keV. The authors conclude that the line is predominately shaped by Doppler/gravitational effects and to a lesser degree by Compton scattering due to reflection.

4.2.4 Super–Eddington luminosities

Recently there has been considerable interest in ultraluminous X–ray sources (ULXs) in external galaxies with 0.5–10 keV luminosities in the range $10^{39} - 10^{40.5}$ erg s^{-1} (Makishima et al. 2000; Fabbiano et al. 2001; Humphrey et al. 2003; Miller et al. 2003b; Ch. 12). The luminosities of ULXs greatly exceed the Eddington limit of a 1.4 $M_\odot$ NS: $L_{\rm Edd} = 1.25 \times 10^{38} (M_1/M_\odot)$ erg s^{-1} . The most luminous systems also exceed by a factor of $\sim$20 the Eddington luminosity of a typical $10 M_\odot$ BH. This fact has led to the suggestion that the most luminous ULXs are a new class of accreting BHs with masses $\sim$100 $M_\odot$ (Makishima et al. 2000; Fabbiano et al. 2001). Alternatively, it has been suggested that the ULXs are powered by conventional stellar–mass BHs that radiate anisotropically (King et al. 2001; Ch. 13). We examine this question by comparing as directly as possible the luminosities of the ULXs to the luminosities of the 18 BHBs listed in Tables 4.1–4.2. We also mention briefly apparent differences between ULXs and BHBs in their spectra and duty cycles.

In terms of the maximum flux density of a BHB, $F_{\rm x,max}$ (Table 4.1), the 2–11 keV luminosity is: $L_x/L_{Edd} \approx\ 2.6 \times 10^{35} \times F_{x,max}(\mu Jy) \times (D/10\ kpc)^2$ (Bradt & McClintock 1983). For a Crab–like spectrum (§4.1.2), the flux in the 0.5–10 keV (ULX) band is a factor of 1.9 greater (although this is somewhat of an overestimate compared to the use of a thermal spectrum). Including this factor and using the distances and peak fluxes in Table 4.1, we find that the three most luminous BHBs are V4641 Sgr (6.2×10^{39} erg s^{-1}), 4U 1543–47 (4.2×10^{39} erg s^{-1}) and GRS 1915+105 (2.4×10^{39} erg s^{-1}). Thus, at peak luminosity these three BHBs appear to be in the same league as many of the ULXs observed in external galaxies. Moreover, using the mass measurements from Table 4.2, it appears that all three BHBs were super–Eddington at maximum (0.5–10 keV): L_x/L_{Edd} = 7.0, 3.5 and 1.4 for V4641 Sgr, 4U 1543–47 and GRS 1915+105, respectively.

This comparison of BHBs and ULXs is somewhat problematic: First, the distances of the BHBs are uncertain, and we have no direct measurements of their fluxes in the 0.5–2 keV band. Nevertheless, the results quoted above suggest that the peak luminosities of a few BHBs approach the peak luminosities observed for ULXs to within a factor of ≈ 5 (e.g., Miller et al. 2003b). Second, the luminosity shortfall of BHBs may be ascribable to the small sample of 18 BHBs compared to the much larger sample of comparable systems that have likely been detected in surveys of external galaxies. Finally, some ULXs exhibit spectral properties unlike those of BHBs. In particular, the cool disk spectra and the longevity at high luminosity of the most luminous ULXs may distinguish them from BHBs in the Milky Way (Miller et al. 2003a; 2003b). The differences among ULX spectra also suggest that the sample may be heterogeneous.

We conclude by noting that super–Eddington luminosities have plainly been observed for a few NS systems. The most clear–cut case is A0535–668, the "LMC transient." This pulsating NS binary with a firm distance of D = 50 kpc (Freedman et al. 2001) achieved a peak luminosity of $L_x\ \approx 1.2 \times 10^{39}$ erg s^{-1} , assuming isotropic emission (Bradt & McClintock 1983, and references therein). This is 6.9 times the Eddington luminosity of a canonical 1.4 $M_\odot$ NS or 3.8 times the Eddington luminosity of a hypothetical 2.5 $M_\odot$ NS.

4.3 Emission states of black hole binaries

As discussed in §4.1 and §4..2, BHBs exhibit thermal and nonthermal components of X–ray emission, both of which can vary widely in intensity. It has long been recognized that BHBs undergo transitions between quasi–stable states in which one or the other of these components may dominate the X–ray luminosity. In the past, the study of BH emission states was based almost exclusively on X–ray spectral and timing studies. More recently, however, the results of X–ray studies have been supplemented with critical contributions by radio, optical and gamma–ray observers to give us a more physical and fruitful framework for regarding the emission states. In the following sections, we review the characteristic behavior that defines each of the principal X–ray states of BHBs. We then describe the current picture of each state in terms of physical structures and the nature of the accretion flow. Finally, we discuss the prospects of using these states to deduce the properties of BHs.

4.3.1 Historical notes on X–ray states

In the spring of 1971, Tananbaum et al. (1972) observed a remarkable X–ray state change in Cyg X–1 during which the average soft flux (2–6 keV) decreased by a factor of 4 and the average hard flux increased by a factor of 2. Simultaneously, the radio counterpart of Cyg X–1 brightened. It was later found that luminous X–ray novae such as A0620–00 exhibited similar spectral transitions, suggesting that common emission mechanisms were at work in both persistent and transient BHCs (Coe et al. 1976). These early results suggested that such global spectral changes might signify important changes in accretion physics.

As the many light curves in §4.2 illustrate, the soft X–ray state is generally seen at higher luminosity, motivating frequent references to the *high/soft* (HS) state. In this state, the spectrum may also display a "hard tail" that contributes a small percentage of the total flux. As shown by the synoptic studies discussed in §4.2.2, the soft state is best explained as ∼1 keV thermal emission from a multi–temperature accretion disk (see §4.1.5), as foreseen in the standard theory for accretion in BHBs (Shakura & Sunyaev 1973). However, it has been found that the soft state of Cyg X–1 is not consistent with a thermal interpretation (Zhang et al. 1997b), and this has caused considerable confusion as to the proper way to understand Cyg X–1 and/or describe the HS state. In seeking a physical basis for describing X–ray states, it turns out that Cyg X–1 is not a good choice as a prototype, and further remarks about the states in Cyg X–1 are given in a separate section below (§4.3.9).

In the hard state the 2–10 keV intensity is comparatively low, prompting the name *low/hard* (LH) state. The spectrum is nonthermal and conforms to a power–law with a typical photon index $\Gamma \sim 1.7$ (2–20 keV). In this state, the disk is either not detected at 2–10 keV (e.g., Belloni et al. 1999), or it appears much cooler and larger than it does in the soft state (Wilms et al. 1999; McClintock et al. 2001b).

An additional X–ray state of BHBs was identified in the *Ginga* era (Miyamoto et al. 1993). It is characterized by the appearance of QPOs in the presence of both disk and power–law components, each of which contributes substantial luminosity (e.g., $> 0.1 L_{\rm Edd}$; van der Klis 1995). In this state, which is referred to as the *very high* (VH) state, the power–law component is observed to be steep ($\Gamma \sim 2.5$). Initially, there were only two BHBs (GX339–4 and Nova Mus 1991) that displayed this behavior, but many additional examples have been seen in the *RXTE* era.

It was first thought that the two nonthermal states (i.e., LH and VH states) could be distinguished through differences in their photon spectral indices, luminosities, and power density spectra. However, as shown below, the latter two differences have become blurred; nevertheless, the spectral index continues to be a valid discriminator. The importance of distinguishing between the LH and VH states was emphasized in a ∼40–500 keV study of seven BHBs with the OSSE instrument aboard the *Compton Gamma Ray Observatory* (Grove et al. 1998). The gamma–ray spectra of these sources separate naturally into two distinct groups which correspond to the LH state and the VH state, respectively: (1) For the first group it was shown that the X–ray LH state corresponds with a "breaking gamma–ray state" in which the spectrum below ∼100 keV is harder than that of the VH state, but then suffers an exponential cutoff near 100 keV. (2) The second group exhibits a power–law gamma–ray spectrum with photon index $2.5 < \Gamma < 3.0$ over the entire range of statistically significant measurements. This gamma–ray photon index is consistent with the X–ray photon index of the VH state. Furthermore, contemporaneous X–ray observations (e.g., with *ASCA*) confirmed that a luminous thermal component coexists with the power–law component, which is one characteristic of the VH state noted above.

4.3.2 X–ray states as different physical accretion systems

Several recent developments in the study of BHBs has taken us beyond a largely phenomenological description of X–ray states to one based on physical elements (e.g., accretion disk, ADAF, jet, and corona). Although this work is still incomplete, the fundamental distinctions between the states are becoming clearer. For example, a key development in this regard is the recognition of a persistent radio jet associated with the LH state that switches off when the source returns to the HS state (§4.3.6; Ch. 9). Another example, revealed by gamma–ray observations, is the very different coronal structure that is responsible for the clear–cut distinction between the LH state and the VH state (§4.3.1). Arguably, each X–ray state can be regarded as a different accretion system that can be used in unique ways to study accretion physics and the properties of accreting BHs.

In the sections below, we review each of the four canonical X–ray states of BHBs, including the long–lived *quiescent* state. We illustrate the uniform X–ray properties of each of the three active states by showing X–ray spectra and power spectra for several BHBs and BHCs observed by *RXTE*. We also examine a possible fifth X–ray state, the *intermediate* state, as part of our discussion of the VH state. While presenting this overview, we suggest an alternative set of state names that are motivated by the kinds of emergent physical pictures mentioned above. Although the new state names depend critically on multiwavelength results (i.e., radio to gamma–ray), we nevertheless attempt to define them on the basis of X–ray data. Furthermore, based on extensive observations of many sources with *RXTE* (e.g., see §4.2.2), *we abandon luminosity as a criterion for defining the states of BHBs* (with the exception of the *quiescent* state). We do not deny that there are correlations between states and luminosity in many sources, in particular the tendency of the HS to occur at higher luminosity compared with the hard state. However, as shown below, there are clear exceptions to these trends and each X-ray state has now been observed to span a range of two or more decades in X-ray luminosity.

4.3.3 Notes on X–ray spectral analyses

Many spectral models have been developed to describe one or more of the spectral states of BHBs. Most models for the nonthermal continuum components invoke inverse Compton or synchrotron emission, but these mechanisms can be applied with many different assumptions and geometric details. Some models closely constrain the relationship between spectral components (e.g., thermal emission providing seed photons for Comptonization), while others allow the spectral components to vary independently. In presenting this review, we have adopted the following pragmatic and generic strategy. As discussed in §4.2.2, the spectra of BHBs are well described by a model consisting of a multi–temperature accretion disk component and a power–law component (which may require an exponential cutoff at high energy). This model provides a robust, first–order description of BHB spectra that covers all of the emission states, and we adopt it to help define the states and to compare the luminosities of the thermal and nonthermal components. We also include additional features in the model, such as Fe line emission and a disk reflection component, when the normalization parameter for such a feature is significant at the level of 5 σ. In the following discussions of each X–ray state, we comment on some physical interpretations and controversies related to the problem of determining the origin of the power–law component.

4.3.4 Quiescent state

A BHB spends most of its life in a *quiescent* state that can be summarized as *an extraordinarily faint state* ($L_x = 10^{30.5} - 10^{33.5}$ *erg* s^{-1} *), with a spectrum that is distinctly nonthermal and hard (*$\Gamma = 1.5 - 2.1$*).* The first short–period X–ray nova to be detected in quiescence was A0620-00 ($P_{\rm orb} = 7.8$ hr); its X–ray luminosity was several times 10^{30} erg s^{-1} , which is only $\sim 10^{-8}$ of its outburst luminosity (McClintock et al. 1995; Narayan et al. 1996). The long–period systems, however, are significantly more luminous in quiescence because their mass transfer rates are driven by the nuclear evolution of their secondaries rather than by gravitational radiation (Menou et al. 1999). For example, the X–ray luminosity of V404 Cyg ($P_{\rm orb} = 155.3$ hr) is typically $L_{\rm x} \sim 10^{33}$ erg s^{-1} (Kong et al. 2002), but can vary by an order of magnitude in one day (Wagner et al. 1994).

It is now possible to make sensitive measurements in the *quiescent* state using *Chandra* and *XMM–Newton.* The minimum quiescent–state luminosities (0.5–10 keV) of five BHs and stringent upper limits on two others have been reported by Garcia et al. (2001) and Narayan et al. (2002). Three additional BHBs were observed in quiescence more recently (Sutaria et al. 2002; Hameury et al. 2003; McClintock et al. 2003a). Considering only the five short–period systems ($P_{\rm orb} \lesssim 1$ day; see Narayan et al. 2002) that have been detected, one finds that four of them (XTE J1118+480, GRO J0422+32, GS 2000+25, and A0620–00) have Eddington–scaled luminosities that are $\approx 10^{-8.5}$. GS 1124–68 is more luminous by about an order–of–magnitude. As Garcia et al. (2001) and Narayan et al. (2002) show, the Eddington–scaled luminosities of several ostensibly similar X–ray novae that contain NS primaries are about 100 times higher, a conclusion that is quite robust. In the context of the advection–dominated accretion flow model, these authors argue that the relative faintness of the BH X–ray novae provides strong evidence that they possess event horizons. For a thorough discussion of their model and several alternative models, see Narayan et al. (2002). Apart from any specific model, it appears quite reasonable to suppose that the established faintness of quiescent BHs is somehow connected with the existence of the event horizon.

The quiescent spectra of BHBs are well fitted by a single power–law plus interstellar absorption. The best–determined photon spectral indices are consistent with the value $\Gamma \approx 2$. Specifically, for A0620–00 and XTE J1118+480, respectively, one has $\Gamma = 2.07(+0.28, -0.19)$ (Kong et al. 2002) and $\Gamma = 2.02 \pm 0.16$ (McClintock et al. 2003a), where the column density is determined from the optical extinction. Only V404 Cyg allows a useful determination of both the column density and the photon index: $N_{\rm H} = (6.98 \pm 0.76) \times 10^{21}$ cm^{-2} and $\Gamma = 1.81 \pm 0.14$ (Kong et al. 2002).

A multiwavelength spectrum of XTE J1118+480 in quiescence is shown in Fig-

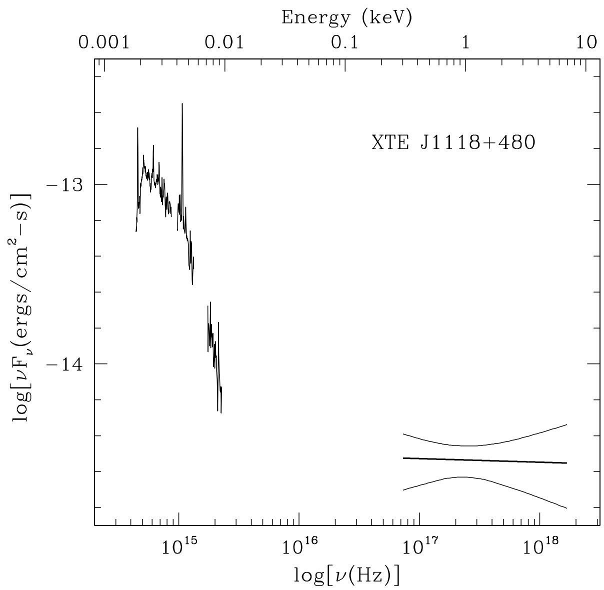

Fig. 4.7. Spectrum of XTE J1118+480 in the *quiescent* state based on simultaneous, multiwavelength observations. The optical spectrum of the mid–K dwarf secondary has been subtracted. Note the Planckian shape of the optical/UV continuum, which is punctuated by a dominant Mg II 2800Å line and a strong Hα line on the far left. The best–fit X–ray model is indicated by the heavy, horizontal line; the 90% error box is defined by the flanking curved lines.

ure 4.7 (McClintock et al. 2003a). This shortest–period BHB ($P_{\rm orb} = 4.1$ hr) is located at b = 62$^{\rm o}$, where the transmission of the ISM is very high (e.g., 70% at 0.3 keV). A very similar multiwavelength spectrum was observed earlier for A0620–00 (McClintock & Remillard 2000), which implies that the spectrum shown in Figure 4.7 represents the canonical spectrum of a BHB radiating at $10^{-8.5} L_{\rm Edd}$. The spectrum is comprised of two apparently disjoint components: a hard X–ray spectrum with a photon index $\Gamma = 2.02 \pm 0.16$, and an optical/UV continuum that resembles a 13,000 K disk blackbody spectrum punctuated by several strong emission lines.

The ADAF/disk model (see §4.1.5) accounts well for the following properties of BHBs in the *quiescent* state: (1) The hard power–law spectra (Narayan et al. 1996; Narayan et al. 1997; Hameury et al. 1997; Quataert & Narayan 1999; McClintock et al. 2003a); (2) the faintness of BHs relative to NSs (Narayan et al. 1997; Garcia et al. 2001; Narayan et al. 2002; (3) the several–day delay in the optical/UV light curve when X–ray novae go into outburst (Hameury et al. 1997); and (4) the broadband spectrum shown in Figure 4.7 (McClintock et al. 2003a). Especially significant is the prediction, confirmed by observations, that the accretion disk is truncated at a large inner radius in both the *quiescent* and LH states (Narayan 1996; Esin et al. 1997; McClintock et al. 2001b; McClintock et al. 2003a).

4.3.5 Thermal–dominant (TD) state or high/soft (HS) state

As discussed in §4.1.5, considerations of basic principles of physics predict that accreting BHs should radiate thermal emission from the inner accretion disk (Shakura & Sunyaev 1973). It was therefore readily accepted that the soft X–ray state of BHBs represents thermal emission. Confirmations of this picture are largely based on the successful ability to describe the soft X–ray component using the simple multi–temperature accretion disk model (MCD model; §4.1.5). In Figures 4.8 & 4.9 we show the energy spectra and power spectra, respectively, of 10 BHBs in the "thermal–dominant" (TD) or *high/soft* (HS) X–ray state as observed by *RXTE*. The thermal component of the model, where it can be distinguished from the data, is shown as a solid line, and the power–law component is shown as a dashed line. Typically, below about 10 keV the thermal component is dominant. With a few exceptions, the temperature of this component is in the range 0.7–1.5 keV (Table 4.4). The power–law component is steep ($\Gamma = 2.1 - 4.8$) and faint. In GRS 1915+105 the power–law falls off even more steeply with an e–folding cutoff energy of 3.5 keV; similar behavior has been reported for GRO J1655–40 (Sobczak et al. 1999).

In Figure 4.8 we feature data for BHBs obtained during pointed observations with *RXTE*, while data for BHCs are shown in Figure 4.9. The spectra of four of the sources in the figures (4U 1543–47, GX 339–4, XTE J1755–324, and XTE J2012+381) correspond to the maximum 2–20 keV luminosities observed during *RXTE* pointings (i.e., considering all possible states). The power density spectra (PDS) in Figures 4.8 & 4.9 show that the variability in the TD state is either weak or the power scales roughly as ν^{-1}, which is a characteristic of many physical processes including turbulence (Mandelbrot 1999). The total rms power (r) integrated over 0.1–10 Hz in these PDS is in the range $0.01 \lesssim r \lesssim 0.06$, which is significantly below that of the LH state. QPOs in the range 0.1–30 Hz are generally not seen in individual TD observations, but large groups of PDS in the TD state have yielded weak QPOs in two cases. A 0.3% (rms) QPO at 27 Hz was seen in a sum of 27 observations ("1997 soft state") of GRO J1655-40 (Remillard et al. 1999), and a similar (0.3%) QPO at 17 Hz was seen in 69 observations of XTE J1550-564 in the soft state during 1998–1999 (MJD 51160–51237; Homan et al. 2001).

In the following section, we show that a transition to the LH state is followed by the appearance of a hard and dominant power–law spectrum, while the accretion disk, if visible, shows a substantial decrease in temperature. On the other hand, a transition to the VH state (§4.3.7) is marked by a steeper power–law spectrum accompanied by either a normal (~ 1 keV) disk or one that appears hot with a small inner radius. This latter transition is also accompanied by the presence of QPOs that appear when the disk contribution to the total, unabsorbed flux at 2–20 keV falls below the level of 0.75 (Sobczak et al. 2000a). *We thus define the TD state as the set of conditions for which the disk–flux fraction is above 75% (2–20 keV), the PDS shows no QPOs or very weak features (rms* $<< 1\%$*), and the power continuum is also weak :* $r \lesssim 0.06$ *integrated over 0.1–10 Hz.*

As further support for a thermal interpretation of the soft X–ray component, many studies have found evidence for disk luminosity variations in which the inner disk radius (which scales as the square root of the MCD normalization parameter) appears constant while the luminosity variations depend only on changes in temperature

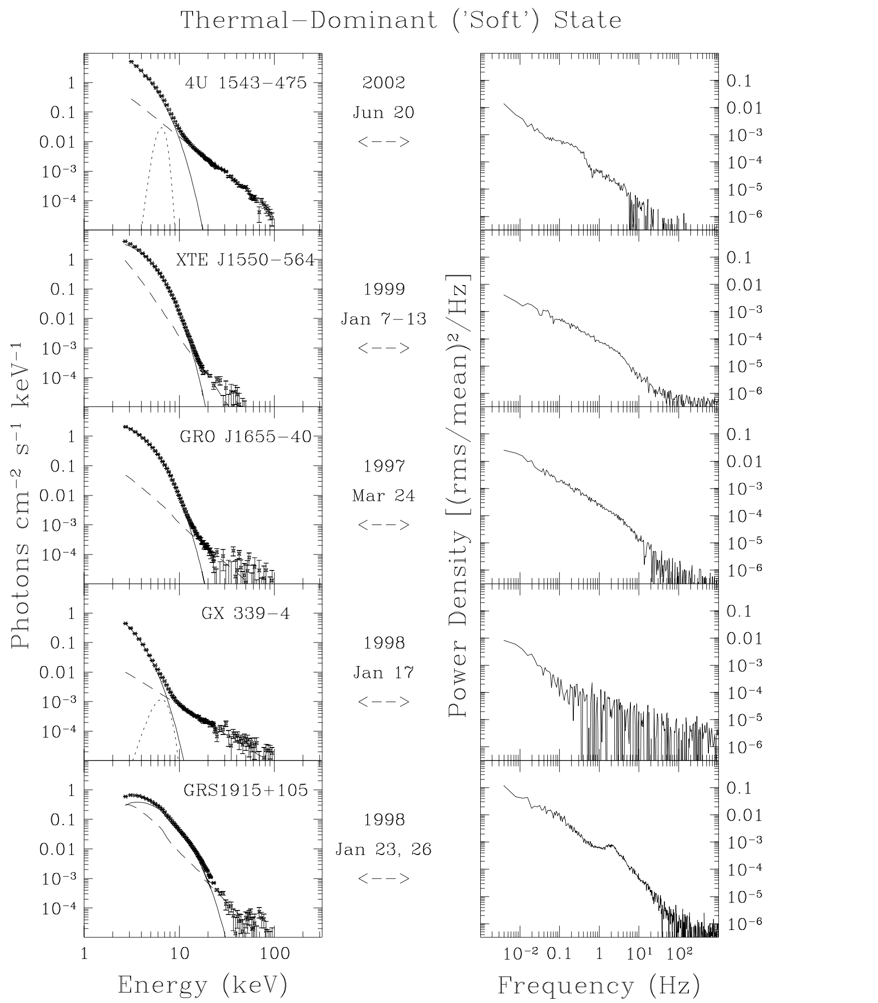

Fig. 4.8. Sample X–ray spectra of BHBs in the X–ray state for which the dominant component is thermal emission from the accretion disk. The energy spectra (left) are decomposed into a thermal component, which dominates below ~10 keV (solid line), and a faint power–law component (dashed line); GRS 1915+105 is modeled with a cutoff power–law (see text). For two of the BHBs, an Fe line component is included in the model (dotted line). The corresponding power spectra are shown in the panels on the right.

(§4.2.2). This effect is reported in a study of LMC X–3 (Kubota et al. 2001) and is illustrated in Figure 4.10. The measured disk flux and apparent temperature successfully track the relation $L \propto T^4$ (solid line) expected for a constant inner disk radius. The figure also shows gross deviations from this relation associated with the VH state of GRO J1655–40, a topic that is addressed below in §4.3.7.

Because of the successes of the simple MCD model, the inner disk radius has been used to provide a type of spectroscopic parallax. In principle, the inner disk radius can be deduced for those sources for which the distance and disk inclination

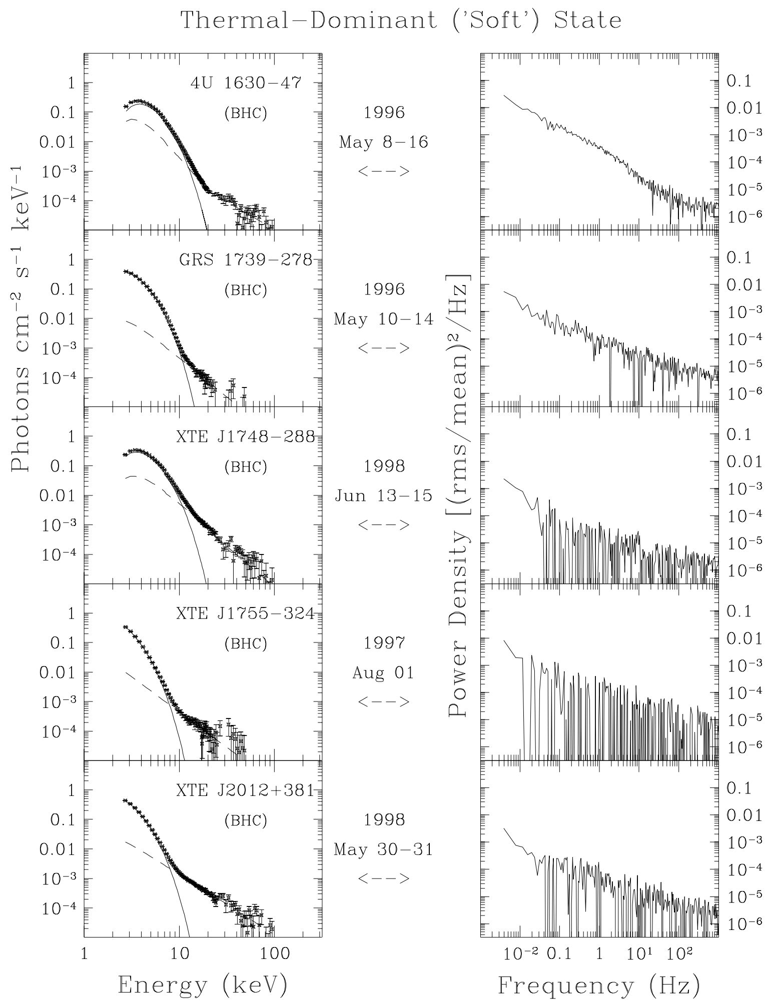

Fig. 4.9. *Left panels:* Sample X–ray spectra of BHCs in the TD X–ray state. In the panels on the left, the energy spectra are shown deconvolved into a thermal component due to the accretion disk (solid line) and a power–law component (dashed line). The corresponding power spectra are shown in the right half of the figure.

are well constrained from the disk normalization parameter, $(R_{\rm in}/{\rm D})^2 \cos\theta$, where $R_{\rm in}$ is the inner disk radius in kilometers, D is the distance to the source in units of 10 kpc, and θ is the inclination angle of the system (e.g., Arnaud & Dorman 2002). However, the MCD model is Newtonian, and the effects of GR and radiative transfer need to be considered. GR predicts a transition from azimuthal to radial accretion flow near $R_{\rm ISCO}$, which depends only on mass and spin and ranges from $1-6R_{\rm g}$ for a prograde disk (§4.1.5). Therefore, for a system with a known distance and inclination, in principle it may be possible to estimate the spin parameter via an X–ray measurement of the inner radius and an optical determination of the mass. In lieu of a fully relativistic MHD model for the accretion disk, one could attempt

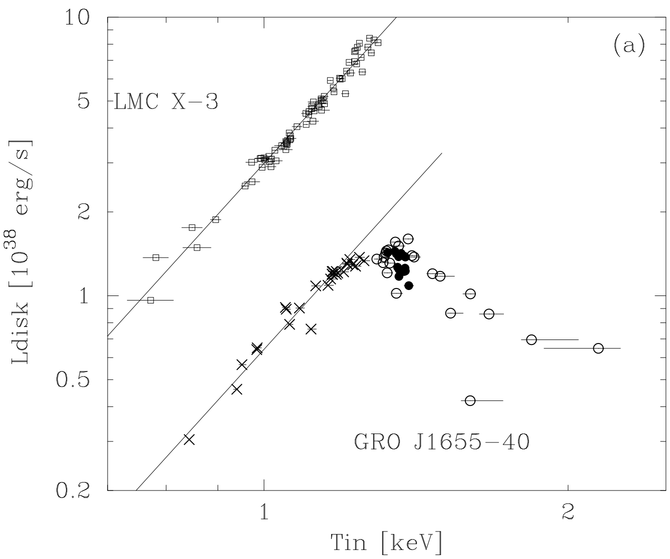

Fig. 4.10. The accretion disk luminosity *vs* temperature at the inner accretion disk (Kubota et al. 2001). For GRO J1655–40, the symbol type denotes the time periods: early outburst (filled circles), first phase (open circles), and second phase (crosses). The solid lines represent the $L_{\rm disk} \propto T_{\rm in}^4$ relation.

to correct the MCD model parameters to account for the effects of radiative transfer through the disk atmosphere (Shimura & Takahara 1995) and for modifications on the structure and emissivity of the inner disk due to GR (Zhang et al. 1997a). However, the accuracy of these corrections has been challenged (Merloni et al. 2000; Gierlinski et al. 1999), and at present the chief value of the MCD model is in monitoring the temperature and the fractional flux contribution from the accretion disk.

4.3.6 Hard X–ray state associated with a steady radio jet

The conventional name for this state is the *low/hard* (LH) state; however, henceforth we refer to it simply as the *hard* state for the reasons given in §4.3.2. As noted earlier (§4.3.1), Cyg X–1 and many transient sources have been observed to undergo transitions to a hard, nonthermal X–ray spectral state. This usually occurs at luminosities below that of the TD state, and the spectrum can be modeled (e.g., 1–20 keV) as a power–law function with a photon index ∼1.7. In some sources, such as Cyg X–1 and GS 1354–64, this *hard* state is accompanied by a broad enhancement at 20–100 keV which is interpreted as reflection of the power–law component from the surface of the inner accretion disk (Di Salvo et al. 2001). This component is discussed further at the end of this section.

In recent years there have been rapid advances in associating the X–ray *hard* state with the presence of a compact and quasi–steady radio jet (for a thorough review, see Ch. 9). This relationship, which constitutes one of the foundations of the "disk : jet" connection, is based on at least three arguments. First, VLBI radio images have shown a spatially–resolved radio jet during episodes of quasi–steady radio and hard X–ray emission from GRS 1915+105 (Dhawan et al. 2000) and Cyg

X–1 (Stirling et al. 2001). In both instances the radio spectrum was flat or inverted. Second, more generally (i.e., when VLBI images are not available), X–ray sources that remain in the *hard* state for prolonged periods (weeks to years) are highly likely to show correlated X–ray and radio intensities and a flat radio spectrum (Fender et al. 1999a; Fender 2001; Corbel et al. 2000; Klein–Wolt et al. 2002; Marti et al. 2002; Corbel et al. 2003). In one of these examples, GX 339–4, the jet interpretation is further supported by the detection of 2% linear radio polarization with a nearly constant position angle (Corbel et al. 2000). Finally, it is now routine to witness the quenching of the persistent radio emission whenever an X–ray source exits the *hard* state and returns to the TD state (Fender et al. 1999b; Brocksopp et al. 1999; Corbel et al. 2000).

In Figure 4.11, the five BHBs shown in the *hard* state are the same sources shown earlier in the TD state (Fig. 4.8). In the following cases, the X–ray data have been selected to coincide with specific radio observations: Flat–spectrum radio emission was reported for both XTE J1550–564 on 2000 June 1 during the decay of its second outburst (Corbel et al. 2001) and for GX 339–4 on 1999 March 3 (Corbel et al. 2000). In addition, both the radio and X–ray emission of GRS 1915+105 are fairly steady on 1997 October 22, which coincides with one of the days in which the core radio image shows the extended structure of a nuclear jet (Dhawan et al. 2000).

A second sample of BHBs and BHCs in the *hard* state is shown in Figure 4.12. The *hard* state for XTE J1748–288 occurred during decay from the HS state (Revnivtsev et al. 2000c). On the other hand, the data shown for XTE J1118+480 and GS 1354–64 correspond with outburst maxima; these outbursts never reached the HS state (Revnivtsev et al. 2000a; Frontera et al. 2001b). Associated radio emission for these two sources was reported with jet interpretations by Fender et al. (2001) and Brocksopp et al. (2001), respectively. Finally, GRS 1758–258 and Cyg X–1 spend most of their time in the *hard* state, and their energy spectra are shown in the bottom two panels of Figure 4.12. These *RXTE* observations happened to coincide with radio observations that confirm a flat radio spectrum. In the case of GRS 1758–258, core radio emission (as distinct from the extended radio lobes observed for this source) was reported on 1998 August 3 and 5 by Marti et al. (2002), and a clear detection of Cyg X–1 during 1997 December 12–17 is evident in the public archive of the Greenbank Interferometer available on the NRAO web site.

The physical condition of the accretion disk in the *hard* state is a subject of great significance in the effort to build a detailed physical model for both the jet and the X–ray source. Observations with *ASCA*, which provided sensitivity in the range 0.5 to 9 keV, showed that the *hard* states of both GX 339–4 (Wilms et al. 1999) and Cyg X–1 (Takahashi et al. 2001) exhibit power–law spectra with an additional soft X–ray excess that can be modeled as a large and cool (∼0.1–0.2 keV) accretion disk. The spectral decompositions illustrated in Figure 4.11 provide some evidence for a soft disk component in both GRO J1655–40 and GRS 1915+105, although *RXTE* is much less sensitive than *ASCA* to thermal spectra with temperatures well below 1 keV. By far, the best direct measurements of the temperature and inner radius of an accretion disk in the *hard* state have been made for XTE J1118+480, which has an extraordinarily small interstellar attenuation (e.g., only 30% at 0.3 keV). Based on simultaneous *HST*, *EUVE* and *Chandra* observations made in outburst,

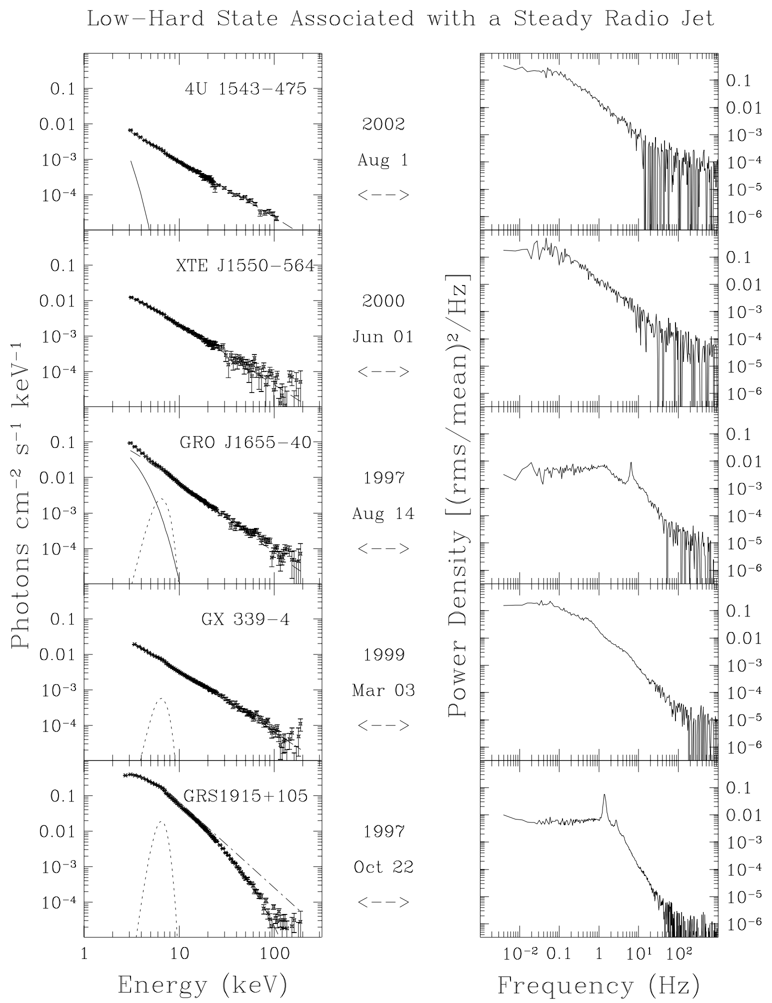

Fig. 4.11. Sample spectra of BHBs in the *hard* state. The energy spectra are characterized by a relatively flat power–law component that dominates the spectrum above 1 keV. A second characteristic of the *hard* state is the elevated continuum power in the PDS. This state is associated with the presence of a steady type of radio jet (see text). The selected X–ray sources are the same BHBs shown in Figure 4.8. The individual spectral components include the power–law (dashed line) and, if detected, the accretion disk (dotted line) and a reflection component (long dashes).

it was determined that the inner disk radius and temperature for the MCD model were $\gtrsim 100\ R_{\rm g}$ and $\approx$ 0.024 keV, respectively (McClintock et al. 2001b). Somewhat higher temperatures ($\approx$ 0.035–0.052 keV) have been inferred from observations using BeppoSAX (Frontera et al. 2003).

While it seems clear that the blackbody radiation appears truncated at a large radius ($\sim 100\ R_{\rm g}$) in the *hard* state, the physical state of the hot material within this

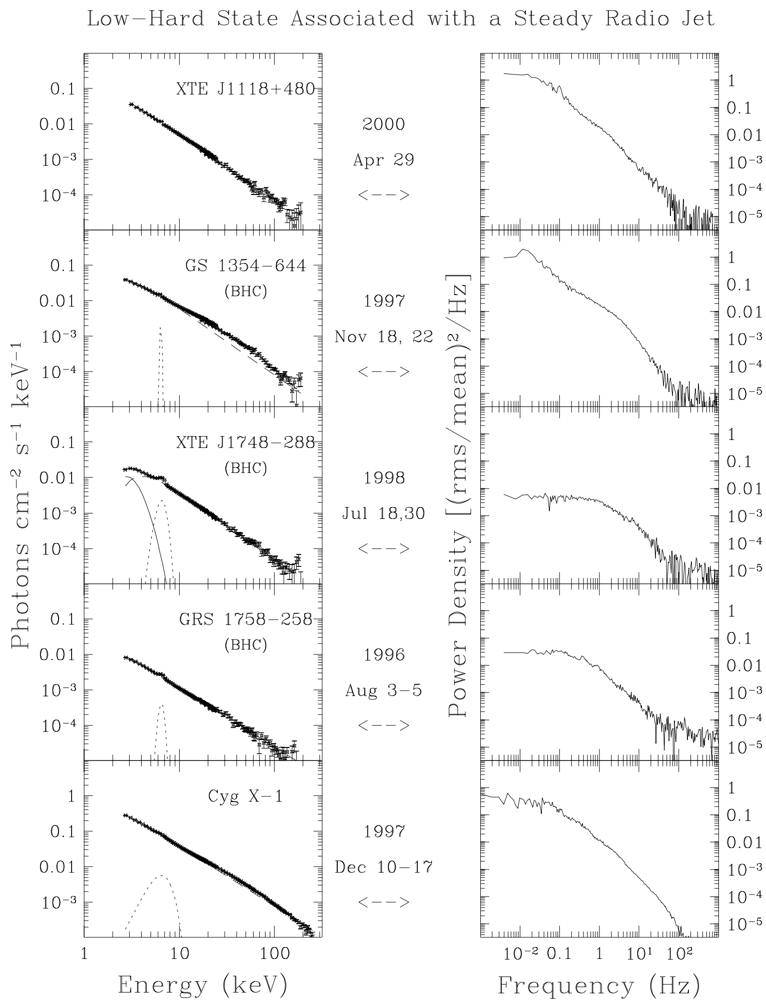

Fig. 4.12. A second sample of BHBs or BHCs seen in the *hard* state. The observations of XTE J1748–288 occurred during outburst decay, while XTE J1118+480 and GS 1354–64 are seen in the *hard* state at the peaks of their respective outbursts. GRS 1758–258 and Cyg X–1 spend most of their time in the *hard* state. There is radio coverage that confirms the presence of a flat radio spectrum for all the sources except XTE J1118+480. The line types denoting the spectral components follow the convention of Figure 4.11
.

large radius is still a matter of debate. Is the disk density truncated at this radius, as envisioned in the ADAF model, or is a substantial amount of matter present in a relativistic flow that is entrained in a jet (e.g., Markoff et al. 2001)? Or is the inner disk basically intact and either depleted of energy or veiled in some type of Compton corona? For the latter possibility, the properties of the corona would be strongly constrained by the absence of any normal ($\sim$1 keV) thermal component in the *hard* state of XTE J1118+480 (Esin et al. 2001; Frontera et al. 2003).

Guidance in sorting out these options may eventually come from other types of investigations, such as the study of correlated optical/X–ray variability (Malzac et al. 2003). Also promising are spectral analyses that focus on broad Fe emission features (§4.2.3) or the X–ray reflection component (Done & Nayakshin 2001). These spectral features depend on substantial density in the inner disk, while the Fe line additionally reveals the pattern of Keplerian flow modified by effects due to GR. Systematic studies of these features during different BHB states and transitions could help to determine the physical changes in the inner disk associated with the *hard* state. The reflection component is most apparent when the disk is observed nearly face-on. One such system is Cyg X–1, and a reflection analysis has been reported by Done & Zycki (1999). They find that the disk is physically truncated, but the transition radius (tens of $R_{\rm g}$) is not as far from the event horizon as suggested by the value of R_{in} inferred from the disk spectrum in the *hard* state (Takahashi et al. 2001).

The origin of the X–ray power–law is another aspect of the controversy concerning the appropriate physical model for the *hard* state. As noted above, we regard the power–law fit as a general signature of nonthermal radiation; however, the observed spectrum can be produced by several different radiation mechanisms. This is well illustrated in the case of XTE J1118+480, where the X–ray spectrum has been fitted by an ADAF model (Esin et al. 2001), a synchrotron model (Markoff et al. 2001) and a thermal–Comptonization model (Frontera et al. 2001b).

Despite the large uncertainties that remain for physical models, it would appear that the association of the *hard* state with a steady radio jet is an important step forward. And it does remain possible to identify the *hard* state solely from X–ray spectral and temporal properties, as had been done in the past (TL95). Using Figures 4.11 & 4.12 and Table 4.4, *we conclude that the hard state is well characterized by three conditions: the spectrum is dominated (> 80% at 2–20 keV) by a power–law spectrum, the spectral index is in the range* $1.5 < \Gamma < 2.1$*, and the integrated power continuum (0.1–10 Hz) is strong and typically in the range* $0.1 < r < 0.3$*.*

4.3.7 Steep power–law (SPL) state or very high (VH) state

There are times when BHBs become exceedingly bright ($L_x > 0.2 L_{\rm Edd}$), and the X–ray spectrum again displays substantial nonthermal radiation, which may constitute 40–90% of the total flux. In such cases the photon index is typically $\Gamma \geq 2.4$, which is steeper than the index ($\Gamma \sim 1.7$) seen in the *hard* state. The strength of this steep power–law component also coincides generally with the onset of X–ray quasi–periodic oscillations (QPOs) in the range 0.1–30 Hz. This suite of characteristics was initially seen in only two instances: during a bright outburst of GX 339–4 (Miyamoto & Kitamoto 1991) and near the time of maximum flux in X–ray Nova Muscae 1991 (= GS/GRS 1124–68; Miyamoto et al. 1993). At the time, this *very high* (VH) state was interpreted as a signature of the highest rate of mass accretion in a BHB system (van der Klis 1995).

As mentioned previously (§4.3.1), the high–energy spectra of several BHCs observed with OSSE on *CGRO* (40–500 keV) reinforced the distinction between the X–ray *hard* and VH states, showing that the *hard*–state spectra exhibit a steep cutoff near 100 keV (Grove et al. 1998). On the other hand, the VH–state spectra showed no evidence for a high–energy cutoff, while the photon index in the X–ray and gamma–ray bands is the same ($\Gamma \sim 2.5$–3.0). The unbroken power–law spectra observed by OSSE for five sources suggested that these BHBs had been observed in the VH state, although most of the observations were not accompanied by X–ray observations that could assess the presence of QPOs.

The monitoring programs of *RXTE* have shown that the VH state is both more common and more complicated than originally envisioned. Some sources display both X–ray QPOs and a steep power–law component at luminosity levels that are well *below* the maxima seen even in their TD (HS) state (Remillard et al. 2002b; §4.5). This topic is considered further in §4.3.8 below. In response to these developments, we hereafter refer to this state as the "steep power–law" state, or the SPL state, rather than the VH state. We adopt this new name because the steep power–law is a fundamental property of this state, whereas a very high luminosity is not. We view the presence of QPOs as a confirming property of the SPL state.

In Figure 4.13 we show examples of the SPL state for the same five BHBs considered in Figures 4.8 & 4.11. The photon index of the steep power–law component covers the range $2.4 < \Gamma < 3.0$ as shown in Table 4.4, and QPOs are present with central frequencies over the range 5–13 Hz . The spectra of XTE J1550–564 and GRO J1655–40 (Fig. 4.13) correspond to the highest luminosities observed for these sources during pointed observations with *RXTE* (Sobczak et al. 2000b; Sobczak et al. 1999). Moreover, both observations revealed the presence of high–frequency QPOs, 186 Hz and 300 Hz, respectively (Remillard et al. 2002b). The relationship between the SPL state and HFQPOs will be discussed further in §4.4.3.

In Figure 4.14 we show spectra of the SPL state for three BHCs and two additional BHBs. For three of the sources we have selected observations near the time of maximum flux, as seen in *RXTE* pointed observations. For the two remaining sources we consider local maxima: the 1996 soft–state episode of Cyg X–1 and the second outburst of 4U 1630–47. X–ray QPOs are seen in the top four panels (5–8 Hz in three cases and 31 Hz in the case of XTE J1748–288). The power spectrum of Cyg X–1 contains broad continuum features but no X–ray QPOs, although the energy spectrum indicates that the source is in an SPL–like state.

We can encompass all of these SPL examples with the following criteria (see also Sobczak et al. 2000a). *The SPL state is defined first by the presence of a power–law component in the X–ray spectrum with photon index* $\Gamma > 2.4$. *Secondly, either there are X–ray QPOs present (0.1–30 Hz) while the power–law contributes more than 20% of the total (unabsorbed) flux at 2–20 keV, or the power–law contributes more than 50% of the total flux without detections of QPOs.*

Transitions between the TD and *hard* states frequently pass through intervals of the SPL state, and this has led some authors to suggest that the SPL (or VH) state is itself an "intermediate state" that lies between the TD and *hard* states (Rutledge et al. 1999; Homan et al. 2001). However, this appears to be a radical suggestion that gives inadequate weight to other SPL observations associated with (1) the episodes of highest absolute luminosity in many BHBs, (2) a distinct gamma–ray spectrum, and (3) occurrences of QPOs at both high and low frequency. We therefore conclude that the SPL state is a bona fide state of BHBs, and we note that nothing in our state definitions constrains the order in which state transitions should occur.

The radio properties of the SPL state are an important and complicated topic

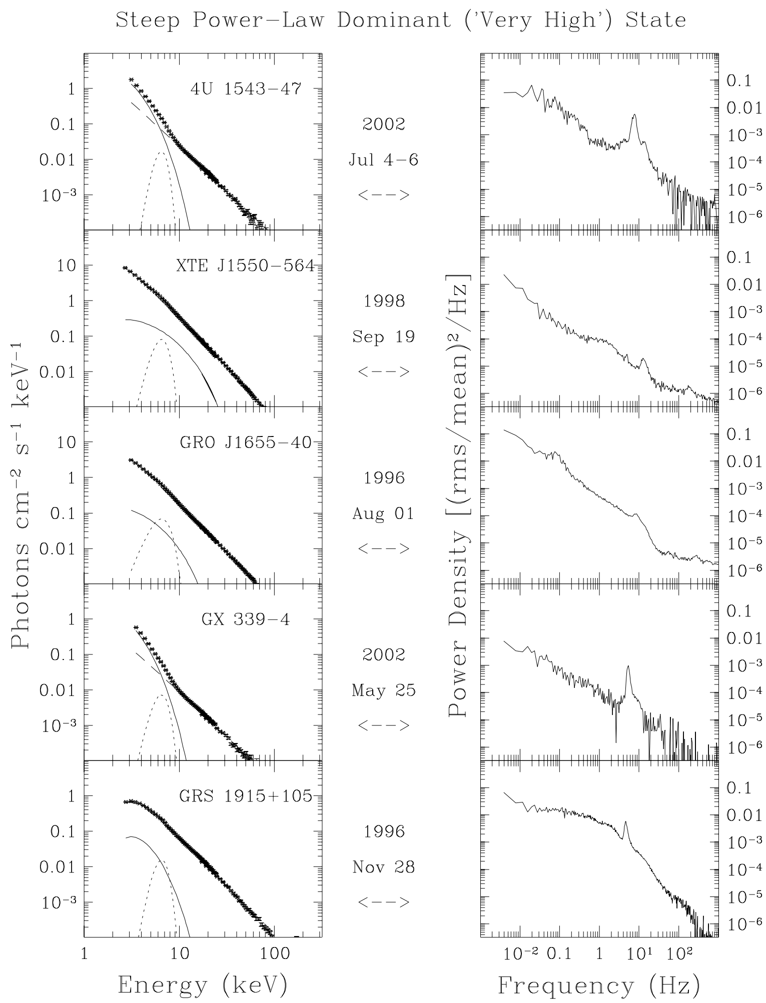

Fig. 4.13. X–ray spectra of BHBs in the SPL state, which is characterized by a strong and steep power–law component in the energy spectrum, along with the presence of X–ray QPOs. The dashed and dotted lines follow the convention of earlier figures.

that calls for the heightened attention of observers. Here we highlight several salient results. The brightest days of GRO J1655–40 during its 1996–1997 outburst occurred in the SPL state (1996 August) when the source appeared radio–quiet (e.g. Tomsick et al. 1999). Similarly, Cyg X–1 becomes radio quiet whenever the spectrum switches from the *hard* state to the SPL state. On the other hand, the SPL state is also associated with the explosive formation of radio jets. For example, the giant X–ray flare in XTE J1550–564 (shown in Fig. 4.2 & 4.13) has been linked to a relativistic mass ejection seen as a superluminal separation of bipolar radio jets (Hannikainen et al. 2001). However, there is a distinct possibility that the X–ray flare in the SPL state may have occurred after the moment of ejection, at a time when the

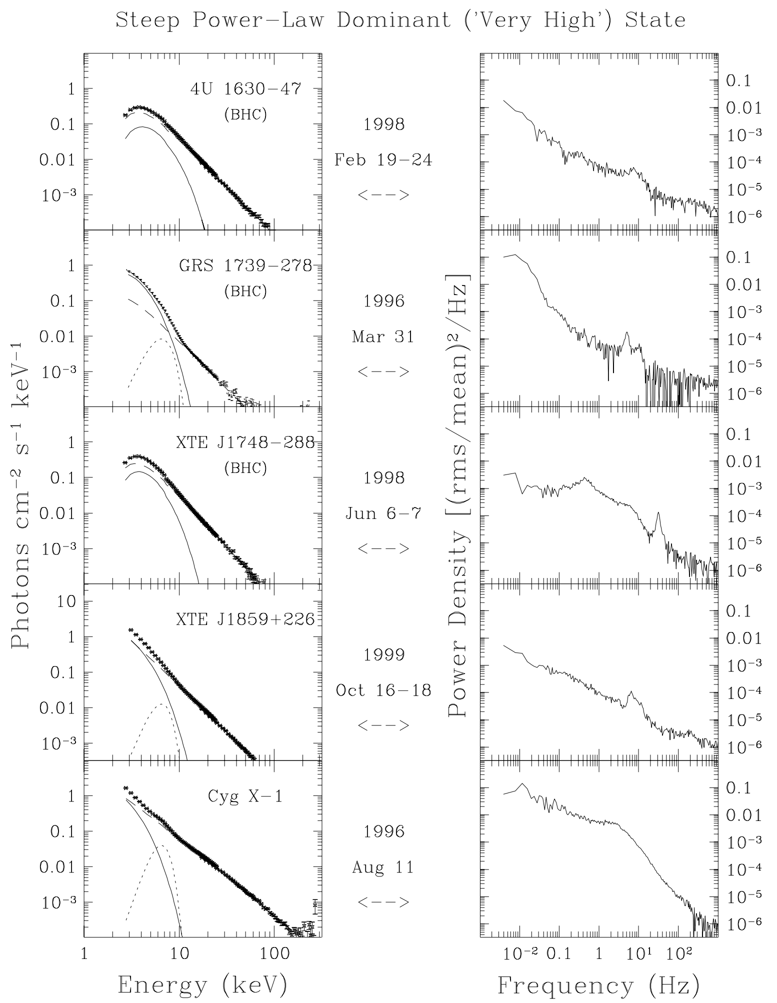

Fig. 4.14. Additional examples of sources in the SPL state. The observations were selected near the times of global or local maxima in the X–ray flux. Cyg X–1 is exceptional for its relatively low luminosity and for the absence of QPOs (see §4.3.9). The dashed and dotted lines follow the convention of earlier figures.

radio properties of the core (i.e., the inner disk) are unknown. This conjecture is supported by radio observations of the same source during the 2000 outburst when a radio flare was observed to decay below detectable levels while the source remained in the SPL (VH) state (Corbel et al. 2001). We conclude that the best available evidence suggests that the SPL state is essentially radio quiet, while the instability that causes impulsive jets is somehow associated with the SPL state.

The physical origin of the SPL spectrum remains one of the outstanding problems in high–energy astrophysics. The SPL spectrum extends to ∼1 MeV in several sources: e.g., Cyg X–1, GRO J1655–40 and GRO J0422+32 (Table 4.2). The spectrum may extend to even higher energies, but present investigations are limited by photon statistics. At stake is our understanding of accretion physics at the extraordinary times of peak BHB luminosity. Equally important is our need to interpret the high–frequency QPOs associated with the SPL state.

Most models for the SPL state invoke inverse Compton scattering as the operant radiation mechanism (e.g., Zdziarski 2000). The MeV photons suggest that the scattering occurs in a nonthermal corona, which may be a simple slab operating on seed photons from the underlying disk (Gierlinski et al. 1999; Zdziarski et al. 2001). Efforts to define the origin of the Comptonizing electrons has led to more complicated geometric models with feedback mechanisms, such as flare regions that erupt from magnetic instabilities in the accretion disk (Poutanen & Fabian 1999). One early model, which was applied to AGN, invokes a strongly magnetized disk and predicts power–law spectra extending to tens of MeV (Field & Rogers 1993). An analysis of extensive *RXTE* observations of GRO J1655–40 and XTE J1550–564 has shown that as the power–law component becomes stronger and steeper, the disk luminosity and radius appear to decrease while maintaining a high temperature (see Fig. 4.10). These results can be interpreted as an observational confirmation of strong Comptonization of disk photons in the SPL state (Kubota et al. 2001; Kubota & Makishima 2003).

There are a number of alternative models for the SPL state. For example, bulk motion Comptonization has been proposed in the context of a converging sub–Keplerian flow within 50 $R_{\rm g}$ of the BH (e.g., Titarchuk & Shrader 2002). Turolla et al. (2002) have suggested pair production as a means of extending the photon spectrum beyond the ∼350 keV limit initially calculated for this model.

As noted above, Comptonization models are hard–pressed to explain the origin of the energetic electrons. As a further difficulty, a viable model must also account for the QPOs in the SPL state. This is important since strong QPOs (see Fig. 4.13 and Fig. 4.14) are common in this state. SPL models and X–ray QPOs are discussed further in §4.4 below.

4.3.8 Intermediate states

The four states described above capture the behavior observed for most BHBs on many occasions. However, other forms of complex behavior are often seen, and these dispel the notion that every BHB observation can be classified via these X–ray states. In the following three subsections, we consider observations that challenge or combine elements of the four–state framework described above.

The *hard*–state energy spectra in Figures 4.11 & 4.12 show little or no contribution from the accretion disk, while the PDS exhibit a "band–limited" power continuum (i.e., a flat power continuum at low frequencies that breaks to a steeper slope between 0.1 and 10 Hz). However, a band–limited power spectrum is sometimes seen in combination with a stronger contribution from the accretion disk. This condition of a BHB has been interpreted as an *intermediate* state that lies between the *hard* and TD states (e.g., Mendez & van der Klis 1997). We agree that the spectra of GRO J1655–40 shown in Figure 4.11 do appear to represent a legitimate example of the *intermediate* state in the sense of a transition between the *hard* and TD states.

Other cases seem to display a different type of intermediate or hybrid emission state. For example, dozens of observations of XTE J1550–564 yielded energy spectra and QPOs that resemble the SPL state (Sobczak et al. 2000b), but the PDS showed band–limited continuum power that is reminiscent of the *intermediate* state described above (Homan et al. 2001). One example is shown in Figure 4.15, along with a similar observation of GRS 1915+105. These observations can be described as SPL states with band–limited power continua. The significance of this PDS shape is yet to be fully understood. It could suggest an *intermediate* state linking the *hard* and SPL states, a detail further supported by the fact that the disks in the two systems appear cooler and larger than they do in the TD state. However, such speculations may be ill–advised without considerations of sensitive radio measurements. We further note that the presence or absence of band–limited power observed in individual SPL–state observations of XTE J1550–564 is closely coupled to the amplitudes and phase lags of the associated QPOs (of types A, B, and C; Remillard et al. 2002a). Finally, while the energy spectra of XTE J1550–564 and GRS 1915+105 in Figure 4.15 are distinctly steep, there is some ambiguity as to whether they are best modeled as a steep power–law or as a flatter power–law with an unusually low cutoff energy (~ 50 keV). In Table 4.4, we show the spectral parameters for the latter model, which is statistically preferred in the case of GRS 1915+105.

We conclude that it is inappropriate to refer to both the observations of XTE J1550–564 (Fig. 4.15) and the very different observations of GRO J1655–40 (Fig. 4.11) as representing a single BHB state, namely, the *intermediate* state. On the other hand, state transitions and hybrid emission properties are to be expected and *X–ray spectra and PDS should be interpreted as intermediate states when necessary, while specifying which states can be combined to yield the the observed X–ray properties.* In summary, we describe the spectra of GRO J1655–40 (Fig. 4.11) as representing primarily a *hard* state or perhaps an *intermediate* state between *hard* and TD. On the other hand, the spectra and PDS of XTE J1550–564 and GRS 1915+105 considered here appear to show an *intermediate* state related to the SPL and *hard* states. Since transitions between these latter two states are not generally seen, this hybrid combination merits further scrutiny.

4.3.9 X–ray states of Cygnus X–1 and GRS 1915+105

In this section we briefly summarize the efforts to integrate the behavior of two uncommon BHBs within the framework of the TD, *hard*/radio jet, and SPL states. We first return to the issue of Cyg X–1 and the nature of its transitions to a soft state of high intensity, which is unlike the canonical TD (HS) state. As noted earlier (§4.2.1.1; §4.3.1), contrary to expectations the 1996 soft–state spectrum of Cyg X–1 revealed a power–law spectrum, rather than a TD spectrum (Zhang et al. 1997a; Frontera et al. 2001a; Fig. 4.14). Cyg X–1 has never been seen in the TD state, and the transition from a hard X–ray spectrum to a soft one must be seen as a transition from the *hard* state to the SPL state (Gierlinski et al. 1999; Zdziarski et al. 2001). However, this SPL–like state is unusual in two respects: the absence of QPOs and the relatively low temperature of the accretion disk (Table 4.4). Less surprising is the low luminosity of the SPL state (Zhang et al. 1997b), since this is also seen in other sources (e.g., XTE J1550–564; Remillard et al. 2002a). Whether the SPL state in Cyg X–1 requires a higher mass accretion rate than the *hard* state is a matter of controversy (Zhang et al. 1997b; Frontera et al. 2001a).

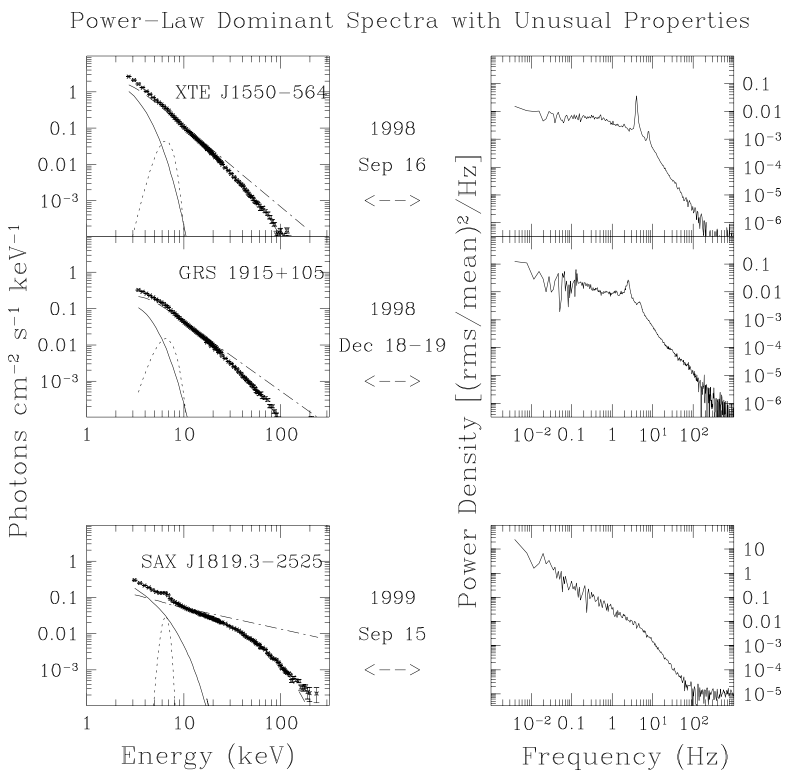

Fig. 4.15. Unusual spectra of three BHBs. The observations of XTE J1550–564 and GRS 1915+105 show spectral properties of the SPL state, but the PDS show a band–limited power continuum that is customarily seen as a characteristic of the *hard* state, rather than the SPL state. In the bottom panel, the flares and rapid fluctuations seen in SAX J1819.3–2525 (V4641 Sgr) do not coincide with any of the typical X–ray states of BHB systems.

In the unique case of GRS 1915+105, the wildly varying X–ray light curves indicate an imposing number of instability modes (Belloni et al. 2000). Nevertheless, within this complexity it is often possible to identify the canonical states of a BHB (Muno et al. 1999; Belloni et al. 2000). About half of the observations of GRS 1915+105 show fairly steady X–ray flux (rms $<$ 15% in 1 s bins at 2–30 keV), and most of these intervals yield spectra and PDS that resemble either the TD or *hard* states (Muno et al. 1999; Fender 2001; Klein–Wolt et al. 2002). There are, however, some noteworthy anomalies encountered while interpreting the behavior of GRS 1915+105 in terms of the canonical X–ray states. First, the condition of steady radio and X–ray emission extends to $L_x > 10^{38}$ erg s^{-1}, which is a factor ~ 100 higher than is observed for other BHBs in the *hard* state. Secondly, the X–ray photon index ($\Gamma \sim 2.2$) is steeper than usual, although it remains flatter than the index seen in in the SPL state ($\Gamma \geq 2.4$) or the hard tail of the TD state ($\Gamma \approx 3$; see Table 4.4). In short, the spectral index for GRS 1915+105 in the *hard* state appears shifted to somewhat high value compared to other BHBs.

Overall, the spectral and temporal properties of Cyg X–1 and GRS 1915+105 are best integrated into the standard description of BH X–ray states if we relax the assumptions regarding the relative or absolute luminosity ranges that are appropriate for the various states. As we will see in §4.5.1, the spectral evolution of XTE J1550–564 motivates a similar conclusion, since the luminosity in the SPL state can lie well below that of the TD state. Undoubtedly, there is an overall correlation between spectral states and luminosity intervals in accreting BHB systems. However, *the canonical X–ray states are most usefully defined in terms of the properties of the energy spectrum and PDS, rather than in terms of luminosity.*

4.3.10 Anomalous behavior of SAX J1819.3–2525

Finally, we consider whether BHBs exhibit characteristics that fall entirely outside the X–ray states considered thus far. The most challenging case may be the BHB SAX J1819.3–2525 (V4641 Sgr; Fig. 4.2). The PCA observations of 1999 September 15.9 show the source in a unique flaring state (Wijnands & van der Klis 2000). The spectral hardness ratio remains remarkably constant throughout the brightest $\sim$500 s of this observation, despite the dramatic intensity fluctuations. The spectrum and PDS for this central time interval are shown in Figure 4.15. The spectral analysis reveals a hot accretion disk and a broad Fe line, while the photon index is extraordinarily hard: $\Gamma = 0.60 \pm 0.03$ with a cutoff energy of 39 keV (Table 4.4). This source is also distinguished as a new prototype for a "fast X–ray nova" (Wijnands & van der Klis 2000) because it exhibited a 12 Crab flare that appeared and decayed in less than 1 day (Fig. 4.2). The multifrequency spectrum near X–ray maximum has been interpreted in terms of super–Eddington accretion with the binary immersed in an extended envelope (Revnivtsev et al. 2002).

4.4 Fast temporal variations: QPOs and broad power peaks

As shown in the preceding sections on X–ray states (§4.3.6–8), QPOs are prevalent in the SPL state, and they are sometimes seen in the *hard* state when thermal emission from the disk contributes some flux above 2 keV (e.g., GRO J1655-40 in Fig. 4.11). In this section we briefly consider the QPOs of BHBs and BHCs in greater detail. For references on PDS computation, defining QPOs, and QPO characteristics of NS systems, see Chapter 2. We supplement this work by discussing X–ray timing results for BHBs. Following van der Klis, we define QPOs as features (usually modeled as a Lorentzian function) in the PDS that have coherence parameter $Q = \nu/\Delta\nu > 2$ (FWHM). Features with significantly lower Q values are regarded as "broad power peaks" and are discussed separately.

4.4.1 Low frequency QPOs and radiation mechanisms

The X–ray PDS of many BH transients display low frequency QPOs (LFQPOs) roughly in the range 0.1 to 30 Hz. The significance of these oscillations can be summarized as follows.

(1) LFQPOs are almost always seen during the SPL state. They can be exceedingly strong (see Figs. 4.13–4.15) with rms amplitudes (expressed as a fraction of the mean count rate) as high as $r > 0.15$ for sources such as GRS 1915+105 (Morgan et al. 1997) and XTE J1550–564 (Sobczak et al. 2000a). More generally, they are seen

Table 4.4. *Spectral Fit Parameters*

X–ray name	N_H (10^{22})	T_{DBB} (keV)	± (keV)	N_{DBB}	±	Γ_{PL}	±	N_{PL}	±	Fe FWHM	N_{Fe}	±	χ^2_ν	additional details
TD State: Figs. 4.8 & 4.9														
4U 1543-475	0.3	1.01	0.02	7419.	165.	2.57	0.02	5.42	0.21	0.61	.0479	.0031	3.62	feature at 4.4 keV
XTE J1550-564	2.0	1.12	0.03	3289.	74.	4.76	0.04	152.	17.	...	...	...	0.98	smedge at 9.2 keV
GRO J1655-40	0.9	1.16	0.03	1559.	21.	2.85	0.23	1.01	0.65	...	...	...	2.00	smedge at 8.0 keV
GX 339-4	0.2	0.71	0.03	2520.	62.	2.02	0.04	0.08	0.01	1.05	.0032	.0003	1.45	
GRS1915+105	6.0	2.19	0.04	62.	5.	3.46	0.02	33.4	1.61	...	...	...	3.13	smedge at 6.7 keV
4U 1630-47	11.0	1.33	0.03	315.	7.	3.75	0.03	17.4	1.40	...	...	...	1.06	break at 20.8 keV to $\Gamma = 1.9$
GRS 1739-278	3.0	0.95	0.04	972.	23.	2.65	0.15	.210	0.008	1.11	.0068	.0008	1.42	
XTE J1748-288	10.4	1.79	0.02	42.4	2.1	2.60	0.02	14.6	0.4	...	...	...	1.18	
XTE J1755-324	0.2	0.75	0.08	1486.	133.	2.40	0.15	0.11	0.04	...	...	...	1.78	
XTE J2012+381	0.8	0.85	0.05	1176.	56.	2.06	0.04	0.16	0.015	...	...	...	1.32	
Hard State: Figs. 4.11 & 4.12														
4U 1543-475	0.3	0.38	0.07	645.	1338.	1.67	0.02	0.041	0.001	...	...		1.57	
XTE J1550-564	2.0	...	...	....	...	1.70	0.10	0.108	0.021	...	...	...	1.13	
GRO J1655-40	0.9	0.77	0.02	228.	37.	1.93	0.02	0.571	0.021	1.00	.0065	.0006	1.83	
GX 339-4	0.2	...	...	....	...	1.75	0.02	0.168	0.028	0.90	.0013	.0003	0.98	plus reflection
GRS1915+105	6.0	...	...	....	...	2.11	0.02	0.231	0.043	0.91	.0458	.0003	2.39	plus reflection
XTE J1118+480	0.01	...	...	....	...	1.72	0.04	0.267	0.024	...	...	...	1.23	
GS 1354-644	0.7	...	...	....	...	1.48	0.09	0.470	0.032	0.1	.0008	.0002	1.15	plus reflection
XTE J1748-288	10.4	0.48	0.05	5302.	479.	1.88	0.09	0.293	0.065	0.66	.0045	.0003	1.65	
GRS 1758-258	1.0	...	...	....	...	1.67	0.07	0.053	0.010	0.36	.0004	.0001	1.84	
Cyg X-1	0.5	...	...	....	...	1.68	0.07	0.446	0.025	1.44	.0206	.0018	3.40	plus reflection
SPL State: Figs. 4.13 & 4.14														
4U 1543-47	0.3	0.93	0.07	3137.	138.	2.47	0.02	6.85	0.21	0.82	.0347	.0034	1.90	
XTE J1550-564	2.0	3.31	0.20	7.76	0.70	2.82	0.05	200.	1.5	1.30	.2136	.0314	2.16	smedge at 8.5 keV
GRO J1655-40	0.9	2.22	0.20	9.89	1.6	2.65	0.05	75.3	1.1	1.32	.2321	.0157	4.45	
GX 339-4	0.2	0.89	0.08	1917.	109.	2.42	0.02	2.34	0.08	0.97	.0178	.0017	1.39	
GRS 1915+105	6.0	1.19	0.07	115.	31.	2.62	0.08	28.5	0.6	0.90	.0396	.0065	4.13	
4U 1630-47	11.0	1.73	0.02	46.0	2.4	2.65	0.02	17.0	0.4	...	...	...	1.10	
GRS 1739-278	3.0	1.01	0.06	1116.	38.	2.61	0.03	2.95	0.19	1.53	.0341	.0021	0.94	
XTE J1748-288	10.4	1.36	0.02	210.	11.	2.92	0.02	26.2	1.2	...	...	...	0.96	
XTE J1859+226	0.5	1.03	0.02	1164.	91.	2.55	0.08	14.5	0.31	1.33	.0426	.0060	1.36	
Cyg X-1	0.5	0.49	0.03	55708.	2962.	2.68	0.03	7.65	0.37	0.73	.0270	.0016	1.78	breaks to $\Gamma = 1.83$ above 12 keV
Unusual Spectra: Fig. 4.15														
XTE J1550-564	2.0	0.74	0.02	6932.	562.	2.24	0.02	23.0	0.87	1.03	.121	.008	1.34	p.l. cutoff energy 51.7 keV
GRS 1915+105	6.0	0.88	0.03	775.	156.	1.91	0.02	4.51	0.18	1.28	.053	.004	1.45	p.l. cutoff energy 50.0 keV
SAX J1819.3-2525	0.3	1.63	0.06	38.	6.	0.59	0.03	0.25	0.02	0.47	.038	.003	1.46	p.l. cutoff energy 39.3 keV

with $0.03 < r < 0.15$ whenever the steep power law contributes more than 20% of the flux at 2–20 keV (Sobczak et al. 2000a). LFQPOs have been observed at energies above 60 keV (Tomsick & Kaaret 2001).

(2) In several sources, the LFQPO frequency is correlated with the total disk flux (but not with temperature or inner disk radius; Sobczak et al. 2000a; Muno et al. 1999; Trudolyubov et al. 1999). This behavior, in combination with the role of the steep power law mentioned directly above, suggests that LFQPOs may provide a vital clue to the mechanism that couples the thermal and SPL components.

(3) LFQPOs can be quasi–stable features that persist for days or weeks. For example, in GRS 1915+105 QPOs at 2.0–4.5 Hz persisted for 6 months during late 1996 and early 1997 (Muno et al. 2001).

(4) In a general sense, it can be argued that oscillations as distinct and strong as these QPOs (often with $Q > 10$), represent global requirements for an organized emitting region. For example, in the context of models in which thermal radiation originates from MHD instabilities, one cannot accept the common picture of numerous and independent magnetic cells distributed throughout the inner disk.

The effort to tie LFQPOs to the geometry and flow of accreting gas is complicated by the fact that LFQPO frequencies are much lower than the Keplerian frequencies for orbits in the inner accretion disk. For example, for a BH mass of 10 $M_{\odot}$, an orbital frequency near 3 Hz coincides with a disk radius near 100 R_g, while the expected radius for maximum X–ray emission lies in the range 1–10 R_g (depending on the value of the BH spin parameter). For the strongest QPOs in GRS 1915+105, the individual oscillations were tracked to determine the origin of frequency drifts and to measure the average "QPO–folded" oscillation profile (Morgan et al. 1997). The results show a random walk in QPO phase and a nearly sinusoidal waveform. The ramifications of these results for QPO models remain uncertain.

There are now a large number of proposed LFQPO mechanisms in the literature, and we mention only a few examples here. The models are driven by the need to account for both the QPO frequency and the fact that the oscillations are strongest at photon energies above 6 keV, i.e., where only the power–law component contributes substantially to the X–ray spectrum. The models include global disk oscillations (Titarchuk & Osherovich 2000), radial oscillations of accretion structures such as shock fronts (Chakrabarti & Manickam 2000), and oscillations in a transition layer between the disk and a hotter Comptonizing region (Nobili et al. 2000). Another alternative, known as the "accretion–ejection instability model," invokes spiral waves in a magnetized disk (Tagger & Pellat 1999) with a transfer of energy out to the radius where material corotates with the spiral wave. This model thereby combines magnetic instabilities with Keplerian motion to explain the observed QPO amplitudes and stability.

Further analyses have revealed phase lags associated with LFQPOs and their harmonics. The analysis technique uses Fourier cross spectra to measure both the phase lags and the coherence parameter (*versus* frequency) between different X–ray energy bands, e.g., 2–6 *vs.* 13–30 keV. Unexpectedly, both positive and negative phase lags have been found (Wijnands et al. 1999; Cui et al. 2000b; Reig et al. 2000; Muno et al. 2001), and efforts have been made to classify LFQPOs by phase lag properties. The expansion of LFQPO subtypes may not be widely viewed as a welcome development. Nevertheless, it has been shown in the case of XTE J1550–564 that the properties of the phase lags clarify how LFQPO parameters correlate with both the accretion–disk and high–frequency QPO parameters (Remillard et al. 2002a).

4.4.2 Broad power peaks and comparisons of BH and NS systems

The study of broad features in the PDS has led recently to important developments. In many NS systems and in the *hard* state of BHBs, the PDS can be decomposed into a set of four or five broad power peaks (Nowak 2000; Belloni et al. 2002), generally with $0.5 < Q < 1.0$. The evolution of these features has been linked to major behavioral changes in Cyg X–1. For example, the disappearance of the third broad power peak occurred just at the time Cyg X–1 left the *hard* state and its steady radio jet was quenched (Pottschmidt et al. 2003).

Broad PDS features are also involved in renewed efforts to contrast accreting BHB and NS systems via their variability characteristics. It has been proposed that the observed high–frequency limit of the power continuum provides a means to distinguish accreting BH and NS systems (Sunyaev & Revnivtsev 2000), since only the latter exhibit intensity variations above 500 Hz.

Finally, some studies have used both QPOs and broad power peaks to examine the relationship between low– and high–frequency features and to make comparisons between different NS subclasses and BHBs. There have been claims of a unified variability scheme that encompasses all X–ray binary types (Psaltis et al. 1999; Belloni et al. 2002). The bottom line of this scheme is that all of the oscillations must originate in the accretion disk. However, important aspects of this work remain controversial, particularly the handling of BH HFQPOs and their association with the lower kHz QPO observed for NSs (Remillard et al. 2002a).

4.4.3 High–frequency QPOs and general relativity

The topic of high–frequency QPOs (HFQPOs) in BHBs (40–450 Hz) continues to evolve in the *RXTE* era. These transient QPOs have been detected in seven sources (4 BHBs and 3 BHCs). HFQPOs have rms amplitudes that are generally ∼1–3% of the mean count rate in a given energy band. Remarkably, three sources exhibit pairs of QPOs that have commensurate frequencies in a 3:2 ratio (Remillard et al. 2002b; Remillard et al. 2003b; Table 4.2). As shown in Figure 4.16, GRO J1655-40 and XTE J1550-564 each exhibit a single such pair of frequencies. GRS 1915+105, on the other hand, shows two pairs of HFQPOs; the complete set of four QPO pairs is shown in Figure 4.16. In addition (see references in Tables 4.2 & 4.3), single–component HFQPOs have been observed in 4U1630–47 (184 Hz), XTE J1859+226 (190 Hz), XTE J1650–500 (250 Hz), and H 1743–322 (240 Hz). Their profiles are similar to the 300 Hz QPO for GRO J1655–40 shown in the top left panel of Figure 4.16. HFQPOs occur in the SPL state, except for the 67 Hz QPO in GRS 1915+105 (see Fig. 4.16) which appears in the TD state, especially when $L_x > 10^{38}$ erg s^{-1}.

The preponderance of evidence indicates that HFQPOs do not shift freely in frequency in response to luminosity changes, as do the kHz QPOs in NS systems (see Ch. 2). Instead, they appear to exhibit an "X–ray voiceprint". That is, the QPOs occur in harmonics of an unseen fundamental frequency which has a unique value for each BH. For the three cases that show 3:2 frequency pairs, the relationship between

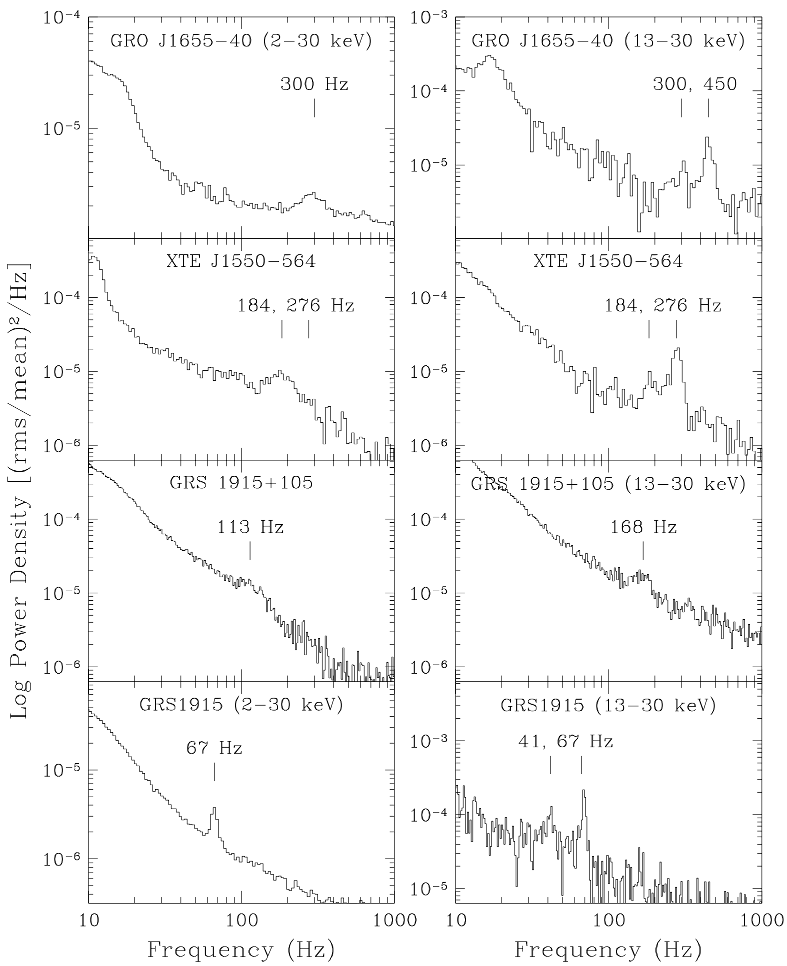

Fig. 4.16. Four pairs of HFQPOs observed in three black–hole binary systems. The energy band is 6–30 keV unless otherwise indicated. These usually subtle oscillations are only visible during a fraction of the observations for each source.

the HFQPO frequencies *vs.* BH mass scales as M_1^{-1}. This relationship is shown in Figure 4.17, where we have plotted the frequency of the stronger feature (i.e. $2 \times \nu_0$), since the fundamental is generally not seen. These results offer strong encouragement for seeking interpretations of BH HFQPOs via GR theory, since each type of GR disk oscillation under strong gravity varies as M_1^{-1}, assuming the sampled BHs have similar values of the dimensionless spin parameter (a_*).

These commensurate frequencies can be seen as strong support for the idea that HFQPOs may represent some type of resonance phenomenon involving oscillations describable by GR, as originally proposed by Abramowicz & Kluzniak (2001). Res-

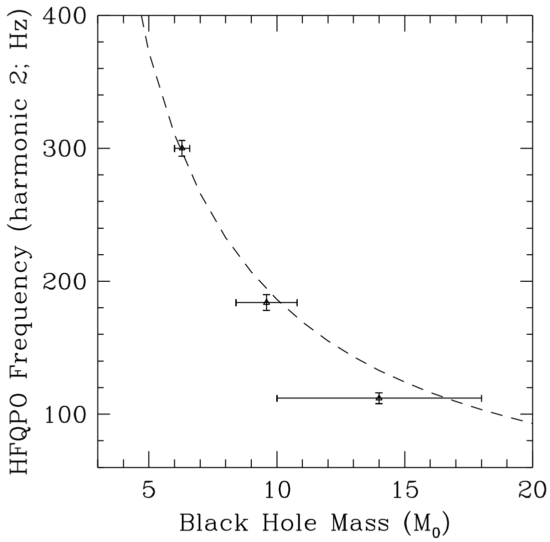

Fig. 4.17. Relationship between HFQPO frequency and BH mass for XTE J1550–564, GRO J1655–40, and GRS 1915+105. These three systems display a pair of HFQPOs with a 3:2 frequency ratio. The frequencies are plotted for the stronger QPO that represents $2 \times \nu_0$. The fundamental is generally not seen in the power spectra. The dashed line shows a relation, ν_0 (Hz) = 931 $(M/M_\odot)^{-1}$, that fits these data.

onances in some form may be applicable to both BH and NS systems (Abramowicz et al. 2003). We note that the 3:2 harmonic pattern cannot be attributed to a distorted sine wave with harmonic content because the individual detections (in a given energy band, on a given day) generally appear as a single peak in the PDS, and the presence of a pair of commensurate frequencies is recognized only when the ensemble of results is examined.

Coordinate frequencies and their differences (i.e., beat frequencies) in GR were proposed earlier to explain some of the X-ray QPOs from both NSs and BHs (Stella et al. 1999); however, this work did not treat the commensurate frequencies of interest here, which were discovered subsequently in three BHB systems. In the resonance hypothesis (Abramowicz & Kluzniak 2001), these harmonic frequencies are discussed in terms of accretion blobs following perturbed orbits in the inner accretion disk. Unlike Newtonian gravity, GR predicts independent oscillation frequencies for each spatial coordinate for orbits around a rotating compact object, as seen from the rest frame of a distant observer. Over the range of radii in the accretion disk where X–rays are expected to originate in the standard disk model, pairs of GR coordinate frequencies have varying, non–integral ratios. Therefore, the discovery of HFQPOs with commensurate frequencies can be seen to suggest enhanced emissivity at a particular radius where a pair of coordinate frequencies are in some type of resonance. Unlike the azimuthal and polar coordinate frequencies, the radial coordinate frequency reaches a maximum value and then falls to zero as the radius decreases toward $R_{\rm ISCO}$ (Kato 2001; Merloni et al. 2001). This ensures the possibility of commensurate coordinate frequencies somewhere in the inner disk. For example, there is a wide range in the dimensionless spin parameter, a_*, where one can find a particular radius that corresponds to a 2:1, 3:1, or 3:2 ratio in the orbital and radial coordinate frequencies. A resonance between the polar and radial coordinate frequencies is also possible. In the resonance scenario, linear perturbations may grow at these radii, ultimately producing X–ray oscillations that represent some combination of the individual resonance frequencies, their sum, or their difference. However, there remain serious uncertainties as to whether such structures could overcome the severe damping forces and emit X–rays with sufficient amplitude and coherence to produce the observed HFQPOs (Markovic & Lamb 1998).

Models for "diskoseismic" oscillations adopt a more global view of the inner disk as a GR resonance cavity (Kato & Fukue 1980; Wagoner 1999). This paradigm has certain attractions for explaining HFQPOs, but integral harmonics are not predicted for the three types of diskoseismic modes derived for adiabatic perturbations in a thin accretion disk. Clearly, there is a need to investigate further the possibility of resonances within the paradigm of diskoseismology. Other models must be considered as well, e.g. the p-mode oscillations of an accretion torus surrounding a black hole (Rezzolla et al. 2003).

It has been argued by Strohmayer (2001a) that HFQPO frequencies are sufficiently high that they require substantial BH spin. For example, in the case of GRO 1655–40 the 450 Hz frequency exceeds the maximum orbital frequency (ν_ϕ) at the ISCO around a Schwarzschild BH (i.e., $a_* = 0$; §4.1.5) of mass $M_1 = 6.3 \pm 0.5\ M_\odot$ (Greene et al. 2001). *If* the maximum Keplerian frequency is the highest frequency at which a QPO can be seen, then the results for GRO J1655–40 require a Kerr BH with prograde spin, for example, $a_* > 0.15$. However, the conclusion that spin is required may not be valid if the QPO represents the sum of two beating frequencies. On the other hand, even higher values of the spin parameter may be required if the QPO represents either resonant coordinate frequencies ($a_* > 0.3$; Remillard et al. 2002b) or diskoseismic oscillations ($a_* > 0.9$; Wagoner et al. 2001).

Accurate and sensitive measurements of X–ray HFQPO frequencies may lead to a determination of the GR mechanism that is responsible for these oscillations, and ultimately to secure measurements of the spin parameter a_* for a number of BHs. These spin measurements would be very valuable in assessing the role of BH rotation in the production of jets (Blandford & Znajek 1977). This is especially true since the three systems with paired frequencies have a history of relativistic mass ejections during some (but not all) of their outbursts.

4.5 Energetics and key variables determining BHB radiation

4.5.1 Division of spectral energy: disk and power–law components

A revealing view of the behavior of a BHB over the course of its entire outburst cycle can be obtained by plotting the flux in the power–law component vs. the flux from the accretion disk. Four such plots are shown in Figure 4.18, where the various plotting symbols identify the emission states described in §4.3. The figure shows the flux diagrams for 3 BHBs, while considering two of the outbursts of XTE J1550–564 (Muno et al. 1999; Remillard et al. 2001; Remillard et al. 2002b).

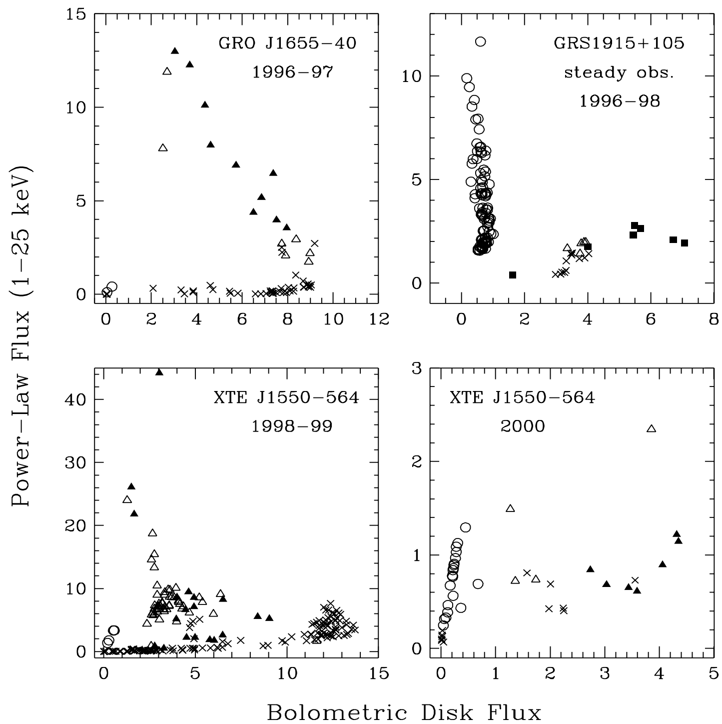

Fig. 4.18. Radiation energy division between the accretion disk and the power–law component. The symbol types denote the X–ray state as TD (x), *hard* (∘), or SPL(Δ). Furthermore, in the SPL state, an open triangle is used when there is only an LFQPO, while a filled triangle denoted the additional presence of an HFQPO. Finally, the TD–like observations that show 67 Hz QPOs in GRS 1915+105 are shown with a filled square. All fluxes are in units of 10^{-8} erg cm^{-2} s^{-1} and corrected for absorption.

It has been shown that the emerging patterns in these flux diagrams are largely unaffected by the choice of integration limits, e.g., whether the energy measurements are computed in terms of bolometric flux or the integrated flux within the 2–25 keV PCA bandpass (Remillard et al. 2002a).

The TD points ("x" symbol; Fig. 4.18) for GRO J1655–40 and XTE J1550–564 (1998–99) appear well organized; they can be described as horizontal tracks in which accretion energy is freely converted to thermal radiation from the accretion disk. These tracks correspond to the standard accretion disk model (Shakura & Sunyaev 1973), and they may also convey moderate Comptonization effects expected from MHD turbulence (e.g., Hawley & Krolik 2001) as these tracks curve upward at high luminosity. The TD points at the highest flux levels correspond to Eddington luminosities of 0.2 for GRO J1655–40, 0.6 for XTE J1550–564 (1998–99), and 0.4 for GRS 1915+105, using the values for mass and distance given in Tables 4.1 & 4.2.

Observations in the *hard* state (i.e., a dominant power–law component with $1.4 < \Gamma < 2.2$) are plotted as circles in Figure 4.18. These points form vertical tracks with only minor flux contributions from the disk. The *hard*–state points coincide with fairly steady radio emission for GRS1915+105 (Muno et al. 2001) and XTE J1550–564 in 2000 (Corbel et al. 2001), as expected for this state.

Observations in the SPL state (defined by a power–law index $\Gamma > 2.4$ and by QPOs) are plotted as triangles in Figure 4.18; a solid symbol is used when there is an additional detection of an HFQPO above 100 Hz. The wide diversity in the relative contributions from the disk and power–law components within the SPL state are especially apparent for XTE J1550–564. It is these results, combined with the wide range in the luminosities of the TD and *hard* tracks shown in Figure 4.18, that have caused us to abandon the luminosity requirements in defining the X–ray states of BHBs (§4.3). Finally, detections of the 67 Hz QPO in GRS 1915+105 are shown as filled squares. They appear to extend the TD branch out to 0.6 L_{Edd}.

4.5.2 Key variables determining BHB radiation

Prior to the *RXTE* era, it was thought that the X–ray states primarily represent a simple progression in luminosity, and that the emission properties depend only on the accretion rate and the BH mass (e.g., Tanaka & Lewin 1995). The behavioral complexity of sources such as XTE J1550–564 (Fig. 4.18) have challenged this viewpoint (Homan et al 2001; Remillard et al. 2002b) because it now appears that any of the three active states of accretion may occur at a given luminosity.

Finally, what other parameters must be considered in the theory of BH accretion? It is clear that BH spin and the angle between the spin and disk axes must also be considered in a complete theory of BH accretion, but these would not help to explain the types of rapid state transitions seen in many systems. As noted in several previous sections, MHD instabilities are widely invoked to explain nonthermal radiation, and magnetic fields are additionally expected to play a leading role in the formation and collimation of jets. It then seems relevant to question whether a parameter of magnetism, such as the ratio of magnetic to gas pressure, should be considered a key variable in accretion physics. The global magnetic field geometry may also play an essential role in the formation of some X-ray states. The continued development of 3–D MHD simulations are expected to be very fruitful in gaining a deeper understanding of the radiation emitted by black hole binaries.

4.6 Concluding remarks

As reviewed in §4.4.3, high frequency QPOs at 40–450 Hz have been observed with *RXTE* for four BHBs and three BHCs. Furthermore, three of these sources show harmonic (3:2) pairs of frequencies that scale as M_{BH}^{-1}. The models for these QPOs (e.g., orbital resonance and diskoseismic oscillations) invoke strong–field GR effects in the inner accretion disk, and they depend on both the mass and spin of the BH. On the other hand, studies of broadened Fe Kα emission lines (§4.2.3), which can also reveal the conditions in the very inner accretion disk, may prove as revealing as timing studies. The line photons that reach a distant observer are gravitationally redshifted and Doppler and transverse–Doppler shifted. Encoded in the line profile are the mass and spin of the BH. The most provocative result has been obtained for the BHC XTE J1650–500 (§4.2.3), where the line profile suggests the presence of an extreme Kerr BH.

The behavior of the massive compact objects reviewed herein supports the view that they are bona fide BHs, which are described by GR and were formed by the complete gravitational collapse of matter. Our challenge is to prove that this conclusion is correct by making clean quantitative measurements of relativistic effects in the strong gravitational fields near these objects. At present, no one can say which future mission can best help us meet this challenge: LISA, MAXIM, Constellation–X, or an X–ray Timing Observatory (XTO). Perhaps all of the approaches will be required. In any case, an XTO with effective area and telemetry ten times that of *RXTE* and with improved energy resolution, would be a powerful probe of physics near the event horizon. Consider that *RXTE* with just 1.6 times the effective area of *Ginga*, broke through to discover kHz QPOs in NSs, a discovery that led quickly to hard constraints on dense matter.

Acknowledgments

We thank Jon Miller, Mike Muno, David Smith, Jean Swank, John Tomsick, and Rudy Wijnands for their help in assembling the catalogue of candidate BHBs presented in Table 4.3, and Keith Arnaud, George Field, Mike Garcia, Aya Kubota, Kazuo Makishima, and Mike Revnivtsev for valuable comments. We are indebted to Andy Fabian, Jon Miller, Ramesh Narayan, Jerry Orosz and Andrej Zdziarski for a careful reading of portions of the manuscript and their valuable comments. We are especially grateful to Jeroen Homan and John Tomsick for their detailed comments on a near–final draft of the manuscript. We thank Ann Esin for supplying Figure 4.1, Jon Miller for supplying Figure 4.6, John Tomsick and Emrah Kalemci for the use of unpublished data on 4U1543–47, John Huchra for advice on the distance to the LMC, and Suresh Kumar for his assistance in typesetting the manuscript. This work was supported in part by NASA under Grants NAG5–10813 and by the NASA contract to M.I.T. for support of *RXTE*.

References

Abramowicz, M.A. (1998) in *Theory of Black Hole Accretion Discs*, eds. M.A. Abramowicz, G. Bjornsson and J.E. Pringle (Cambridge U. Press, Cambridge), 50–60
Abramowicz, M.A., Karas, V. and Kluzniak, W., et al. (2003), PASJ **55**, 467–471
Abramowicz, M.A. and Kluzniak, W. (2001), A&A **374**, L19–L20
Agol, E. and Krolik, J.H. (2000), ApJ **528**, 161–170
Agol, E., Kamionkowski, M., Koopmans, L.V.E. and Blandford, R.D. (2002), ApJ **576**, L131–L135
Arnaud, K. and Dorman, B. (2002), XSPEC (An X–ray Spectral Fitting Package), version 11.2x (NASA/GSFC/HEASARC, Greenbelt)
Augusteijn, T., Kuulkers, E. and van Kerkwijk, M.H. (2001), ApJ **375**, 447–454
Baganoff, F.K., Bautz, M.W., Brandt, W.N., et al. (2001), Nature **413**, 45–48
Bahcall, J. N. (1986), ARA&A **24**, 577–611
Ball, L., Kesteven, M.J., Campbell–Wilson, D., et al. (1995), MNRAS **273**, 722–730
Balucinska–Church, M. and Church M.J. (2000), MNRAS **312**, L55–L59
Barr, P., White, N.E. and Page, C.G. (1985), MNRAS **216**, 65P–70P
Barret, D., Grindlay, J.E., Bloser, P.F., et al. (1996a), IAU Circ. 6519
Barret, D., McClintock, J.E. and Grindlay, J.E. (1996b), ApJ **473**, 963–973
Barret, D., Olive, J.F. and Boirin, L. (2000), ApJ **533**, 329–351
Barret, D., Roques, J.P., Mandrou, P., et al. (1992), ApJ **392**, L19–L22
Belloni, T., Klein-Wolt, M., Mendez, M., et al. (2000), A&A **355**, 271–290
Belloni, T., Mendez, M., van der Klis, M., et al. (1999), ApJ **519**, L159–L163

Belloni, T., Psaltis, D. and van der Klis, M. (2002), ApJ, **572**, 392–406
Belloni, T., van der Klis, M., Lewin, W.H.G., et al. (1997), A&A **322**, 857–867
Blandford, R.D. (2002), to appear in *Lighthouses of the Universe*, eds. M. Gilfanov, R. Sunyaev, et al. (Springer, Berlin), (astro–ph 0202265)
Blandford, R.D. and Begelman, M.C. (1999), MNRAS **303**, L1–L5
Blandford, R.D. and Znajek, R.L. (1977), MNRAS **179**, 433–456
Bolton, C.T. (1972), Nature **240**, 124–126
Borozdin, K.N., Aleksandrovich, N.L., Aref'ev, V.A., et al. (1995), AstL **21**, 212–216
Borozdin, K.N., Revnivtsev, M.G., Trudolyubov, S.P., et al. (1998), AstL **24**, 435–444
Boyd, P.T., Smale, A.P., Homan, J., et al. (2000), ApJ **542**, L127–L130
Bradt, H., Levine, A.M., Remillard, R.A. and Smith, D.A. (2001), MmSAI **73**, 256–271
Bradt, H.V.D. and McClintock, J.E. (1983), ARA&A **21**, 13–66
Branduardi, G., Ives, J.C., Sanford, P.W., et al. (1976), MNRAS **175**, 47P–56P
Brocksopp, C., Fender, R. P., Larionov, V., et al. (1999), MNRAS **309**, 1063–1073
Brocksopp, C., Fender, R.P., McCollough, M., et al. (2002), MNRAS **331**, 765–775
Brocksopp, C., Jonker, P.G., Fender, R.P., et al. (2001), MNRAS **323**, 517–528
Bronfman, L., Cohen, R.S., Alvarez, H., et al. (1988), ApJ **324**, 248–266
Brown, G.E. and Bethe, H.A. (1994), ApJ **423**, 659–664
Brown, G.E., Lee, C.-H, Wijers, R.A.M.J. and Bethe, H.A. (2000a), Phys. Rep. **333–334**, 471–504
Brown, G.E., Lee, C.-H., Wijers, R.A.M., et al. (2000b), NewA **5**, 191–210
Campana, S., Stella, L., Belloni, T., et al. (2002), A&A **384**, 163–170
Cannizzo, J.K. (1993), ApJ **419**, 318–336
Casares, J., Charles, P.A. and Marsh, T.R. (1995), MNRAS **277**, L45–L50
Casares, J. and Charles, P.A. (1994), MNRAS **271**, L5–L9
Casares, J., Charles, P.A., Naylor, T. and Pavlenko, E.P. (1993), MNRAS **265**, 834–852
Chakrabarti, S.K. and Manickam, S.G. (2000), ApJ **531**, L41–L44
Chaty, S., Mignani, R.P. and Israel, G.L. (2002), MNRAS **337**, L23–L26
Chen, W., Shrader, C.R. and Livio, M. (1997), ApJ **491**, 312–338
Churazov, E., Gilfanov, M. and Revnivtsev, M. (2001), MNRAS **321**, 759
Churazov, E., Gilfanov, M., Sunyaev, R., et al. (1993), ApJ **407**, 752–757
Coe, M.J., Engel, A.R. and Quenby, J.J. (1976), Nature **259**, 544–545
Cooke, B.A., Levine, A.M., Lang, F.L., et al. (1984), ApJ **285**, 258–263
Corbel, S., Fender, R.P., Tzioumis, A.K., et al. (2000), A&A **359**, 251–268
Corbel, S., Fender, R.P., Tzioumis, A.K., et al. (2002), Science **298**, 196–199
Corbel, S., Kaaret, P., Jain, R.K., et al. (2001), ApJ **554**, 43–48
Corbel, S., Nowak, M.A., Fender, R.P., et al. (2003), A&A, **400**, 1007–1012
Cowley, A.P., Crampton, D. and Hutchings, J.B. (1987), AJ **92**, 195–199
Cowley, A.P., Crampton, D., Hutchings, J.B., et al. (1983), ApJ **272**, 118–122
Cowley, A.P., Schmidtke, P.C., Anderson, A.L. and McGrath, T.K. (1995), PASP **107**, 145–147
Cowley, A.P., Schmidtke, P.C., Ebisawa, K., et al. (1991), ApJ **381**, 526–533
Cui, W., Heindl, W.A., Swank, J.H., et al. (1997a), ApJ **487**, L73–L76
Cui, W., Schulz, N.S., Baganoff, F.K., et al. (2001), ApJ **548**, 394–400
Cui, W., Shrader, C.R., Haswell, C.A. and Hynes, R.I. (2000a), ApJ **535**, L123–L127
Cui, W., Zhang, S.N. and Chen, W. (2000b), ApJ **531**, L45–L48
Cui, W., Zhang, S.N., Focke, W. and Swank, J.H. (1997b), ApJ **484**, 383–393
Dal Fiume, D., Frontera, F., Orlandini, M., et al. (1999), IAU Circ. 7291
Davies, R.D., Walsh, D. and Browne, I.W.A., et al. (1976), Nature **261**, 476–478
Dhawan, V., Mirabel, I.F. and Rodriguez, L.F. (2000), ApJ **543**, 373–385
Dieters, S.W., Belloni, T., Kuulkers, E., et al. (2000), ApJ **538**, 307–314
di Matteo, T., Celotti, A. and Fabian, A.C. (1999), MNRAS **304**, 809–820
Di Salvo, T., Done, C., Zycki, P.T., et al. (2001), ApJ **547**, 1024–1033
Done, C. and Nayakshin, S. (2001), MNRAS **328**, 616–622
Done, C., Mulchaey, J.S., Mushotzky, R.F. and Arnaud, K.A. (1992), ApJ **395**, 275-288
Done, C. and Zycki, P.T. (1999), MNRAS **305**, 457–468
Dove, J.B., Wilms, J. and Begelman, M.C. (1997a), ApJ **487** 747–758
Dove, J.B., Wilms, J., Maisack, M. and Begelman, M.C. (1997b), ApJ **487**, 759–768
Dubus, G., Hameury, J.-M and Lasota, J.-P. (2001), A&A **373**, 251–271

Ebisawa, K., Makino, F., Mitsuda, K., et al. (1993), ApJ **403**, 684–689
Ebisawa, K., Mitsuda, K. and Inoue, H. (1989), PASJ **41**, 519–530
Ebisawa, K., Mitsuda, K. and Tomoyuki, H. (1991), ApJ **367**, 213–220
Ebisawa, K., Ogawa, M., Aoki, T., et al. (1994), PASJ **46**, 375–394
Elvis, M., Page, C.G., Pounds, K.A., et al. (1975), Nature **257**, 656–657
Esin, A.A., McClintock, J.E. and Narayan, R. (1997), ApJ **489**, 865–889
Esin, A.A., McClintock, J.E., Drake, J.J., et al. (2001), ApJ **555**, 483–488
Esin, A.A., Narayan, R., Cui, W., et al. (1998), ApJ **505**, 854–868
Fabbiano, G., Zezas, A. and Murray, S.S. (2001), ApJ **554**, 1035–1043
Fabian, A.C., Iwasawa, K., Reynolds, C.S. and Young, A.J. (2000), PASP **112**, 1145–1161
Fabian, A.C., Rees, M.J., Stella, L. and White, N.E. (1989), MNRAS **238**, 729–736
Falcke, H. and Biermann, P.L. (1995), A&A **293**, 665–682
Fender, R.P. (2001), MNRAS, **322**, 31–42
Fender, R., Corbel, S., Tzioumis, T., et al. (1999a), ApJ **519**, L165–L168
Fender, R.P., Garrington, S.T., McKay, D.J., et al. (1999b), MNRAS **304**, 865–876
Fender, R.P., Hjellming, R.M., Tilanus, R.P.J., et al. (2001), MNRAS **322**, L23–L27
Feng, Y.X., Zhang, S.N., Sun, X., et al. (2001), ApJ **553**, 394–398
Field, G.B. and Rogers, R.D. (1993), ApJ **403**, 94–109
Filippenko, A. V., Matheson, T. and Ho, L.C. (1995a), ApJ **455**, 614–622
Filippenko, A.V. and Chornock, R. (2001), IAU Circ. 7644
Filippenko, A.V., Leonard, D.C., Matheson, T., et al. (1999), PASP **111**, 969–979
Filippenko, A.V., Matheson, T. and Barth, A.J. (1995b), ApJ **455**, L139–L142
Filippenko, A.V., Matheson, T., Leonard, D.C., et al. (1997), PASP **109**, 461–467
Freedman, W.L., Madore, B.F., Gibson, B.K., et al. (2001), ApJ **553**, 47–72
Frontera, F., Amati, L., Zdziarski, A.A., et al. (2003), ApJ **592**, 1110-1118
Frontera, F., Palazzi, E., Zdziarski, A. A., et al. (2001a), ApJ **546**, 1027–1037
Frontera, F., Zdziarski, A. A., Amati, L., et al. (2001b), ApJ **561**, 1006–1015
Fryer, C. and Kalogera V. (2001), ApJ **554**, 548–560
Garcia, M.R., McClintock, J.E., Narayan, R., et al. (2001), ApJ **553**, L47–L50
Gelino, D.M., Harrison, T.E. and McNamara, B.J. (2001a), AJ **122**, 971–978
Gelino, D.M., Harrison, T.E. and Orosz, J.A. (2001b) AJ **122**, 2668–2678
George, I.M. and Fabian, A.C. (1991), MNRAS **249**, 352–367
Gierlinski, M., Maciolek–Niedzwiecki, A. and Ebisawa, K. (2001), MNRAS **325**, 1253–1265
Gierlinski, M., Zdziarski, A.A., Poutanen, J., et al. (1999), MNRAS **309**, 496–512
Gies, D.R. and Bolton, C.T. (1982), ApJ **260**, 240–248
Goldoni, P., Vargas, M., Goldwurm, A., et al. (1999), ApJ **511**, 847–851
Greene, J., Bailyn, C.D. and Orosz, J.A. (2001), ApJ **554**, 1290–1297
Greiner, J., Cuby, J.G. and McCaughrean, M.J (2001a), Nature **414**, 522–525
Greiner, J., Cuby, J.G., McCaughrean, M.J., et al. (2001b), A&A **373**, L37–L40
Greiner, J., Dennerl, K. and Predehl, P. (1996), A&A **314**, L21–L24
Groot, P., Tingay, S., Udalski, A. and Miller, J. (2001), IAU Circ. 7708
Grove, J.E., Johnson, W.N., Kroeger, R.A., et al. (1998), ApJ **500**, 899–908
Gursky, H., Bradt, H., Doxsey, R., et al. (1978), ApJ **223**, 973–978
Haardt, F. and Maraschi, L. (1991), ApJ **380**, L51–L54
Hameury, J.-M., Barret, D., Lasota, J.-P., et al. (2003), A&A **399**, 631–637
Hameury, J.-M., Lasota, J.-P., McClintock, J.E. and Narayan, R. (1997), ApJ **489**, 234–243
Han, X. and Hjellming, R.M. (1992), ApJ **400**, 304–314
Hannikainen, D., Campbell–Wilson, D., Hunstead, R., et al. (2001), ApSSS **276**, 45–48
Hannikainen, D.C., Hunstead, R.W., Campbell–Wilson, D., et al. (2000), ApJ **540**, 521–534
Harlaftis, E.T., Horne, K. and Filippenko, A.V. (1996), PASP **108**, 762–771
Hawley, J.F. and Krolik, J.H. (2001), ApJ **548** 348–367
Hjellming, R.M. and Rupen, M.P. (1995), Nature **375**, 464–468
Hjellming, R.M., Calovini, T.A. and Han, X.H. (1988), ApJ **335**, L75–L78
Hjellming, R.M., Rupen, M.P. and Mioduszewski, A.J. (1998a), IAU Circ. 6924
Hjellming, R.M., Rupen, M.P. and Mioduszewski, A.J. (1998b), IAU Circ. 6934
Hjellming, R.M., Rupen, M.P., Hunstead, R.W., et al. (2000), ApJ **544**, 977–992
Hjellming, R.M., Rupen, M.P., Mioduszewski, A.J., et al. (1999), ApJ **514**, 383–387

Homan, J., Klein–Wolt, M., Rossi, S., et al. (2003a), ApJ **586**, 1262–1267
Homan, J., Miller J.M., Wijnands, R., et al. (2003b), ATEL 162
Homan, J., Wijnands, R., van der Klis, M., et al. (2001), ApJS **132**, 377–402
Humphrey, P.J., Fabbiano, G., Elvis, M., et al. (2003), MNRAS, in press (astro–ph/0305345)
Hutchings, J.B., Crampton, D., Cowley, A.P., et al. (1987), AJ **94**, 340–344
Hynes, R.I., Roche, P., Charles, P.A and Coe, M.J. (1999), MNRAS **305**, L49–L53
Hynes, R.I., Steeghs, D., Casares, J., et al. (2003), ApJ **583**, L95–L98
Igumenshchev, I.V. and Abramowicz, M.A. (1999), MNRAS **303**, 309–320
in't Zand, J.J.M., Markwardt, C.B., Bazzano, A., et al. (2002a), A&A **390**, 597–609
in't Zand, J.J.M., Miller, J.M., Oosterbroeck, T. and Parmar, A.N. (2002b), A&A **394**, 553–560
Israelian, G., Rebolo, R., Basri, G. (1999), Nature **401**, 142–144
Jones, C., Forman, W., Tananbaum, H. and Turner, M.J.L. (1976), ApJ **210**, L9–L11
Kalemci, E., Tomsick, J.A., Rothschild, R.E., et al. (2002) ApJ **586**, 419–426
Kalogera, V. and Baym, G. (1996), ApJ **470**, L61–L64
Kaluzienski, L.J., Holt, S.S., Boldt, E.A., et al. (1975), ApJ **201**, L121–L124
Kato, S. (2001), PASJ **53**, 1–24
Kato, S. and Fukue, J. (1980), PASJ **32**, 377–388
Kato, S., Fukue, J. and Mineshige, S. (1998), *Black–Hole Accretion Disks* (Kyoto U. Press, Japan)
Kawaguchi, T., Shimura, T. and Mineshige, S. (2000), NewAR **44**, 443–445
Kennea, J.A. and Skinner, G.K. (1996), PASJ **48**, L117–L117
King, A.R., Davies, M.B., Ward, M.J., et al. (2001), ApJ **552**, L109–L112
Kitamoto, S., Tsunemi, H., Pedersen, H., et al. (1990), ApJ **361**, 590–595
Klein–Wolt, M., Fender, R.P., Pooley, G.G., et al. (2002), MNRAS **331**, 745–764
Kong, A.K.H., Charles, P.A., Kuulkers, E. and Kitamoto, S. (2002), MNRAS **329**, 588–596
Kong, A.K.H., McClintock, J.E., Garcia, M.R., et al. (2002), ApJ **570**, 277–286
Kotani, T., Kawai, N., Nagase, F., et al. (2000), ApJ **543**, L133–L136
Kubota, A. and Makishima, K. 2003, ApJ, submitted
Kubota, A., Makishima, K. and Ebisawa, K. (2001), ApJ **560**, L147–L150
Kuulkers, E., Fender, R.P., Spencer, R.E., et al. (1999), MNRAS **306**, 919–925
Kuulkers, E., Wijnands, R., Belloni, T., et al. (1998), ApJ **494**, 753–758
Laor, A. (1991), ApJ **376**, 90–94
Lasota, J.-P. (2001), NewAR **45**, 449–508
Levine, A.M., Bradt, H., Cui, W., et al. (1996), ApJ **469**, 33–36
Ling, J.C., Mahoney, W.A., Wheaton, Wm.A. and Jacobson, A.S. (1987), ApJ **321**, L117–L122
Ling, J.C., Wheaton, Wm.A., Wallyn, P., et al. (2000), ApJS **127**, 79–124
Liu, B.F., Mineshige, S. and Shibata, K. (2002), ApJ **572**, L173–L176
Liu, Q.Z., van Paradijs, J. and van den Heuvel, E.P.J. (2001), A&A **368**, 1021–1054
Liu, Q.Z., van Paradijs, J. and van den Heuvel, E.P.J. (2000), A&As **147**, 25–49
Loewenstein, M., Mushotzky, R.F., Angelini, L., et al. (2001), ApJ **555**, L21–L24
Lowes, P., in 't Zand, J.J.M., Heise, J., et al. (2002), IAU Circ. 7843
Lynden–Bell, D. and Pringle, J.E. (1974), MNRAS **168**, 603–637
Makishima, K., Kubota, A, Mizuno, T., et al. (2000), ApJ **535**, 632–643
Makishima, K., Maejima, Y., Mitsuday, K., et al. (1986), ApJ **308**, 635–643
Malzac, J., Belloni, T., Spruit, H.C. and Kanbach, G. (2003), A&A, in press, (astro-ph/0306256)
Mandelbrot, B. B. (1999), *Multifractals and 1/f Noise: Wild Self-Affinity in Physics* (Springer-Verlag: Heidelberg)
Margon, B., Thorstensen, J.R. and Bowyer, S. (1978), ApJ **221**, 907–911
Markert, T.H., Canizares, C.R., Clark, G.W., et al. (1973), ApJ **184**, L67–L70
Markoff, S., Falcke, H. and Fender, R. (2001), A&A **372**, L25–L28
Markovic, D. and Lamb, F.K. (1998), ApJ **507**, 316–326
Markwardt, C. (2001), ApSS **276**, 209–212
Markwardt, C.B. and Swank, J.H. (2003), IAU Circ. 8056
Marsh, T.R., Robinson, E.L. and Wood, J.H. (1994), MNRAS **266**, 137–154
Marti, J., Mirabel, I.F., Chaty, S. and Rodriguez, L.F. (2000), A&A **363**, 184–187
Marti, J., Mirabel, I.F., Duc, P.-A. and Rodriguez, L.F. (1997), A&A **323**, 158–162
Marti, J., Mirabel, I.F., Rodriguez, L.F. and Smith, I A. (2002), A&A **386**, 571–575
Martocchia, A., Matt, G., Karas, G., et al. (2002), A&A **387**, 215–221

Matt, G., Perola, G.C. and Piro, L. (1991), A&A **247**, 25–34
Mendez, M. and van der Klis, M. (1997), ApJ **479**, 926–932
McClintock, J.E., Garcia, M.R., Caldwell, N., et al. (2001a), ApJ **551**, L147–L150
McClintock, J.E., Haswell, C.A., Garcia, M.R., et al. (2001b), ApJ **555**, 477–482
McClintock, J.E., Horne, K. and Remillard, R.A. (1995), ApJ **442**, 358–365
McClintock, J.E., Narayan, R., Garcia, M.R., et al. (2003a), ApJ, in press (astro-ph/0304535)
McClintock, J.E. and Remillard, R.A. (1986), ApJ **308**, 110–122
McClintock, J.E. and Remillard, R.A. (2000), ApJ **531**, 956–962
McConnell, M.L., Zdziarski, A.A., Bennett, K., et al. (2002), ApJ **572**, 984–995
McKinney, J.C. and Gammie, C.F. (2002), ApJ **573**, 728–737
Menou, K., Esin, A.A., Narayan, R., et al. (1999), ApJ **520**, 276–291
Mendez, M. and van der Klis, M. (1997), ApJ **479**, 926–932
Merloni, A. and Fabian, A.C. (2001a), MNRAS **321**, 549–552
Merloni, A. and Fabian, A.C. (2001b), MNRAS **328**, 958–968
Merloni, A. and Fabian, A.C. (2002), MNRAS **332**, 165–175
Merloni, A., Fabian, A. C. and Ross, R. R. (2000), MNRAS **313**, 193–197
Merloni, A., Vietri, M., Stella, L. and Bini, D. (2001), MNRAS **304**, 155–159
Meyer, F., Liu, B.F. and Meyer–Hofmeister, E. (2000), A&A **361**, 175–188
Miller, J. M., Fabbiano, G., Miller, M.C., and Fabian, A. C. (2003a), ApJ 585, L37–L40
Miller, J.M., Fabian, A.C., in't Zand, J.J.M., et al. (2002a), ApJ **577**, L15–L18
Miller, J.M., Fabian, A.C., Wijnands, R., et al. (2002b), ApJ **570**, L69–L73
Miller, J.M., Fabian, A.C., Wijnands, R., et al. (2002c), ApJ **578**, 348–356
Miller, J.M., Fox, D.W., Di Matteo, T., et al. (2001), ApJ **546**, 1055–1067
Miller, J.M., Wijnands, R., Rodriguez–Pascual, P.M., et al. (2002d), ApJ **566**, 358–364
Miller, J. M., Zezas, A., Fabbiano, G. and Schweizer, F. (2003b), ApJ, submitted (astro-ph/0302535)
Mirabel, I.F. and Rodriguez, L.F. (1994), Nature **371**, 46–48
Mirabel, I.F. and Rodriguez, L.F. (1999), ARA&A **37**, 409–443
Mirabel, I.F. and Rodriguez, L.F. (2003), Science **300**, 1119–1120
Mirabel, I.F., Rodriguez, L.F. and Cordier, B. (1993), IAU Circ. 5876
Mitsuda, K., Inoue, H., Koyama, K., et al. (1984), PASJ **36**, 741–759
Miyamoto, S., Iga, S., Kitamoto, S. and Kamado, Y. (1993), ApJ **403**, L39–L42
Miyamoto, S. and Kitamoto, S. (1991), ApJ **374**, 741–743
Morgan, E.H., Remillard, R.A. and Greiner, J. (1997), ApJ **482**, 993–1010
Motch, C., Guillout, P., Haberl, F., et al. (1998), A&AS **132**, 341–359
Muno, M.P., Morgan, E.H. and Remillard, R.A. (1999), ApJ **527**, 321–340
Muno, M.P., Morgan, E.H., Remillard, R.A., et al. (2001), ApJ, **556**, 515–532
Murdin, P., Griffiths, R.E., Pounds, K.A., et al. (1977), MNRAS **178**, 27P–32P
Narayan, R. (1996), ApJ **462**, 136–141
Narayan, R. (2002), to appear in it Lighthouses of the Universe, eds. M. Gilfanov, R. Sunyaev, et al. (Springer, Berlin)
Narayan, R., Garcia, M.R. and McClintock, J.E. (1997), ApJ **478**, L79–L82
Narayan, R., Garcia, M. R. and McClintock, J. E. (2002), in *Proc. Ninth Marcel Grossmann Meeting*, eds. V.G. Gurzadyan et al. (World Scientific, Singapore), 405–425
Narayan, R. and Insu, Y. (1994), ApJ **428**, L13–L16
Narayan, R. and Insu, Y. (1995), ApJ **444**, 231–243
Narayan, R., Igumenshchev, I.V. and Abramowicz, M.A. (2000), ApJ **539**, 798–808
Narayan, R., McClintock, J.E. and Yi, I. (1996), ApJ **457**, 821–833
Nelemans, G. and van den Heuvel, E.P.J. (2001), A&A **376**, 950–954
Nobili, L., Turolla, R., Zampieri, L. and Belloni, T. (2000), ApJ **538**, L137–L140
Novikov, I.D. and Thorne, K.S. (1973), in *Black Holes*, eds. C. DeWitt and B. DeWitt, (Gordon & Breach, NY)
Nowak, M.A. (2000), MNRAS **318**, 361–367
Nowak, M.A. and Wilms, J. (1999), ApJ **522**, 476–486
Nowak, M.A., Wilms, J. and Dove, J.B. (2002), MNRAS **332**, 856–878
Nowak, M.A., Wilms, J., Heindl, W.A., et al. (2001), MNRAS **320**, 316–326
Ogley, R.N., Ash, T.D.C. and Fender, R.P. (1997), IAU Circ. 6726

Orosz, J.A. and Bailyn, C.D. (1997), ApJ **477**, 876–896
Orosz, J.A., Bailyn, C.D., McClintock, J.E. and Remillard, R.A. (1996), ApJ **468**, 380–390
Orosz, J.A., Groot, P.J., van der Klis, M., et al. (2002a), ApJ **568**, 845–861
Orosz, J.A., Jain, R.K., Bailyn, C.D., et al. (1998), ApJ **499**, 375–384
Orosz, J.A., Kuulkers, E., van der Klis, M., et al. (2001), ApJ **555**, 489–503
Orosz, J.A., Polisensky, E.J., Bailyn, C.D., et al. (2002b), BAAS 201, 1511
Osaki, Y. (1974), PASJ **26**, 429–436
Owen, F.N., Balonek, T.J., Dickey, J., et al. (1976), ApJ **203**, L15–L16
Pan, H.C., Skinner, G.K., Sunyaev, R.A. and Borozdin, K.N. (1995), MNRAS **274**, L15–L18
Parmar, A.N., Angelini, L., Roche, P. and White, N.E. (1993), A&A **279**, 179–187
Pottschmidt, K., Wilms, J., Nowak, M.A., et al. (2003), submitted to A&A (astro–ph/0202258)
Poutanen, J. and Fabian, A. C. (1999), MNRAS **306**, L31–L37
Pringle, J.E. (1981), Ann. Rev. Astron. Astrophys. **19**, 137-162
Pringle, J.E. and Rees, M.J. (1972), A&A **21**, 1–9
Psaltis, D., Belloni, T. and van der Klis, M. (1999), ApJ **520**, 262–270
Quataert, E. and Gruzinov, A. (2000), ApJ **539**, 809–814
Quataert, E. and Narayan, R. (1999), ApJ **520**, 298–315
Reig, P., Belloni, T., van der Klis, M., et al. (2000), ApJ **541**, 883–888
Remillard, R., Levine, A., Swank, J. and Strohmayer, T. (1997), IAU Circ. 6710
Remillard, R.A., Levine, A.M., Morgan, E.H., et al. (2003a), IAU Circ. 8050
Remillard, R.A. and Morgan, E.H., (1999), Bull. AAS **31**, 1421
Remillard, R.A., Morgan, E.H., McClintock, J.E., et al. (1999), ApJ **522**, 397–412
Remillard, R.A., Morgan, E.H. and Muno, M. (2001), in it Proc. Ninth Marcel Grossmann Meeting, eds. V.G. Gurzadyan et al. (World Scientific, Singapore), 2220-2223
Remillard, R.A., Muno, M.P., McClintock, J.E. and Orosz, J.A. (2002a), ApJ **580**, 1030–1042
Remillard, R.A., Muno, M.P., McClintock, J.E. and Orosz, J.A. (2003b), BAAS **35**, 648
Remillard, R.A., Orosz, J.A., McClintock, J.E. and Bailyn, C.D. (1996), ApJ **459**, 226–235
Remillard, R.A., Sobczak, G.J., Muno, M.P. and McClintock, J.E. (2002b), ApJ **564**, 962–973
Revnivtsev, M., Borozdin, K.N., Priedhorsky, W.C. and Vikhlinin, A. (2000a), ApJ **530**, 955-965
Revnivtsev, M., Gilfanov, M. and Churazov, E. (1998a), A&A **339**, 483–488
Revnivtsev, M., Gilfanov, M. and Churazov, E. (2001), A&A **380**, 520–525
Revnivtsev, M., Gilfanov, M., Churazov, E., et al. (1998b), A&A **331**, 557–563
Revnivtsev, M., Gilfanov, M., Churazov, E. and Sunyaev, R. (2002), A&A **391**, 1013–1022
Revnivtsev, M., Sunyaev, R. and Borozdin, K. (2000b), A&A **361** L37–L39
Revnivtsev, M., Trudolyubov, S.P. and Borozdin, K.N. (2000c), MNRAS **312**, 151–158
Revnivtsev, M., Chernvakova, M., Capitanio, F., et al. (2003), ATEL 132
Reynolds, C.S. and Nowak, M.A. (2003), Phys.Rept. *377*, 389-466
Reynolds, A.P., Quaintrell, H., Still, M.D., et al. (1997), MNRAS **288**, 43–52
Rezzolla, L., Yoshida, S'i, Maccarone, T. J., & Zanotti, O. (2003), MNRAS **344**, L37–L41
Rhoades, C.E. and Ruffini, R. (1974), Phys.Rev.Lett. **32**, 324–
Rodriguez, L.F., Mirabel, I.F. and Marti, J. (1992), ApJ **401**, L15–L18
Romani, R.W. (1998), A&A **333**, 583–590
Rothschild, R.E., Blanco, P.R., Gruber, D.E., et al. (1998), ApJ **496**, 538–549
Rothstein, D.M., Eikenberry, S.S., Chatterjee, S., et al. (2002), ApJ **580**, L61–L63
Rozanska, A. and Czerny, B. (2000), A&A **360**, 1170–1186
Rupen, M.P., Brocksopp, C., Mioduszewski, A.J., et al. (2003), IAU Circ. 8054
Rupen, M.P., Dhawan, V. and Mioduszewski, A.J. (2002), IAU Circ. 7874
Rupen, M.P., Hjellming, R.M. and Mioduszewski, A.J. (1998), IAU Circ. 6938
Rutledge, R.E., Lewin, W.H.G., van der Klis, M., et al. (1999), ApJS **124**, 265–283
Sanchez–Fernandez, C., Zurita, C., Casares, J., et al. (2002), IAU Circ. 7989
Seon, K., Min, K., Kenji, Y., et al. (1995), ApJ **454**, 463–471
Shahbaz, T., Naylor, T. and Charles, P.A. (1997), MNRAS **285**, 607–612
Shahbaz, T., Ringwald, F.A., Bunn, J.C., et al. (1994), MNRAS **271**, L10–L14
Shahbaz, T., van der Hooft, F., Casares, J., et al. (1999), MNRAS **306**, 89–94
Shakura, N.I. and Sunyaev, R.A. (1973), A&A **24**, 337–366
Shapiro, S.L. and Teukolsky, S.A. (1983), *Black Holes, White Dwarfs and Neutron Stars: The Physics of Compact Objects* (Wiley, New York)

Shimura, T. and Takahara, F. (1995), ApJ **445**, 780–788
Shrader, C.R., Wagner, R.M., Hjellming, R.M., et al. (1994), ApJ **434**, 698–706
Skinner, G.K., Foster, A.J., Willmore, A.P. and Eyles, C.J. (1990), MNRAS **243**, 72–77
Smak, J. (1971), Acta Astron. **21**, 15–21
Smith, D.M., Heindl, W.A. and Swank, J. (2002), ApJ **578**, L129–L132
Smith, D.M., Heindl, W.A., Markwardt, C.B. and Swank, J.H. (2001), ApJ **554**, L41–L44
Smith, D.M., Heindl, W.A., Swank, J., et al. (1997), ApJ **489**, L51–L54
Sobczak, G.J., McClintock, J.E., Remillard, R.A., et al. (1999), ApJ **520**, 776–787
Sobczak, G.J., McClintock, J.E., Remillard, R.A., et al. (2000a), ApJ **531**, 537-545
Sobczak, G.J., McClintock, J.E., Remillard, R.A., et al. (2000b), ApJ **544**, 993–1015
Steeghs, D., Miller, J.M., Kaplan, D. and Rupen, M. (2003), ATEL 146
Stella, L., Vietri, M. and Morsink, S.M. (1999), ApJ **524**, L63–L66
Stirling, A.M., Spencer, R.E., de la Force, C.J., et al. (2001), MNRAS **327**, 1273–1278
Stone, J.M., Pringle, J.E. and Begelman, M.C. (1999), MNRAS **310**, 1002–1016
Strohmayer, T.E. (2001a), ApJ **552**, L49–L53
Strohmayer, T.E. (2001b), ApJ **554**, L169–L172
Sunyaev, R., Churazov, E., Gilfanov, M., et al. (1992), ApJ **389**, L75–L78
Sunyaev, R., Gilfanov, M., Churazov, E., et al. (1991a), SvAL **17**, 50–54
Sunyaev, R.A., Kaniovskii, A.S., Efremov, V.V., et al. (1991b), SvAL **17**, 123–130
Sunyaev, R.A., Lapshov, I.Yu., Grebenev, S.A., et al. (1988), SvAL **14**, 327–333
Sunyaev, R. and Revnivtsev, M. (2000), A&A **358**, 617–623
Sutaria, F. K., Kolb, U., Charles, P., et al. (2002), A&A **391**, 993–997
Swank, J. (1998), in *The Active X–ray Sky: Results from BeppoSAX and Rossi–XTE*, eds. L. Scarsi et al., Nuclear Physics B Proceedings Supplements (astro–ph/9802188)
Tagger, M. and Pellat, R. (1999), A&A **349**, 1003–1016
Takahashi, K., Inoue, H. and Dotani, T. (2001), PASJ **53**, 1171–1177
Tanaka, Y. and Lewin, W.H.G. (1995), in **X–ray Binaries**, eds. W.H.G. Lewin, J. van Paradijs and E.P.J. van den Heuvel, (Cambridge U. Press, Cambridge) 126–174, TL95
Tanaka, Y. and Shibazaki, N. (1996), ARA&A **34**, 607–644, TS96
Tanaka, Y., Nandra, K., Fabian, A.C. (1995), Nature **375**, 659–661
Tananbaum, H., Gursky, H., Kellogg, E., et al. (1972), ApJ **177**, L5–L10
Timmes, F.X., Woosley, S.E. and Weaver, T.A. (1996), ApJ 457, 834–843
Titarchuk, L. and Osherovich, V. (2000), ApJ **542**, L111–L114
Titarchuk, L. and Shrader, C. (2002), ApJ **567**, 1057–1066
Tomsick, J.A. and Kaaret, P. (2000), ApJ **537**, 448–460
Tomsick J.A. and Kaaret, P. (2001), ApJ **548**, 401–409
Tomsick, J.A., Kaaret, P., Kroeger, R.A. and Remillard, R.A. (1999), ApJ **512**, 892–900
Trudolyubov, S., Churazov, E., Gilfanov, M., et al. (1999), A&A **342**, 496–501
Turner, M.J.L., Thomas, H.D., Patchett, B.E., et al. (1989), PASJ **41**, 345–372
Turner, N.J., Stone, J.M. and Sano, T. (2002), ApJ **566**, 148–163
Turolla, R., Zane, S. and Titarchuk, L. (2002), ApJ **576**, 349–356
Ueda, Y., Dotani, T., Uno, S, et al. (1997), IAU Circ. 6627
van den Heuvel, E.P.J. (1992), in *ESA, Environment Observation and Climate Modelling Through International Space Projects* (SEE N93–23878 08–88)
van der Hooft, F., Kouveliotou, C., van Paradijs, J., et al. (1996), ApJ **458**, L75–L78
van der Hooft, F., Kouveliotou, C., van Paradijs, J., et al. (1999), ApJ **513**, 477–490
van der Klis M. (1994), ApJS **92**, 511–519
van Dijk, R., Bennett, K., Collmar, W., et al. (1995), A&A 296, L33–L36
van der Klis M. (1995) in *X–ray Binaries*, eds. W.H.G. Lewin, J. van Paradijs and E.P.J. van den Heuvel, (Cambridge U. Press, Cambridge), 252–307
van Paradijs, J. (1995) in *X–ray Binaries*, eds. W.H.G. Lewin, J. van Paradijs and E.P.J. van den Heuvel, (Cambridge U. Press, Cambridge), 536–577
van Paradijs, J. and McClintock, J.E. (1995) in *X–ray Binaries*, eds. W.H.G. Lewin, J. van Paradijs and E.P.J. van den Heuvel, (Cambridge U. Press, Cambridge), 58–125
Vargas, M., Goldwurm, A., Laurent, P., et al. (1997), ApJ **476**, L23–L26
Vargas, M., Goldwurm, A., Paul, J., et al. (1996), A&A **313**, 828–832
Vasiliev, L., Trudolyubov, S. and Revnivtsev, M. (2000), A&A **362**, L53–L56

Vikhlinin, A., Churazov, E., Gilfanov, M., et al. (1994), ApJ **424**, 395–400
Vikhlinin, A., Finoguenov, A., Sitdikov, A., et al. (1992), IAU Circ. 5608
Wagner, R.M., Foltz, C.B., Shahbaz, T., et al. (2001), ApJ **556**, 42–46
Wagner, R.M., Starrfield, S.G., Hjellming, R.M., et al. (1994), ApJ **429**, L25–L28
Wagoner, R.V. (1999), Phys.Rept. **311**, 259–269
Wagoner, R.V., Silbergleit, A.S. and Ortega-Rodriguez, M. (2001), ApJ **559**, L25–L28
Wardzinski, G., Zdziarski, A.A., Gierlinski, M., et al. (2002), MNRAS **337**, 829-839
Weaver, K.A., Gelbord, J. and Yaqoob, T. (2001), ApJ **550**, 261–279
Webster, B.L and Murdin, P. (1972), Nature **235**, 37–38
White, N.E. and Marshall, F.E. (1984), ApJ **281**, 354–359
White, N.E. and van Paradijs, J. (1996), ApJ **473**, L25–L29
White, N.E., Nagase, F. and Parmar, A.N. (1995) in *X–ray Binaries*, eds. W.H.G. Lewin, J. van Paradijs and E.P.J. van den Heuvel, (Cambridge U. Press, Cambridge) 1–57
White, N.E., Stella, L. and Parmar, A.N. (1988), ApJ **324**, 363–378
Wijnands, R. and Miller, J.M. (2002), ApJ **564**, 974–980
Wijnands, R. and van der Klis, M. (2000), ApJ **528**, L93–L96
Wijnands, R., Homan, J. and van der Klis, M. (1999), ApJ **526**, L33–L36
Wijnands, R., Mendez, M., Miller, J.M. and Homan, J. (2001), MNRAS **328**, 451–460
Wijnands, R., Miller, J.M. and van der Klis, M. (2002), MNRAS **331**, 60–70
Wilms, J., Nowak, M.A., Dove, J.B., et al. (1999), ApJ **522**, 460–475
Wilms, J., Nowak, M.A., Pottschmidt, K., et al. (2001a), MNRAS **320**, 327–340
Wilms, J., Reynolds, C.S., Begelman, M.C., et al. (2001b), MNRAS **328**, L27–L31
Wilson, A.M., Carpenter, G.F., Eyles, C.J., et al. (1977), ApJ **215**, L111–L115
Wilson, C.K. and Rothschild, R.E. (1983), ApJ **274**, 717–722
Wood, K.S., Ray, P.S., Bandyopadhyay, R.M., et al. (2000), ApJ **544**, L45–L48
Woods, P.M., Kouveliotou, C., Finger, M.H., et al. (2002), IAU Circ. 7856
Woosley, S.E., Heger, A. and Weaver, T.A. (2002), RvMP **74**, 1015–1071
Wu, K., Soria, R., Campbell–Wilson, D., et al. (2002), ApJ **565**, 1161–1168
Yaqoob, T., Ebisawa, K. and Mitsuda, K. (1993), MNRAS **264**, 411–420
Zdziarski, A.A. (2000), in *Highly Energetic Physical Processes*, Procs. IAU Symposium #195, eds. C.H. Martens, S. Tsuruta and M.A. Weber, ASP, 153-170, (astro-ph/0001078)
Zdziarski, A.A., Grove, J.E., Poutanen, J., et al. (2001), ApJ **554**, L45–L48
Zdziarski, A.A., Lubinski, P., Gilfanov, M. and Revnivtsev, M. (2003), MNRAS **342**, 355–372
Zdziarski, A., Poutanen, J., Paciesas, W.S. and Wen, L. (2002), ApJ **578**, 357–373
Zhang, S.N., Cui, W. and Chen, W. (1997a), ApJ **482**, L155–L158
Zhang, S.N., Cui, W., Harmon, B.A., et al. (1997b), ApJ **477**, L95–L98
Zurita, C., Sanchez–Fernandez, C., Casares, J., et al. (2002), MNRAS **334**, 999–1008
Zycki, P.T., Done, C. and Smith, D.A. (1999a), MNRAS **305**, 231–240
Zycki, P.T., Done, C. and Smith, D.A. (1999b), MNRAS **309**, 561–575